

**PRECONCENTRATION OF VOLATILE ELEMENTS ON QUARTZ
SURFACE PRIOR TO DETERMINATION BY ATOMIC SPECTROMETRY**

**A THESIS SUBMITTED TO
THE GRADUATE SCHOOL OF NATURAL AND APPLIED SCIENCES
OF
MIDDLE EAST TECHNICAL UNIVERSITY**

BY

DENİZ KORKMAZ

**IN PARTIAL FULFILLMENT OF THE REQUIREMENTS FOR
THE DEGREE OF DOCTOR OF PHILOSOPHY**

IN

CHEMISTRY

MAY 2004

Approval of the Graduate School of Natural and Applied Sciences

Prof. Dr. Canan Özgen
Director

I certify that this thesis satisfies all the requirements as a thesis for the degree of Doctor of Philosophy.

Prof. Dr. Hüseyin İşçi
Chair of Chemistry Department

This is to certify that we have read this thesis and that in our opinion it is fully adequate, in scope and quality, as a thesis for the degree of Doctor of Philosophy.

Prof. Dr. O. Yavuz Ataman
Supervisor

Examining Committee Members

Prof. Dr. Mehmet DOĞAN (Hacettepe University) _____

Prof. Dr. O. Yavuz ATAMAN (METU) _____

Dr. Jiří DĚDINA (Academy of Sciences of Czech Rep.) _____

Prof. Dr. E. Hale GÖKTÜRK (METU) _____

Prof. Dr. Mürvet VOLKAN (METU) _____

I hereby declare that all information in this document has been obtained and presented in accordance with academic rules and ethical conduct. I also declare that, as required by these rules and conduct, I have fully cited and referenced all material and results that are not original to this work.

Name, Last name : Deniz KORKMAZ

Signature :

ABSTRACT

PRECONCENTRATION OF VOLATILE ELEMENTS ON QUARTZ SURFACE PRIOR TO DETERMINATION BY ATOMIC SPECTROMETRY

Korkmaz, Deniz

Ph.D., Department of Chemistry

Supervisor: Prof. Dr. O. Yavuz Ataman

May 2004, 156 Pages

Hydride generation technique is frequently used for the detection of elements as As, Se, Sb, Sn, Bi, Ge, Te and Pb that form volatile hydrides in solution using a reductant. In this study, a novel quartz trap for on-line preconcentration of volatile analyte species was designed. Pb, Sb and Cd were selected as analyte elements and chemical vapour generation technique was employed for generation of their volatile species in flow systems. The trapping medium was formed by external heating of either the inlet arm of the quartz tube atomizer or a separate cylindrical quartz tube. Generated analyte species were trapped on quartz surface heated to the collection temperature and the collected species were revolatilized when the trap was heated further to releasing temperature and hydrogen gas was introduced in the trapping medium. The conventional quartz T-tube and multiple microflame quartz tube were employed as atomizers. The influence of relevant experimental parameters on the generation, collection and revolatilization efficiencies was investigated. Optimum

conditions, performance characteristics of the trap and analytical figures of merit are presented. Experimental design was used for optimizations in some cases. Standard reference materials were analyzed to assess the accuracy of the proposed method. For a collection period of 1.0 minute for Pb, 2.0 minutes for Sb and 3.0 minutes for Cd, 3σ limit of detections, in pg ml^{-1} , were 19, 3.9 and 1.8, respectively. In cases of Sb and Cd, the limits of detections obtained are the same as the best attained with *in-situ* trapping in graphite furnaces.

Keywords: Hydride Generation, Cold Vapour Generation, On-line Preconcentration, Quartz Trap, Pb, Sb, Cd

ÖZ

UÇUCU ELEMENTLERİN ATOMİK SPEKTROMETRİ İLE TAYİNİNDEN ÖNCE KUVARS YÜZEY ÜZERİNDE ÖNZENGİNLEŞTİRİLMESİ

Korkmaz, Deniz

Doktora, Kimya Bölümü

Tez Yöneticisi : Prof. Dr. O. Yavuz Ataman

Mayıs 2004, 156 sayfa

Hidrür oluşturma tekniği, As, Se, Sb, Sn, Bi, Ge, Te ve Pb gibi bir indirgeyici ile reaksiyon sonucu uçucu hidrürler oluşturan elementlerin tayininde sıklıkla kullanılır. Bu çalışmada, uçucu analit türlerinin hat-üstü önzenginleştirilmesi için yeni bir kuvars tuzak tasarlanmıştır. Analit olarak Pb, Sb ve Cd elementleri seçilmiş ve bu elementlerin uçucu bileşiklerinin oluşturulması için akış sistemlerinde kimyasal buhar oluşturma tekniği kullanılmıştır. Tuzak ortamı, kuvars tüp atomlaştırıcının giriş kolu veya ayrı bir silindirik kuvars tüp dışarıdan ısıtılarak oluşturulmuştur. Oluşturulan analit türleri toplama sıcaklığına ısıtılmış olan kuvars yüzey üzerinde tuzaklanmış ve tuzağın salınma sıcaklığına getirilip ortama hidrojen gazının girişiyle tekrar buharlaştırılmıştır. Atomlaştırıcı olarak, kuvars T tüp veya çoklu mikroalevli kuvars tüp kullanılmıştır. Oluşturma, toplama, tekrar buharlaştırma verimine etki eden parametreler incelenmiştir. Optimum koşullar, tuzağın performans karakteristikleri ve analitik performans sayıları sunulmuştur. Bazı durumlarda optimizasyonlar için deneysel tasarım kullanılmıştır. Önerilen yöntemin

dođruluđunu deđerlendirmek için standard referans maddeler analiz edilmiştir. Pb için 1.0, Sb için 2.0 ve Cd için 3.0 dakika toplama süreleri kullanılarak, 3σ tayin limitleri, pg ml^{-1} cinsinden sırasıyla, 19, 3.9 ve 1.8'dir. Sb ve Cd için, elde edilen tayin limitleri grafit tüpte yerinde tuzaklama ile elde edilen en iyi tayin limitleri ile aynıdır.

Anahtar Kelimeler: Hidrür Oluşturma, Sođuk Buhar Oluşturma, Hat-üstü Önzenginleştirme, Kuvars Tuzak, Pb, Sb, Cd

ACKNOWLEDGEMENTS

I owe a debt of gratitude to many individuals without whose efforts this work would not have been possible.

First and foremost, I would like to thank Prof. Dr. O. Yavuz Ataman. In many ways he has always set an example to emulate in my life. I am deeply grateful for his invaluable guidance and support throughout all stages of this thesis.

I am much indebted to Assist. Prof. Dr. Nusret Ertaş for the innumerable insights and suggestions he has provided at all stages of this work.

During a three months stay in his laboratory, I learned much from Dr. Jiří Dědina who proposed numerous improvements to this work and has always given inspiration and encouragement to me. Our discussions were most helpful and are deeply appreciated. Thanks are also due to Anna Selecká, Dr. Vlasta Korunová, Honza Kratzer, Dr. Alessandro D'Ulivo and Dr. Bohumil Dočekal for their helps and friendship which made the life easier for me in Prague.

I would like to thank my examining committee members for their advice, time and interest in this work.

My deepest thanks are to my husband, Ilgaz Korkmaz, for his unconditional love, patience, understanding and support. His love and joy lights up my world everyday.

Grateful thanks are due to my friends, Dr. Eftade Gaga, Oktay Cankur and Süleyman Can for all their support. I would like to extend special thanks to my dearest and extremely talented friend Dr. Gülay Ertaş with whom I have had the

pleasure of working with for the past several years with very many memorable times.

The continued support of Assoc. Prof. Dr. Cevdet Demir for chemometric studies is gratefully acknowledged .

This work was financially supported by Middle East Technical University Research Fund and TÜBİTAK NATO Science Fellowship Programme through grants BAP 2001-07-02-00-08 and NATO A2, respectively.

TABLE OF CONTENTS

ABSTRACT.....	iv
ÖZ.....	vi
ACKNOWLEDGEMENTS.....	viii
TABLE OF CONTENTS.....	x
LIST OF TABLES.....	xv
LIST OF FIGURES.....	xvii
LIST OF ABBREVIATIONS.....	xx
 CHAPTER	
1. INTRODUCTION.....	1
1.1 Atomic Absorption Spectrometry.....	1
1.2 Hydride Generation Atomic Absorption Spectrometry.....	2
1.2.1 Hydride Formation.....	5
1.2.2 Hydride Transport.....	8
1.2.3 Hydride Atomization.....	10
1.2.3.1 Flame-in-Tube Atomizers.....	10
1.2.3.2 Externally Heated Quartz Tube Atomizers.....	12
1.2.3.2.1 Multiple Microflame Quartz Tube Atomizer.....	14
1.2.3.3 Electrothermal Atomizers.....	16

1.2.3.4 Tungsten Atomizers.....	16
1.3 Cold Vapour Generation Technique.....	17
1.4 Chemical Vapour Generation of Transition and Noble Metals.....	18
1.5 Metal Devices for Preconcentration of Hydrides.....	20
1.6 Quartz Traps for Flame AAS.....	21
1.7 Pb.....	22
1.7.1 Determination of Pb by HG.....	23
1.7.2 Atomization Mechanism of Pb in Quartz T-Tube.....	24
1.8 Sb.....	25
1.8.1 Determination of Sb by HG.....	26
1.9 Cd.....	27
1.9.1 Determination of Cd by Cold Vapour Generation.....	27
1.10 Chemometrics.....	29
1.10.1 Experimental Design and Optimization.....	30
1.10.1.1 Two-Level Designs: Screening Designs.....	32
1.10.1.1.1 Factorial Designs.....	32
1.10.1.2 Three Level Designs: Response Surface Designs.....	34
1.10.1.2.1 Central Composite Design.....	34
1.11 Aim of This Study.....	36
2. EXPERIMENTAL.....	37
2.1 Pb.....	37

2.1.1 Reagents.....	37
2.1.2 Spectrometer.....	37
2.1.3 Hydride Generator.....	38
2.1.4 Trap.....	38
2.1.5 Atomizer.....	39
2.1.6 Procedure.....	41
2.1.7 Accuracy Check.....	42
2.2 Sb.....	43
2.2.1 Reagents.....	43
2.2.2 Spectrometer.....	43
2.2.3 Hydride Generator.....	44
2.2.4 Trap.....	45
2.2.5 Atomizer.....	47
2.2.6 Procedure.....	48
2.3 Cd.....	50
2.3.1 Reagents.....	50
2.3.2 Spectrometer.....	50
2.3.3 Cold Vapour Generator.....	51
2.3.4 Trap.....	52
2.3.5 Quartz T-Tube.....	54
2.3.6 Procedure.....	55
2.3.7 Accuracy Check.....	56

3. RESULTS AND DISCUSSION	58
3.1 Pb.....	58
3.1.1 Optimization of Conditions for Continuous Flow HGAAS.....	58
3.1.1.1 Potassium Hexacyanoferrate(III) and HCl Concentrations.....	58
3.1.1.2 NaBH ₄ and NaOH Concentrations.....	60
3.1.1.3 Pumping Rate and Argon Flow Rate.....	61
3.1.1.4 The Length of Reaction Coil.....	62
3.1.2 Trapping PbH ₄ on Inlet Arm of Quartz Tube Atomizer.....	62
3.1.3 Observation of Pre-peaks	66
3.1.4 Trapping PbH ₄ on Separated Quartz Trap	68
3.1.5 Effect of Carrier Gas	69
3.1.6 Effect of Hydrogen Radicals	70
3.1.7 The Form of Revolatilized Species	71
3.1.8 Analytical Figures of Merit	72
3.2 Sb.....	74
3.2.1 Hydride Generation Conditions for Continuous Flow HGAAS.....	74
3.2.2 Preliminary Observations.....	75
3.2.3 Optimization of Collection and Revolatilization.....	76
3.2.4 Influence of the Length of Inlet Arm of Atomizer	81
3.2.5 Influence of Oxygen.....	81

3.2.6 Observation of Pre-peaks	83
3.2.7 Analytical Figures of Merit	84
3.3 Cd.....	86
3.3.1 Optimization of Conditions for FI HGAAS.....	86
3.3.2 Data Analysis.....	89
3.3.3 Double Peaks in FI Cold Vapour Generation of Cd.....	102
3.3.4 Optimization of Collection and Revolatilization.....	103
3.3.5 Effect of Carrier Gas.....	105
3.3.6 Effect of H ₂ Flow.....	106
3.3.7 Effect of Filling Materials.....	107
3.3.8 Analytical Figures of Merit.....	109
3. CONCLUSIONS	113
REFERENCES.....	117
VITA.....	136

LIST OF TABLES

TABLES

2.1 The relation between voltage difference applied to the trap and the inside temperature for separated quartz trap.....	41
2.2 Microwave program for digestion.....	43
2.3 The relation between voltage difference applied to the trap and the inside temperature for Sb.....	46
2.4 The relation between voltage difference applied to the trap and the inside temperature for Cd.....	54
2.5 Microwave program for digestion.....	57
3.1 Comparison of analytical figures of merit using peak height. Collection time for separated quartz trap was 60 s with a sample solution flow rate of 6.0 ml min ⁻¹	74
3.2 Analysis results of standard reference materials.....	74
3.3 Integrated absorbances for introducing H ₂ before or after reaching to volatilization temperature.....	77
3.4 The influence of the auxiliary H ₂ flow rate on peak area for direct transfer and collection modes of measurements.....	79
3.5 The influence of auxiliary air flow rate on signals observed in the collection mode of measurements; 5 ng Sb.....	82
3.6 Uncoded design matrix.....	88
3.7 Coding of factors.....	88
3.8 Coded design matrix with average response values.....	90
3.9 The coefficients for the model.....	92

3.10 Construction of a central composite design for three factors.....	93
3.11 Real values corresponding to the coded levels.....	93
3.12 Coded central composite design matrix with average response values..	96
3.13 Coefficients for the model.....	97
3.14 The predicted responses and residuals.....	97
3.15 Calculation of t-statistics.....	98
3.16 Coded and real optimum values for generation of Cd species.....	100
3.17 Comparison of analytical figures of merit using integrated absorbances. Collection time for quartz trap was 180 s with a sample solution flow rate of 2.0 ml min ⁻¹	111
3.18 Determination of Cd in SRMs.....	112
4.1 Summary of 3σ LODs and characteristic masses (m ₀) attained.....	115

LIST OF FIGURES

FIGURES

1.1. Chemical vapour forming elements by reaction with NaBH_4	6
1.2 Representation of a three factor, two level a) full factorial and b) fractional factorial designs.....	33
1.3 Elements of a central composite design.....	35
2.1 Continuous flow system with separated quartz trap on-line.....	39
2.2 Top view of quartz tube atomizer with trap. Trap (a) close to (b) away from T-junction.....	40
2.3 Temperature inside the quartz trap vs. time after increasing the applied voltage from 30 V (500°C) to 90 V; temperature was steady state at $t = 0$	42
2.4 Scheme of the hydride generator.....	45
2.5 Temperature inside the trap vs. the time after increasing the applied voltage from 4.4 V (650°C) to 8.0 V; temperature was steady state at $t = 0$	47
2.6 Multiple microflame quartz tube atomizer.....	48
2.7 Scheme of the hydride generator.....	51
2.8 Temperature inside the inlet arm vs. the time after increasing the applied voltage from 1.4 V (350°C) to 4.4 V; temperature was steady state at $t = 0$	54
2.9 Top view of quartz T-tube with trap.....	55
3.1 Surface plot for absorbance signal versus $\text{K}_3\text{Fe}(\text{CN})_6$ and HCl concentrations.....	59

3.2 Surface plot for absorbance signal versus NaBH ₄ and NaOH concentrations.....	60
3.3 Surface plot for absorbance signal versus pumping rate and Ar flow.....	61
3.4 Changes in signal when the trap was operated during continuous flow of PbH ₄ , 10 ng ml ⁻¹ Pb. Trap (a) close to (b) away from T-junction of quartz tube atomizer.....	63
3.5 Time profile of thermal atomization signal. 20 ng/mL Pb collected for 2 minutes on quartz T-tube, close to T-junction. No hydrogen was allowed into the atomizer during atomization (b) 20 ng/mL Pb collected for 2 minutes. Trap was heated and pump was activated on different instants of heating.....	65
3.6 Time profile of atomization signal for (a) separated quartz trap, 6.0 ml of 1 ng ml ⁻¹ Pb collected for 60 s; (b) continuous flow HGAAS, 1 ng ml ⁻¹ Pb.....	69
3.7 Experimental set-up to understand the effect of hydrogen radicals.....	71
3.8 Calibration plot for 60 s trapping.....	72
3.9 Analytical signal vs. collection time for 0.5 ng ml ⁻¹ Pb.....	73
3.10 Influence of collection temperature (squares, volatilization temperature of 920 °C) and volatilization temperature (triangles, collection temperature of 650 °C) on the observed signal; 5 ng Sb.....	78
3.11 The typical signal shape observed. Collection temperature: 650 °C; revolatilization temperature: 920 °C; 4 ng Sb.....	80
3.12 The signal observed for the collection temperature of 700 °C. Revolatilization temperature: 920 °C; 5 ng Sb.....	81
3.13 Peak area and peak height calibration for the collection mode. Collection time: 120 s; sample volume: 8 ml.....	85
3.14 Relationship between response, design matrix and coefficients.....	91
3.15 Estimated response surface for length of reaction coil vs carrier HCl concentration.....	100

3.16 Estimated response surface for length of reaction coil vs NaBH ₄ concentration.....	101
3.17 Estimated response surface for carrier HCl concentration vs NaBH ₄ concentration.....	101
3.18 Effect of Ar flow on FI signal. 1 ng ml ⁻¹ Cd, 100 μL loop.....	102
3.19 Changes in signal when the trap was operated during FI of 100 μL, 1.0 ng ml ⁻¹ Cd.....	104
3.20 Influence of collection temperature (squares, volatilization temperature of 1000 °C) and revolatilization temperature (triangles, collection temperature of 350 °C) on the observed signal; 0.3 ng Cd....	105
3.21 The influence of the H ₂ flow rate on peak area for revolatilization.....	107
3.22 The typical signal shape observed. Collection temperature: 350 °C; revolatilization temperature: 1000 °C; 20 pg ml ⁻¹ Cd, 3 min. collection. Peak height: 0.057; peak area: 0.051. Seven pieces of quartz piece as filling material in the trapping medium.....	108
3.23 The signal shape observed for 3 pieces of quartz piece as filling material in the trapping medium. Collection temperature: 350 °C; revolatilization temperature: 1000 °C; 75 pg ml ⁻¹ Cd, 3 min. collection. Peak height: 0.155; peak area: 0.079.....	109
3.24 Calibration plot for 180 s collection; total sample volume was 6.0 ml..	110
3.25 Analytical signal vs collection time for 0.1 ng ml ⁻¹ Cd flowing at a rate of 2 ml min ⁻¹	111

LIST OF ABBREVIATIONS

AAS.....	Atomic Absorption Spectrometry
CVG.....	Chemical Vapour Generation
FI.....	Flow Injection
FWHM.....	Full Width at Half Maximum
GLS.....	Gas Liquid Separator
HG.....	Hydride Generation
HGAAS	Hydride Generation Atomic Absorption Spectrometry
i.d.....	inner diameter
LOD.....	Limit of Detection
o.d.....	outer diameter
RSD.....	Relative Standard Deviation
SRM.....	Standard Reference Material

CHAPTER 1

INTRODUCTION

1.1 Atomic Absorption Spectrometry

Atomic absorption spectrometry (AAS) is a spectroanalytical technique for the qualitative detection and quantitative determination of elements employing the absorption of optical radiation by free atoms in the gaseous state [1]. It was introduced as an analytical tool by Walsh [2]. In AAS, the absorption of resonance radiation by ground state atoms of the analyte is used as the analytical signal. Accordingly, a source delivering the resonance radiation of the analyte is required as well as an atomizer into which the analyte is introduced. The absorption of resonance radiation is highly selective as well as sensitive and thus, AAS became a powerful method of analysis, which is now used for trace elemental determinations in most analytical laboratories for a wide variety of applications [3].

The atomizer is the place in which the analyte is atomized, i.e. the flame, the graphite furnace, or the quartz tube. The atomization step, i.e. the transfer of the sample, and especially the analyte, into free atoms in the gaseous state, is without doubt the most important process in an analysis by AAS. Flame atomization is the oldest one of the AAS techniques. In flame atomization, either an indeterminate volume or a fixed aliquot of the measurement solution is converted into an aerosol

by a nebulizer and transported into the flame. The flame must possess enough energy not only to vaporize but also to atomize the sample. The chemical composition of the flame can have a major influence on these processes. For electrothermal atomization, a measured volume of the sample solution, usually 10-50 μL , is dispensed into the graphite furnace and the temperature is increased stepwise to remove the solvents and concomitants as completely as possible before atomization. An inert atmosphere of N_2 or Ar is used. Since the entire aliquot introduced into the graphite furnace is atomized within a short time (typically 1 s), a peak-shaped, time-dependent signal is generated whose integrated absorbance is proportional to the mass of the analyte in the measurement solution. Furnace techniques exhibit higher sensitivity than flames. Quartz tubes can be employed as absorption cells or atomizers for the analytes that can be vaporized in the atomic state or as molecules, like hydrides, by chemical reaction at ambient temperature [1].

1.2 Hydride Generation Atomic Absorption Spectrometry

In chemical vapour generation (CVG), the analyte is separated from the sample matrix by the generation of gaseous species as a result of a chemical reaction [4]. There are several CVG techniques to convert analytes into their volatile derivatives such as hydrides, chelates, alkyls, carbonyls, oxides or halides before their detection [5]. Since its introduction in 1969 [6], hydride generation (HG) has been one of the most frequently used sample introduction techniques for the determination of volatile hydride forming elements *viz.*, As, Bi, Ge, Pb, Sb, Se, Sn, and Te in AAS. Though not very widely used, generation of hydrides of In [7], P [8], S [9] and Tl [7] for analytical purposes have also been reported. Chemical HG involves the conversion of analyte in an acidified solution, to its gaseous hydride by a reducing agent, mostly sodium tetrahydroborate, NaBH_4 , under ambient conditions. Then the

hydride is driven out of the solution and transported to the atomizer which is usually an externally heated quartz T-tube. There is no need to heat the atomizer in case of Hg and Cd both of which can produce atomic vapour at room temperature and be determined by cold vapour generation technique. The popularity of HG arises for the significant advantages it offers: increased transport efficiency, separation of analyte from matrix which in effect suppresses the interferences, preconcentration potentiality, improved sensitivity, simplicity, automation, good sampling frequencies, low cost, and well established methodology. HG can also be coupled with other atomic spectrometric, chromatographic or flow injection (FI) techniques for certain speciation possibilities, better detection limits and on-line sample/analyte treatments such as decomposition, prereduction, enrichment etc. [10]. Hydride generation atomic absorption spectrometry (HGAAS) is widely applied to analysis of environmental, biological, food, agricultural, geological, metallurgical and other sample types [5].

In addition to its advantages, several intrinsic limitations and drawbacks of HGAAS are worth bearing in mind. CVG is essentially a chemical separation of the analyte element (or species) from the sample/matrix solution, which is performed *in situ* and instantaneously; hence rather complex, on-line chemistry is involved; high and consistent chemical yields of reaction products are required; specific chemical pretreatment is needed so as to reliably transform the analyte element into a definite, reactive chemical form and oxidation state. Thus selenium and tellurium analytes have to be prereduced to their hydride forming oxidation states, Se(IV) and Te(IV); lead should be preoxidized to its metastable Pb(IV) form; while arsenic and antimony exhibit much better sensitivity in their As(III) and Sb(III) oxidation states and typically call for a prereduction step. Hence reagent blanks and chemical interferences in aqueous and gaseous phase are involved. Because of specific HG conditions for individual elements (and species), multielement capabilities of HG technique are rather limited [11].

Electrochemical [12] and thermochemical [13] HG systems have also been proposed as alternatives to chemical HG although they were not commercialized and not used as widely as chemical HG in routine analysis. In electrochemical HG, the hydride is formed in the cathodic space of an electrolytic cell. The process is considered to take place in at least three sequential events: reduction and deposition of the analyte onto the surface of the cathode (or at specific surface sites), stepwise reduction of the deposited metal with nascent hydrogen (hydrogen atom) generated on the cathode by reduction of protons, and desorption of the hydride. Simultaneously, water is oxidized in the separated anodic space and oxygen is formed. Its advantages include requirement of fewer reagents, less critical experimental parameters, reduction of interferences from transition metals compared to chemical HG and the reduced influence of the oxidation state of the analyte on the hydride yield, depending on the type of cathode material used [14]. On the other hand, electrochemical HG is not without problems. The production of a reproducible solid electrode surface is not simple. A strong relationship between the conditions of the surface of the cathode, the operating parameters, the type of solid cathode and the cathode material itself exists. The conditioning of the cathode surface has to be done daily or before changing the sample type, or when the signal does not return to the baseline. The formation of hydrides can be negatively or positively affected by concomitant ions dependent on the cathode material and operating parameters and the efficiency of HG strongly depends on the analyte form, similar to chemical HG [12].

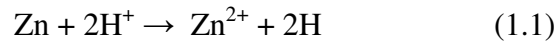
Thermochemical HG, which actually is a specific kind of quartz tube atomization, was first proposed for the determination of arsenobetaine, arsenocholine, and tetramethylarsonium cations which do not react with reducing agents [15]. After their chromatographic separation, the eluent was nebulized by thermospray effect and pyrolyzed in a methanol/oxygen flame and the atomized organometallic analytes were thermochemically derivatized to the hydride in the presence of excess

hydrogen at 900-1000 °C. The volatile derivative was then transported to hydrogen/oxygen diffusion flame atomizer.

Within last few years, the scope of CVG with NaBH₄ has been expanded to include several unconventional transitional and noble elements. It is not clear at this point the nature and mechanism of formation of those volatile species but the recent studies confirm that the resulting species are relatively unstable in solution and are quickly lost during their generation and subsequent transport, requiring rapid phase separation for their detection [16]. The overall scheme of chemical vapour forming elements by reaction with NaBH₄ can be seen in Figure 1.1.

1.2.1 Hydride Formation

Generally, either a metal/acid or tetrahydroborate reduction is employed for HG. The earlier technique, March reaction, used a metal/acid system, which was most often Zn/HCl, to produce nascent hydrogen for analyte reduction to hydride:



where m and n, respectively, are valencies of the analyte A in the sample solution and in hydride.

9

IA												VIII A					
IIA												IIIA	IVA	VA	VIA	VIIA	VIII A
		IIIB	IVB	VB	VIB	VII B	VIII B			IB	IIB						
			Ti		Cr	Mn	Fe	Co	Ni	Cu	Zn		Ge	As	Se		
							Ru	Rh	Pd	Ag	Cd	In	Sn	Sb	Te		
							Os	Ir	Pt	Au	Hg	Tl	Pb	Bi			

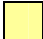


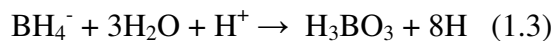
-  Hydride forming elements
-  Cold atomic vapour forming elements
-  Chemical vapour forming elements

Figure 1.1. Chemical vapour forming elements by reaction with NaBH₄

The second technique for hydride formation is $\text{BH}_4^-/\text{acid}$ reaction. The following generally accepted mechanism was first postulated by Robbins and Caruso [17]:



The resulting nascent hydrogen reduces analyte to hydride according to reaction 1.2. The upper mechanism of hydride suggests that the nascent hydrogen is the effective derivatizing agent for the formation of hydride. Another hypothesis of hydride formation includes mechanisms based on the direct transfer of hydrogen bound to boron to the hydride forming element [18]. Considering the estimated standard potential of H^+/H couple [$E^0(\text{H}^+/\text{H}) = -2.106 \text{ V}$], it was claimed that neither tetrahydroborate [$E^0(\text{H}_3\text{BO}_3/\text{BH}_4^-) = -0.482 \text{ V}$] nor zinc [$E^0(\text{Zn}^{2+}/\text{Zn}) = -0.763 \text{ V}$] would be able to perform the reduction reaction of protons to atomic hydrogen [19]. In a study by Pergantis et al. [20] mass spectrometry was used to detect transfer of deuterium from labelled reagents to arsines following hydride generation reactions. The results showed that hydrogen of hydride was from tetrahydroborate in most cases.

Sodium (most often) or potassium salt of tetrahydroborate is employed for generation of hydrides. Tetrahydroborate concentration varies depending on analyte element and on the type of hydride generators used. It should be underlined that even alkaline NaBH_4 solutions slowly decompose forming hydrogen; the decomposition is probably surface catalyzed and is slower in more concentrated hydroxide solutions. Filtration, or preferably, membrane ultrafiltration is therefore advisable. Large excess of NaOH could be detrimental, since it has to be neutralized as well as for higher blanks entailed [5]. The use of cyanoborohydride [21] and very recently aminoboranes [22] have also been reported as reagents for the chemical generation of volatile species of the elements forming volatile hydrides.

The $\text{BH}_4^-/\text{acid}$ system is currently almost exclusively used since it is superior to the metal/acid reduction method with respect to reduction yield, reaction time, blank contamination and to applicability to the elements concerned. Technically, the reducing reaction is performed by mixing an excess of acidic sample volume with tetrahydroborate so that the reacted out mixture is still acidic. The optimum conditions for hydride release involving the effects of various acids as reaction media, their concentration, sometimes the presence of reaction controllers or buffers depend on analyte identity and its valency. It should be mentioned that analytes can be reduced by tetrahydroborate in alkaline solution and generated from the solution by acidification [5].

There is always excess, usually many orders of magnitude, of the reducing agent over the analyte under typical conditions of hydride generation. Resulting hydrogen drives the hydride from the reaction mixture to the gaseous phase. This is the additional function of the reducing agent. In some designs of hydride generators the purge gas is mixed with or bubbled through the reaction mixture. This supports the release of reduced hydride from the solution and can partially reduce the demand of the reducing agent. It can be assumed that under the optimum conditions and in the absence of a matrix, the hydride release efficiency approaches to unity. This has been convincingly shown for Se, As, Sb, Sn and Bi employing radiotracers [5].

1.1.1 Hydride Transport

The hydride released from sample solution is transported by a flow of the purge gas to an atomizer. Losses of hydride on glass or plastic surfaces during its transport can be serious. Losses or delay of transported hydrides are probably due to their decomposition or sorption. Water traces which are typically present in hydride generators can also enhance the losses or delay. The reason is high solubility of

some hydrides in water. These effects can reduce hydride transport efficiency, thus the observed sensitivity, but mainly deteriorate reproducibility of measurements. An efficient way to prevent losses of hydrides on glass surfaces is their silanization. However, silanization is not very stable and has to be repeated often which is not practical for routine analysis. The magnitude of hydride interaction with surfaces obviously decreases with increasing the gas flow rate and with decreasing the surface area, i.e. with decreasing diameter of tubing and the size of the generator vessel. In conclusion, hydride transport losses can be made negligible in an optimized experimental set-up. The optimization includes the use of a reasonably high flow rate, minimization of surfaces coming into contact with hydride and, if necessary, silanization of glass surfaces [5].

The tubing serving for the transport of hydrides to the atomizer should be as short as possible to avoid the transport losses. The interaction of hydride with the tubing surface is reduced in narrower tubings; however, a too narrow tubing increases the risk of overpressure problems. The flow of gases also transports together with generated hydride a certain amount of spray of the reaction mixture stripped out of the reaction vessel. Condensation of the reagent mist and/or water vapour in the transfer line should be avoided because of the above mentioned losses or delay of hydrides. The spray can also negatively influence the performance of hydride atomizer. Desiccants can be employed but they should be chosen with care since the desiccant may fail to adequately remove the water or irreversibly trap the hydride. Further means to avoid carryover of liquid drops is to employ liquid trap, hygroscopic membrane dryer tube or membrane gas-liquid separator (GLS) [5].

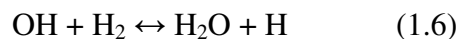
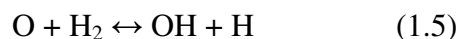
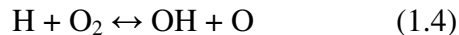
1.1.2 Hydride Atomization

Hydride atomizers are expected to convert analyte hydride to free atoms with maximum efficiency, independent of the sample composition and with minimum dilution. They should keep free atoms in the observation volume as long as possible in order to achieve high sensitivity [5]. Most frequently used hydride atomizers are flame-in-tube, externally heated quartz tube and electrothermal atomizers.

1.1.2.1 Flame-in-Tube Atomizers

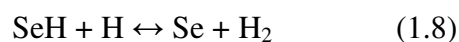
Flame-in-tube atomizer was introduced by Siemer and Hagemann [23]. It is an externally unheated quartz T-tube with a highly fuel rich, essentially invisible hydrogen-oxygen microflame burning near the T-tube junction. It employs a capillary to introduce oxygen to the atomizer in order to support the microflame. The temperature in the atomizer bar tube depends on hydrogen and oxygen flows and usually does not exceed 200 °C at the hottest part [24]. A wide range of hydrogen and oxygen flows were used: 2 to 200 ml s⁻¹ for hydrogen and 0.05 to 3.5 ml s⁻¹ for oxygen. There is a very marked dependence of analytical response on oxygen inlet flow to the flame. With increasing oxygen flow, a rapid rise of the signal is observed followed by a plateau, indicating that increasing the oxygen flow beyond the optimum value does not change the atomization efficiency [24].

Dědina and Rubeska [25] investigated atomization mechanism of selenium hydride in a flame-in-tube atomizer. Since heating of the inlet part of the atomizer up to 900 °C at oxygen flow rates below the optimum value never led to a peak area increase, it was concluded that the atomization of selenium hydride was not caused by thermal decomposition but was due to free radicals generated in the reaction zone of the diffusion flame by the following reactions:

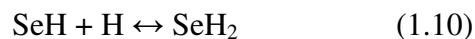


Consequently, only OH and H radicals were formed in the presence of excess hydrogen. Due to the very fast reaction (1.6), a balanced state between H and OH radicals was readily established. Since the equilibrium constant of reaction 1.6 was very large and further since the hydrogen concentration in the atomizer was much higher than the water concentration, H radicals outnumbered OH radicals at least by a few orders of magnitude. Thus, OH radicals could be neglected and it could be assumed that only H radicals are produced, in quantities corresponding to the total amount of oxygen, i.e. two radicals for each oxygen molecule [25].

The actual mechanism of the atomization proceeded most probably by two consecutive reactions for selenium:



Analogous reactions took place for arsenic hydride [26, 27] and probably for other hydrides as well. Recombination reactions of the type



were probably not significant because they were strongly exothermic, and consequently, their rate constants should be relatively small [25].

The direct experimental evidence to support the presence and involvement of hydrogen radicals in the atomization step of hydrides was provided by Tesfalidet et al. [28]. By employing a miniaturized oxygen/hydrogen flame torch fitting in the centre of the electron spin resonance (ESR) cavity, it was possible to directly monitor the production of hydrogen radicals in the flame, as well as their consumption upon introduction of arsine into the flame. Furthermore, it was found that the radicals that were produced in the flame were confined to a small region in the cavity.

1.1.2.2 Externally Heated Quartz Tube Atomizers

Externally heated quartz tube atomizers can either be heated by flame, or more often and more conveniently, electrically. The use of air-acetylene flame to heat the atomizer was first suggested by Thompson and Thomerson [29] and electrically heated atomizer was introduced by Chu et al. [30]. Since then, externally heated atomizers have become the most commonly used atomizers. The design is usually very similar to flame-in-tube atomizers; a T-tube with its bar tube aligned in the optical path and the central arm of T serving for delivery of hydrides carried by a flow of gas from a generator [24]. The horizontal bar of the T-tube can be heated up to 1100 °C. The ends of the horizontal bar tube can be closed by removable quartz windows. When using flame for heating the atomizer, the end windows can be replaced by graphite rings. Windows or graphite rings are used to prevent ignition of hydrogen escaping from the ends of the bar tube. This is important since hydrogen flame burning at the optical path increases noise levels particularly at shorter wavelengths. Several variations of the externally heated quartz tubes have been employed, most of them based on the T shape, differing in dimensions and design of the bar tube [5].

There is no sharp division between externally heated quartz tube and flame-in-tube atomizers regarding the mechanism of atomization. This is not only because of similar design but primarily since oxygen is often introduced into the atomizer mainly because of its beneficial effect on sensitivity [5]. A very small amount of oxygen, which is present in sufficient quantities as a concomitant in the gas and/or solutions, is necessary to reach optimum sensitivity for almost all hydride forming elements even at a temperature of 1000 °C. Much more oxygen is needed at lower heating temperatures [5, 31].

It can be concluded that for optimum sensitivity there is a minimum oxygen supply to the atomizer, which depends, for a given atomizer and gas flow rate, on temperature – the higher the temperature the lower the oxygen supply necessary. It was shown that in the absence of hydrogen, arsine is decomposed in a heated quartz cell but is not atomized; the arsenic species formed in that thermal decomposition are in part volatile and/or can be revolatilized and, in the presence of hydrogen, atomized [31, 32]. The following scheme of hydride atomization emerges for the externally heated quartz tubes: at the beginning of the hot zone of the atomizer a cloud of hydrogen radicals, analogous as in flame-in-tube atomizers, is formed by reactions 1.4-1.6 between oxygen and hydrogen. Hydride is atomized within the cloud by the same reactions as in flame-in-tube atomizers. The exact position of the cloud is controlled by the temperature profile within the atomizer, by the purge gas flow rate and composition, and by atomizer design. For example, the cloud may be located well upstream in the inlet arm, in the T-tube junction or even in the horizontal bar tube of the atomizer depending on heating temperature and gas flow rate to the atomizer. The number of radicals is determined mainly by the oxygen supply to the atomizer; however, the amount of radicals is not a decisive factor in ensuring that an efficient atomization is achieved but their cross-sectional density in the cloud is. Consequently, the oxygen demand is controlled by the inner diameter

(i.d.) of the atomizer section where the hydrogen radical cloud is situated. Most probably, radical cloud fills only a small portion of the volume of the atomizer [5].

The same mechanism of hydride atomization in externally heated quartz tubes as in flame-in-tube atomizers indicates that these two types of quartz tube atomizers are, in principal, identical. The main difference between externally heated quartz tubes and flame-in- atomizers is the technique of creating the hydrogen radical cloud. Both atomizers are based on a flame burning inside the atomizer tube [5].

1.1.2.2.1 Multiple Microflame Quartz Tube Atomizers

In both types of quartz tube atomizers described above, hydride is, under optimum conditions, fully atomized in the cloud by reactions with extremely energetic hydrogen radicals. The free analyte atoms are transported further into the optical tube. There are two processes removing free analyte atoms from the atomizer optical tube [33]. The first one is mechanical, the forced convection which drives them out by the flow of gas. The second removal process is due to chemical reactions. Since free analyte atoms are thermodynamically forbidden outside the cloud of hydrogen radicals [5], they start to decay immediately after leaving the cloud. Although the exact mechanism of free atom decay is unclear, it is proved that it is critically influenced by the state of the atomizer inner surface [35, 36] and that the decay products are removed from the optical tube by the flow of carrier gas [5, 35, 27]. Quartz tube atomizer provides a long residence time of free atoms in the optical path and subsequently very high sensitivity. Additionally, the background noise is low so that the limit of detection is very good. However, there are also fundamental disadvantages inherent in quartz tube atomizer: poor resistance to atomization interferences, often unsatisfactory linearity of calibration graphs, and poor long term

stability of the observed sensitivity. The last one is due to the changes of the inner atomizer surface. To sum up, the source of all difficulties inborn to quartz tube atomizer is that free atoms, after leaving the hydrogen cloud, undergo chemical reactions. Consequently, all disadvantages of quartz tube atomizer would be eliminated if the analyte was maintained in the state of free atoms. This situation can be approached by recurrent atomization of the decaying analyte. The decay products can be reatomized with an additional hydrogen cloud. Such an additional hydrogen radical cloud can be formed only in another flame or upon introduction of additional oxygen to the hot atomizer to create a microflame [33].

The performance of a flame heated, holed quartz T-tube was investigated by Grinberg et al. [37] with regard to hydride forming element interferences. It was observed that the holed quartz T-tube was able to induce larger tolerance to interferences compared to conventional quartz tube atomizer. An extended linear range was obtained for most of the elements studied.

A more advanced approach to hydride atomization based on a recurrent atomization of analyte was reported by Dědina and Matoušek [33]. Multiple microflame quartz tube atomizer was designed to provide multiple microflames to the optical tube in order to reduce the zones without hydrogen radicals. The central section of the horizontal arm consisted of two concentric tubes. The inner tube had multiple tiny orifices through its length. The outer concentric tube of the horizontal arm was without orifices and was heated by the same device as conventional quartz tube atomizer. The purpose of the cavity between two concentric tubes was to admit an oxygen-argon mixture through orifices to the inside of the optical tube. The employed design of multiple microflame quartz tube atomizer eliminated the disadvantages of conventional quartz tube atomizer: poor resistance to atomization interferences and unsatisfactory linearity of calibration graphs while providing the same sensitivity [33].

1.1.2.3 Electrothermal Atomizers

Graphite furnaces have been used for hydride atomization almost since the introduction of hydride generation techniques. There are two approaches to using graphite furnaces: *in-situ* trapping of hydrides in the furnace and on-line atomization [5]. *In-situ* trapping techniques which couple hydride generation with the graphite furnace permit significant enhancement in relative detection power over conventional batch and continuous generation approaches for the ultratrace determination of metallic hydrides. Graphite furnace is used to decompose the volatile hydride and trap analyte species on the tube surface, thereby effecting a clean, rapid separation from the matrix as well as collection. The technique can therefore provide a useful simultaneous separation-concentration step prior to electrothermal vaporization-plasma source spectrometric analysis [34]. On-line atomization utilizes direct transfer of hydride from the generator to the furnace, which is preheated to atomization temperature. The generated hydrides are introduced to the internal gas line of commercial furnaces. This arrangement, though very simple, has the same disadvantage as *in-situ* trapping: hydrides can be captured on cooler metal or graphite parts. Naturally, sensitivity for on-line atomization is generally lower than with *in-situ* trapping. It is also lower than in quartz tube atomizers [5].

1.1.2.4 Tungsten Atomizers

The physical and chemical properties of metallic tungsten make these devices versatile alternative electrothermal atomizers and vaporizers for analytical atomic spectrometry. Most of the tungsten atomizers can be electrically heated up to 3000 °C at very high heating rates, with a simple power supply. Usually, a tungsten device is employed in one of two modes: as an electrothermal atomizer with which the

sample vapour is probed directly, or as an electrothermal vaporizer, which produces a sample aerosol that is then carried to a separate atomizer for analysis. Tungsten devices may take various physical shapes: tubes, cups, boats, ribbons, wires, filaments, coils and loops. Tungsten atomizers have been coupled to almost all conventional atomic spectroscopic techniques, often providing analytical figures of merit comparable to those associated with graphite atomizers. On the other hand, tungsten devices are not without their drawbacks. The shortcomings of these devices usually include the addition of hazardous hydrogen to the purge gas and the potential for corrosion of samples having high acid content. Also, when tungsten is used for samples having high carbon content the formation of the carbide may lower the melting point of the atomizer, thus limiting the number of detectable elements and the device lifetime. As with most electrothermal atomizers, a fast response detection system is needed due to the transient nature of signals from the tungsten devices. Finally, metals such as Mo and W can not be determined with a tungsten device [38].

1.2 Cold Vapour Generation Technique

Hg is the only metallic element that has a vapour pressure as high as 0.0016 mbar at 20⁰C, which corresponds to a concentration of approximately 14 mg/m³ of atomic Hg in the vapour phase. The possibility thus exists of determining Hg directly by AAS without an atomizer. The element must merely be reduced to the metal from its compounds and transferred to the vapour phase. This procedure is termed the cold vapour generation technique. It is widely used for the determination of Hg by reduction either with stannous chloride, SnCl₂, or with NaBH₄ [1].

A highly sensitive determination of cadmium by the use of cold vapour generation technique was introduced in 1995 [39]. It was speculated that some types of volatile

cadmium species, presumably hydride, can be produced by reduction with NaBH_4 but this intermediate was unstable subsequently dissociating into atomic Cd. The technique provided very favourable sensitivity as compared to electrothermal atomizer for the determination of Cd.

1.3 Chemical Vapour Generation of Transition and Noble Metals

Within the last decade, HG technique by the reaction of NaBH_4 in acid media has expanded in scope. As apparent from recent publications, several transition and noble metals have been found to be forming volatile species, probably molecular in nature, by this reaction [40]. They are tentatively suspected to exit as hydrides [41]. So far, generation of volatile species of Ag [17, 41-47], Au [41-43, 46, 48-50], Co [17, 43, 46, 51], Cr [51], Cu [17, 41-43, 45, 46, 51, 52], Fe [51], Ir [17, 43, 53], Mn [43], Ni [43, 46, 51, 54, 55], Os [53], Pd [17, 42, 43, 49], Pt [43, 49], Rh [17, 42, 43, 53], Ru [53], Ti [43] and Zn [41, 45, 46, 51, 56, 57] have been reported. In contrast to conventional hydride forming elements, transition and noble metals require rapid separation of the volatile species from the reaction medium, suggesting the product is very unstable in the liquid phase. This leads to relatively poor overall generation efficiencies [17].

The literature on the identity and/or mechanism of formation of these species is yet limited. Feng et al. [43] described the application of a modified Burgener Teflon parallel path nebulizer for rapid generation of Pt, Co, Ag, Cu, Rh, Pd, Au, Ni, Ir, Ti and Mn vapour species by controlled and rapid mixing of convergent, concentric streams of NaBH_4 reductant and acid solutions. In an effort to ensure that all signals detected originated from the generation of volatile metal species of the elements studied, rather than as an aerosol by-product of the reaction between acid and NaBH_4 reductant, test solutions containing magnesium were investigated.

Magnesium was considered to be unlikely to form a volatile product during this reaction and any signal detected was accepted to be a consequence of transport of an aerosol fraction exiting the spray chamber. It was concluded that for the majority of the elements examined, the contribution to their signals arising from physical aerosol carry over does not exceed 1%.

Matoušek and Sturgeon [47] suggested that the production of volatile Ag species proceeded in two steps. The first step, formation of the volatile species, or more likely, their precursor, might correspond to the reduction of Ag^+ to Ag^0 . This was a rather fast process, a black precipitate was observed at the point of sample/reductant mixing. The second step, formation of the actual volatile species and/or its release from the liquid phase was much slower. Only about 30% of the volatile species was released prior to or upon contact of the reaction mixture with the GLS surface. The volatilization of Ag from the liquid pool of GLS required the presence of decomposing NaBH_4 , either as the agent for further reduction, as a source of atomic (nascent) hydrogen, or simply as a source of very fine bubbles assisting the release of the volatile compound. The precursor could be retained on the walls of the GLS wetted by the pool; the retained portion could be released into the liquid and, upon contact with fresh reaction mixture, produced volatile Ag species. This process was suggested to be responsible for the long washout times.

Feng et al. [17] showed that the nature of the spray chamber surface affects the efficiency of the vapour generation process for Ag, Pd, Co, Rh, Ir, and Cu. In the presence of a Rytan (poly(p-phenylene) sulfide) surface, no drift or memory effects were evident for any of these elements in contrast to glass spray chamber. It was stated that generation of volatile species appeared to proceed via a two-step mechanism, in which the surface may play a role in stabilizing an intermediate atomic species. The signals for all elements studied either disappeared completely or

were significantly suppressed if the glass surface was silanized prior to use, further implicating the role of the surface in mediating these reactions.

The first report on the observation of selective absorption of metal atoms in aqueous solution appeared in 1998 [58]. 0.0025% (m/v) solution of NaBH₄ merged with mg l⁻¹ concentration solutions of Ag, Pd, and Cu in a custom spectrophotometric flow cell produced transient background corrected atomic absorption signals during the initial few seconds of the reaction. Use of more concentrated NaBH₄ reagent or more concentrated solutions of analyte resulted in the immediate and rapid formation of black precipitates. In the presence of surfactants, acting as stabilizing agents, selective absorption on the line of an element developed more slowly and was more reproducible than in their absence. It was concluded that the initial stages of chemical reduction of metallic ions in solution must proceed through the formation of single atoms, followed by the rapid formation of clusters with other atoms until continued coalescence produced observable precipitates or evidence of stable sol formation.

To conclude, the volatile species of interest generated in the reaction with NaBH₄ have not been identified, so the mechanisms of formation, release and transport of the species are not properly understood. Precision and overall efficiency should also be improved [40].

1.4 Metal Devices for Preconcentration of Hydrides

In recent years, metal devices have been used as preconcentration medium for hydrides. A feasible collection method for the determination of selenium, which was very similar to mercury amalgamation technique, was reported by Guo and Guo [59]. SeH₂ was collected on the gold wire heated to 200 °C and was released upon heating the trap further to 600 °C. In that design, gold wire was placed in the inlet

arm of the quartz tube atomizer. Later, use of tungsten wires as concentration medium for the hydride of Bi [60] and both as concentration medium and atomizer for hydride of Se [61] have also been reported. These works proposed simple and inexpensive devices with comparable detection limits to those obtained with *in-situ* trapping of hydrides in the furnace.

1.5 Quartz Traps for Flame AAS

The development of atoms traps stemmed from the desire of introducing a technique with improved sensitivity. The procedure should also be simple and the cost should be low. The purpose of traps is to collect the analyte atoms within the body of the flame. In this way, preconcentration in the flame is achieved without the use of additional chemicals, which may cause contamination. It is therefore possible to analyze samples without time-consuming and potentially contaminating handling procedures. Various traps have been developed.

The use of a slotted quartz tube for momentary sensitivity enhancements in flame AAS was first described by Watling [62]. This device, as used by Watling, was not a preconcentration device. In water-cooled U-shaped quartz traps [63] analyte was collected on a U-shaped quartz tube through which water was circulating and atomized by heating the trap. A water-cooled U-shaped quartz trap combined with a slotted quartz tube was first built by Ertaş et al. [64]. Two novel atomization techniques, flame alteration [64] and organic solvent aspiration [65], were introduced. For flame alteration, after the collection cycle, the fuel content of the flame is increased, causing revolatilization of the collected analyte species. Organic solvent aspiration, on the other hand, can be performed by aspirating 7-50 μL of

organic solvent in order to cause revolatilization. The detailed experiments had shown that heating was not necessarily associated with revolatilization [66].

Huang et al. [67] were first to use a Watling [62] type slotted quartz tube for preconcentration. Compared to other traps, the slotted quartz tube trap was simpler and easier to operate. The sample solution was aspirated for a fixed collection time and, in order to atomize the preconcentrated atoms, flame conditions were changed using the technique offered by Ertaş et al. [64]. Slotted quartz tube trap had been successfully applied to determination of elements like Bi, Cd, In, Pb and Sb [68, 69].

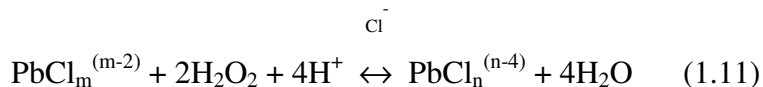
1.6 Pb

Pb is one of the most ubiquitous heavy metals and has been detected in virtually all phases of the environment (air, soil, sediment, surface and ground water) and biological systems occurring both naturally and from human activities. In surface water, Pb is likely to form insoluble compounds with other substances in the water. In soil and sediment, lead complexes with other particles, thereby reducing its bioavailability to organisms living in those environments. Plants may contain small amounts of Pb as a result of atmospheric deposition or root absorption from soil. Pb is not as pervasive in the environment as it once was, due principally to the commercial introduction of Pb free gasoline and the reduced use of Pb in manufacturing processes and consumer products. The scientific and medical consensus is that a child's primary route of Pb exposure is oral ingestion of Pb based paint and Pb containing dust and, to a lesser extent, Pb contaminated soil. For adults, the primary route of exposure is inhalation of Pb containing dusts and fumes in occupational settings, particularly during mining, smelting, and refining operations or during battery manufacturing and reclamation operations [70].

1.6.1 Determination of Pb by HG

The generation of lead hydride (PbH_4 , plumbane) has been relatively less studied compared to the other hydrides. This can be attributed to the difficulties with lead hydride formation, low yield and low stability of the volatile hydride [71]. The generation of lead hydride is performed as a vigorous reaction between the acidified sample with added strong oxidant and large amounts of tetrahydroborate. The role of the added reagent is believed to be the oxidation of Pb(II) to an unstable intermediate, Pb(IV) , which forms the hydride. Several oxidants like H_2O_2 , $(\text{NH}_2)_2\text{S}_2\text{O}_8$, $\text{K}_2\text{Cr}_2\text{O}_7$, $\text{K}_3\text{Fe(CN)}_6$, Ce(III) , Ce(IV) , KBrO_3 , KMnO_4 have been used to increase the efficiency of lead hydride generation [5, 72]. Castillo et al. [73] found a linear relation between logarithm of absorbance values obtained and reduction potentials of $\text{Cr}_2\text{O}_7^{2-}$, MnO_4^- , Ce^{4+} , H_2O_2 and $\text{S}_2\text{O}_8^{2-}$ as oxidizing agents, $\text{S}_2\text{O}_8^{2-}$ providing the best sensitivity. Highest sensitivity was obtained when $\text{K}_3\text{Fe(CN)}_6$ was used in the hydride generating medium [74]. Since the oxidation potency of this reagent is not sufficiently high, the reaction mechanism may be more complex than a simple oxidation [75]. The mechanism of plumbane generation remains unresolved at this point. The determination of Pb using nitroso-R salt (1-nitroso-2-naphthol-3,6-disulphonic acid disodium salt) was described by Zhang et al. [76]. The method was superior in sensitivity to those using dichromate, hydrogen peroxide or peroxodisulphate as oxidants. It is known that nitroso-R salt reacts with Co^{2+} and forms a Co^{3+} chelate on air oxidation. The authors suggested that Pb may react similarly, Pb(II) is oxidized to Pb(IV) while chelated with nitroso-R salt which increases the efficiency of hydride generation. Chen et al. [77] tested a series of chelating reagents for plumbane generation and found that 1-(2-Pyridylazo)-2-naphthol-6-sulphonic acid (PAN-S) is among the most effective. Since o-hydroxyl pyridylazo compounds are not oxidizing agents, the effect of PAN-S was not accounted for in the formation of Pb(IV) . Thus it was assumed that the plumbane was generated directly from the PAN-S chelated Pb(II) . The higher generation

efficiency of lead hydride in the PAN-S system was probably chelated Pb(II) being kinetically more easily reduced by NaBH₄ than free Pb(II). D'Ulivo and Papoff [78] reported that in hydrogen peroxide medium, presence of chloride and bromide enhanced the lead signal by up to 50%. This was explained by assuming that Pb(IV) formed more stable complexes with chloride than Pb(II), so the redox reaction

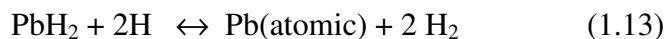
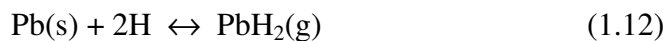


was shifted toward the right and the yield of PbH₄ in the subsequent reaction with borohydride increased.

Pb had been determined in a variety of samples like environmental [72, 76, 77, 79-90], biological [72, 88, 91-93], food and beverage [72, 84, 94, 95], agricultural [72, 96], metallurgical [86, 96], geological [75, 91] and drug [97] by means of HG technique.

1.6.2 Atomization Mechanism of Pb in Quartz T-Tube

Two atomization mechanisms have been suggested for the formation of lead atoms in externally heated quartz tube atomizers. Forsyth and Marshall [98] studied the decomposition and atomization process of alkyllead compounds in a heated quartz tube coupled to a gas chromatograph. It was stated that a certain quantity of hydrogen make-up gas must be present in addition to helium as the carrier gas in the atomizer for maximum atomization of the analyte and the resulting hydrogen radicals act as scavengers for metallic lead as the initial decomposition product of alkylleads. Atomization from the wall was effected by the action of hydrogen radicals. Observation of a very sharp signal as soon as hydrogen was admitted into the furnace was reported. The suggested mechanism was for atomization was:



In addition, temperature variations above 800⁰C were not found to affect the sensitivity, indicating a non-thermal process. On the other hand, Johansson et al. [99] investigated longitudinal and cross-sectional spatial distributions of lead atoms from alkyllead compounds in a quartz tube atomizer. A sharp decrease in free lead atom density was noted towards the end of the atomizer. It was suggested that this decline is due to the ingress of atmospheric oxygen, and thus the formation of lead oxide. Carbon monoxide was found to be as effective as hydrogen in increasing sensitivity when used as make-up gas, and it was concluded that the effects of both carbon monoxide and hydrogen are to reduce the partial pressure oxygen in the atomizer volume, and thus promote the atomization of lead. It was concluded that thermal atomization occurs under reducing conditions.

1.7 Sb

Sb can exist in a variety of oxidation states (-III, 0, III, V) but it is mainly found as Sb(III) and Sb(V) in environmental, biological and geochemical samples. It is used in semiconductors for making infrared detectors, diodes and Hall-effect devices. The presence of Sb greatly increases the hardness and mechanical strength of Pb. Batteries, antifriction alloys, small arms and tracer bullets, and cable sheathing are the main products containing Sb. Antimony trioxide, Sb₂O₃, has many uses including as a flame-proof retardant of textiles, papers, plastics and adhesives; as a paint pigment, ceramic opacifier, catalyst, mordant and glass decolouriser. Antimony tetraoxide, Sb₄O₈, is used as an oxidation catalyst, particularly for the

oxidative dehydrogenation of olefins [100]. To date, no indications are known of the essentiality of Sb for human. The toxicological and physiological behaviour of Sb depends on its oxidation state, the presence of binding partners and potential ligands, and on the solubility of Sb compound. Sb salts are more toxic than elemental Sb and trivalent Sb exert a ten times higher acute toxicity than pentavalent Sb. Sb(III) shows a high affinity for red blood cells and sulfhydryl groups of cell constituents. Sb_2O_3 has been assigned to the group of substances which are suspected of being carcinogenic in humans. Many health threatening effects of Sb compounds are known [101].

1.7.1 Determination of Sb by HG

The generation of antimony hydride (SbH_3 , stibine) is among the most suitable techniques for determination of sub- μg to pg amounts of Sb, with quantification by AAS or other relevant techniques. Among the other hydride-forming elements, Sb is one of the least problematic: the hydride is generated instantaneously within a very broad interval of acidity and NaBH_4 concentration, and determinations are relatively selective [5].

Different oxidation and binding states of Sb exhibit different behaviour in HG, i.e. Sb(III), Sb(V), and methylantimony species would differ as far as the sensitivity, the interference pattern, and the pH range of hydride evolution are concerned. The standard additions technique does not eliminate these problems. Thus, most HG procedures would require an efficient and reliable pre-reduction of Sb (V) to Sb(III) since Sb(III), as compared to Sb(V), is reduced to SbH_3 faster, with higher chemical yield, within a broader pH interval and with a better tolerance to interferences. HG is

a routine and widely used technique for determination of Sb in a wide variety of samples [5].

1.8 Cd

The major uses of Cd are in batteries (67%) and coatings (7%). In the form of its compounds it is used as pigments and plastics stabilizer to prevent degradation by heat or ultraviolet radiation. The most noticeable features compared with other metals are its low melting and boiling points [102]. Cadmium and cadmium compounds are carcinogenic to humans. Cadmium enters the body mainly by inhalation and by ingestion. Occupational exposure to cadmium and cadmium compounds occurs mainly in the form of airborne dust and fume. Occupations in which the highest potential exposures occur include cadmium production and refining, nickel-cadmium battery manufacture, cadmium pigment manufacture and formulation, cadmium alloy production, mechanical plating, zinc smelting, soldering and polyvinylchloride compounding. Urinary and blood cadmium concentrations are generally much lower in non-occupationally exposed people, for whom the most important sources of exposure are cigarette smoking and, especially in polluted areas, eating certain foods. [103].

1.8.1 Determination of Cd by Cold Vapour Generation

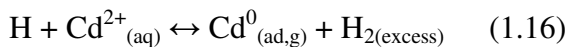
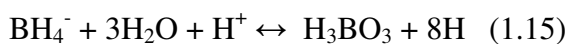
Volatile Cd species were first generated by ethylation [104] and by using NaBH₄ in organic medium [105], and detected by atomization in flame and externally heated quartz tube atomizer, respectively. Vapour generation of Cd with atomization in flame [104, 107], quartz tube atomizer [105, 107, 108], inductively coupled plasma [109-116] and mostly electrothermal atomizer [112, 113, 116-122] as a trapping

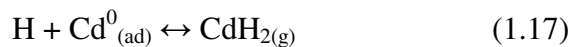
medium and/or atomizer have been well documented. An excellent overview of literature data on vapour generation techniques for cadmium was recently reported by Lampugnani and co-workers [122].

Sanz-Medel et al. [39] discovered that the generated Cd species had sufficiently long lifetime to be determined at room temperature and this was rapidly confirmed by Guo and Guo [123]. A value of 2.9 was obtained for the ratio of detection limits obtained for atomizers at room temperature and 900 °C [39]. A chemical formation of atoms was proposed for Cd according to the following decomposition reaction of initially generated, unstable CdH₂ by reaction with NaBH₄ [39]:



Generation of atomic and molecular Cd species from aqueous media was investigated recently by Feng et al. [124]. It was stated that once generated, atomic species are stable in water, having a half-life of 2.2 minutes. The authors claimed that the initial products of the reduction reaction appeared to be free atoms, not the hydride, and subsequent interaction with nascent hydrogen gave rise to the molecular hydride. The process was found to be moderated by the chemistry of surface groups exposed to the reaction products; i.e., use of a glass spray chamber resulted in a predominance of atomic vapour whereas polymeric spray chamber released the volatile molecular species. This was attributed to the binding property of sulfur to metals forming soft acids; sulfur functional groups present on the surface of the Ryton spray chamber might have reacted with newly generated atomic Cd, prohibiting its escape from the generator system. A two step mechanism for the generation of volatile Cd species was suggested:





The second step reaction (1.16) was reported to be significant because it occurred on the surface and was mediated by its chemistry.

The optimum conditions for the determination of Cd by CVG exhibits apparent variations and inconsistency. Critical parameters of VG/transportation are relatively narrow HCl interval and high NaBH₄ levels; flow rate of purge gas; design of gas-liquid separator and vapour transfer lines because of vigorous reaction entailing aerosol formation and foaming [122]. VG efficiency was claimed to increase by means of surfactant based organized assemblies, such as micelles and vesicles [39, 125], on the other hand some workers observed that the use of surfactants was not necessary [126] and could even be troublesome [122]. Despite the difficulties, determination of Cd by cold vapour generation had been successfully used for different sample types as a sensitive alternative to electrothermal atomizers [39, 126-130].

1.9 Chemometrics

Chemometrics is the chemical discipline that uses mathematical and statistical models to design or select optimal measurement procedures and experiments, and to provide maximum chemical information by analyzing chemical data. Chemometric methods include descriptive and inference statistics, signal processing, experimental design, modelling, optimization, pattern recognition, classification, artificial intelligence methods, image processing and information and system theory [131].

1.9.1 Experimental Design and Optimization

Before proceeding to the principles of experimental design and optimization, some terms should be defined. A *factor* is any aspect of the experimental conditions which affects the result obtained from an experiment. The different values that a factor takes are known as different *levels* [133]. Some factors are termed *qualitative* in respect of the fact that they may only be present or absent, on or off and so on [134]. Other types of factors are *quantitative* since their possible values could be arranged in numerical order. The factors are *controlled* when they could be altered at will by the experimenter or *uncontrolled* in the opposite case [133]. The conditions which are particular to one experiment is called *treatment*. The result or value obtained from an experiment is called the *response* [134]. Most experiments result in some sort of *model*, which is a mathematical way of relating an experimental response to the value or state of a number of factors. The *design matrix* is simply one in which the *rows* refer to experiments and the *columns* refer to individual parameters in the mathematical model or equation linking the response to the values of individual factors. In order to have a better idea of significance it is useful to put each variable on a comparable scale. It is common to *code* experimental data since then the design matrix simplifies considerably. Each variable is placed on a common scale, often with the highest coded value of each variable equal to +1 and the lowest to -1 [132].

The term experimental design is usually used to describe the stages of:

1. identifying the factors which may affect the results of an experiment;
2. designing the experiment so that the effects of uncontrolled factors are minimized;
3. using statistical analysis to separate and evaluate the effects of the various factors involved [133].

The fundamental requirements of an experimental design are replication, randomization and running experiments in blocks.

Replication of measurements for a given combination of factors is necessary for estimation of the experimental error. Furthermore, the error can be reduced by taking replicate measurements and averaging [131].

Randomization means running experiments in a random order. Randomized experiments are obligatory if systematic errors cannot be avoided and must be detected [131]. In measurements made over a period of time, variation in an uncontrolled factor may produce a trend in the result. As a result the errors due to uncontrolled variation are no longer random since the errors in successive measurements are correlated [133]. Carrying out the experiments in a random sequence will be one of the suppositions for being able to measure independent, uncorrelated and usually normally distributed data. Random sequences should be read from random number tables or from a random number generator which eliminates subjective selections [131].

Uncontrolled factors lead to higher experimental errors. Therefore, the experiments should be designed such that uncontrolled factors can be detected and, by means of a further step, can be kept constant or eliminated. There are two categories of uncontrolled factors. Uncontrolled influences might arise from either unknown factors or from known factors that cannot be controlled. The eventual impurity of a reagent is an example of an unknown factor. The changing quality of an experimenter's work is a factor that is difficult to control. No account can be taken of completely unknown factors. Known or presumably known factors can be detected by blocking the experiments. The idea is to run the experiments in blocks that show a minimum experimental variance within one block. For example, if a systematic investigation requires 12 experiments and one can only make four

experiments a day the experiments should be arranged in three blocks with four experiments each day. Day-to-day effects could then be detected by considering the block effects with an adequate mathematical model. Naturally, the experiments within a block should be run at random. Randomized experimentation with regard to some factors, and blocking the experiments with regard to some other factors exclude each other. Therefore, in practice a compromise between randomized runs and blocked experiments must be found [131].

1.9.1.1 Two-Level Designs: Screening Designs

Designs on the basis of two levels for each factor are called screening designs.

1.9.1.1.1 Factorial Designs

Full factorial designs at two levels are mainly used for screening, that is, to determine the influence of a number of effects on a response, and to eliminate those that are not significant, the next stage being to undertake a more detailed study. The number of experiments is given by $N = l^k$, where l is the number of levels and k the number of factors. A weakness of full factorial design is the large number of experiments that must be performed. For example, for a 10 factor design at two levels, 1024 experiments are required, which may be impracticable. These extra experiments do not always result in useful or interesting extra information and so are wasteful of time and resources. Two level fractional factorial designs are used to reduce the number of experiments by 1/2, 1/4, 1/8 and so on, systematically and safely. Figure 1.2 is a symbolic representation of the experiments of a three factor,

two level design experiments, often presented on the corners of a cube, whose axes correspond to each factor.

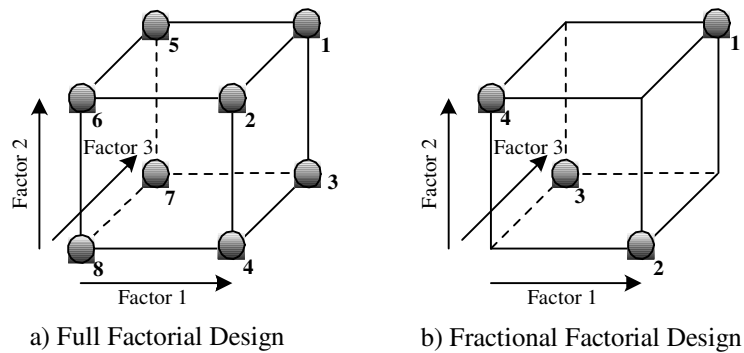


Figure 1.2 Representation of a three factor, two level a) full factorial and b) fractional factorial designs [132]

Rules have been developed to select a correct subset of the original experiments that allows to study all three factors. Half the experiments have been removed in Figure 1.2.b. For the remainder, each face of the cube now corresponds to two rather than four experiments, and every alternate corner corresponds to an experiment. A half factorial design involves reducing the number of experiments from 2^k to 2^{k-1} . As the number experiments is reduced, the amount of information is correspondingly reduced. Since only four experiments are performed, it is only possible to measure four unique factors. The interaction between factors 1 and 2 is said to be confounded with factor three. This means that using this design, the interaction between factors 1 and 2 is indistinguishable from the influence of factor 3 alone. However, not all interactions will be significant, and the purpose of a preliminary experiment is often simply to sort out which main factors should be studied in detail later [132].

1.9.1.2 Three-Level Designs: Response Surface Designs

Two level factorial designs are primarily used for explanatory purposes. It is often important, though, to provide a more detailed model of a system. There are two prime reasons. The first is for optimization – to find the conditions that result in a maximum or minimum, as appropriate. The second is to produce a detailed quantitative model: to predict mathematically how a response relates to the values of various factors. Most explanatory designs do not involve recording replicates, nor do they provide information on squared terms; some do not even provide details of interactions. In case of detailed modelling it is often desirable at a first stage to reduce the number of factors via explanatory designs to a small number of main factors that are to be studied in detail, for which both squared and interaction terms in the model are of interest [132].

1.9.1.2.1 Central Composite Design

Many designs for use in chemistry for modelling are based on the central composite design. The first issue is to code the factors, and it is always important to choose sensible physical values for each of the factors. It is assumed that the central point for each factor is 0, and the design is symmetric around this. A central composite design constructed as several superimposed designs. In Figure 1.3, this is illustrated for three factors, each axis corresponding to a factor.

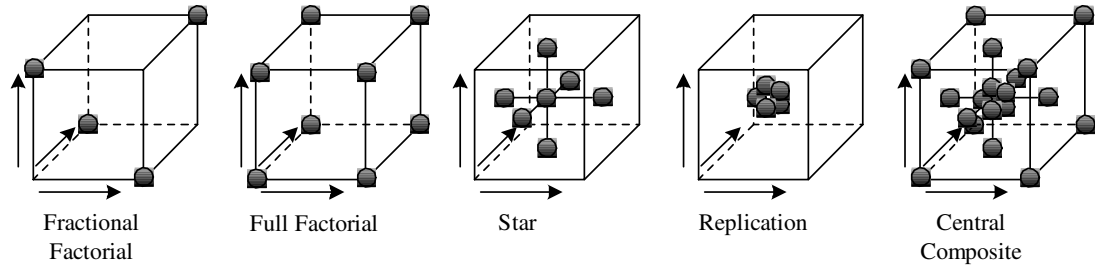


Figure 1.3 Elements of a central composite design [132]

The smallest possible fractional factorial three factor design consists of four experiments, used to estimate the three linear terms and the intercept. Such a design will not provide estimates of the interactions, replicates or squared terms. Extending this to eight experiments provides estimates of all interaction terms. When represented by a cube, these experiments are placed on the eight corners, and consist of a full factorial design. All possible combinations of +1 and -1 for the three factors are observed. Another type of design, often designated a star design, can be employed to estimate the squared terms. In order to do this, at least three levels are required for each factor, often denoted by +a, 0 and -a, with level 0 being in the centre. The reason for this is there must be at least three points to fit a quadratic. Points where one is at level +a are called axial points. For three factors, a star design consists of the centre point, and six in the centre each of the faces of the cube. Finally it is often useful to be able to estimate the experimental error, and one method is to perform extra replicates (typically five) in the centre and assume that the error is the same throughout the response surface. Performing a full factorial design, a star design and five replicates, results in 20 experiments. This design is a type of central composite design [132].

1.10 Aim of This Study

Use of a quartz surface for atom trapping has been suggested in some previous studies; atomic vapours in contact with quartz surfaces can be efficiently trapped prior to a reatomization process resulting in a final analytical signal. A slotted quartz tube and flame atomic absorption spectrometry can be used for this purpose [63, 65, 66].

In this study, a different approach using quartz as a trapping surface was investigated. A novel quartz trap for on-line preconcentration of volatile analyte species was designed. CVG was employed for Pb, Sb and Cd determinations in flow systems. The conventional quartz T-tube and multiple microflame quartz tube were employed as atomizers. The analyte species were trapped either in inlet arm of quartz tube atomizer or in a separate cylindrical quartz tube both of which were resistively heated. The heated quartz surface was found to trap the analyte hydride generated in a conventional manner. Following the trapping stage, the quartz trap was heated to a desired temperature in the presence of H₂ to effect revolatilization of the analyte. Conditions were optimized to generate, collect and revolatilize analyte species on-line. Experimental design was used for optimizations in some cases.

CHAPTER 2

EXPERIMENTAL

2.1 Pb

2.1.1 Reagents

All reagents used in all parts of this work were of analytical grade or higher purity. Standard solutions of Pb were prepared in $K_3Fe(CN)_6$ (Merck) and HCl (Merck) from 1010 mg/L Pb stock solution (Aldrich). $NaBH_4$ solution was prepared from the solid reagent (Merck) in NaOH (Carlo Erba) as stabilizer. The solutions were diluted to final volume using de-ionized water from a Milli-Q Water Purification System. All the solutions were prepared daily. Argon, carbon monoxide and 1% oxygen + 99% argon mixture were supplied from Habaş Industrial and Medical Gas Products, Ankara.

2.1.2 Spectrometer

A Perkin Elmer 305B atomic absorption spectrometer equipped with a deuterium arc background corrector, a 10.0-cm air-acetylene burner assembly and a Philips coded Pb hollow cathode lamp operated at 8 mA were used. Absorbance was measured as

peak height at the 283.3 nm line and recorded with a model BD 121 chart recorder (Kipp&Zonnen). Slit width was 0.7 nm.

2.1.3 Hydride Generator

The analyte solution was mixed with NaBH₄ solution using a Gilson Minipuls 3 peristaltic pump. The flow rate for both NaBH₄ and HCl carrier streams was 6.0 ml min⁻¹. A commercially available Philips (Unicam) hydrostatic type, U-shaped GLS was employed, as used in a PU 9360 vapour system. The inner volume of GLS was 25 ml. Argon or gas combinations as described in procedure were used as carrier gas with a flow of 150 ml min⁻¹. The analyte vapour was transported from the gas-liquid separator to the trap through a 3.0 cm of Masterflex[®] 8.0 cm o.d. and 6.0 cm i.d., platinum-cured Tygon[®] silicone tubing. The other end of the separated trap was connected to the atomizer by 30.0 cm of polytetrafluoroethylene (PTFE) tubing having an inner diameter of 7 mm. Gas flows rates were controlled by flowmeters (Cole-Parmer). Either HCl or analyte in K₃Fe(CN)₆ was introduced from the sample channel. The schematic diagram of the continuous flow system constructed is given in Figure 2.1.

2.1.4 Trap

The analyte vapour was trapped either on the inlet arm of the atomizer (Figure 2.2) or on a separate cylindrical quartz tube (Figure 2.1) to provide on-line preconcentration. Three pieces of broken quartz were inserted in trapping region to increase surface area and trapping efficiency. Broken quartz pieces were produced by crashing a quartz tubing of 4 mm i.d. and 6 mm o.d.; among the pieces produced,

those with longest dimension of about 3 mm were selected. To collect the analyte vapour, trap was electrically heated from the outer surface using a variable potential power supply and a 0.4 mm, 3.5 m long nickel-chromium wire. The wire was coiled around a house-made heat resistant cylindrical piece of ceramic which was 4.0 cm in length. This piece of ceramic was fitted snugly onto the quartz tube to be heated.

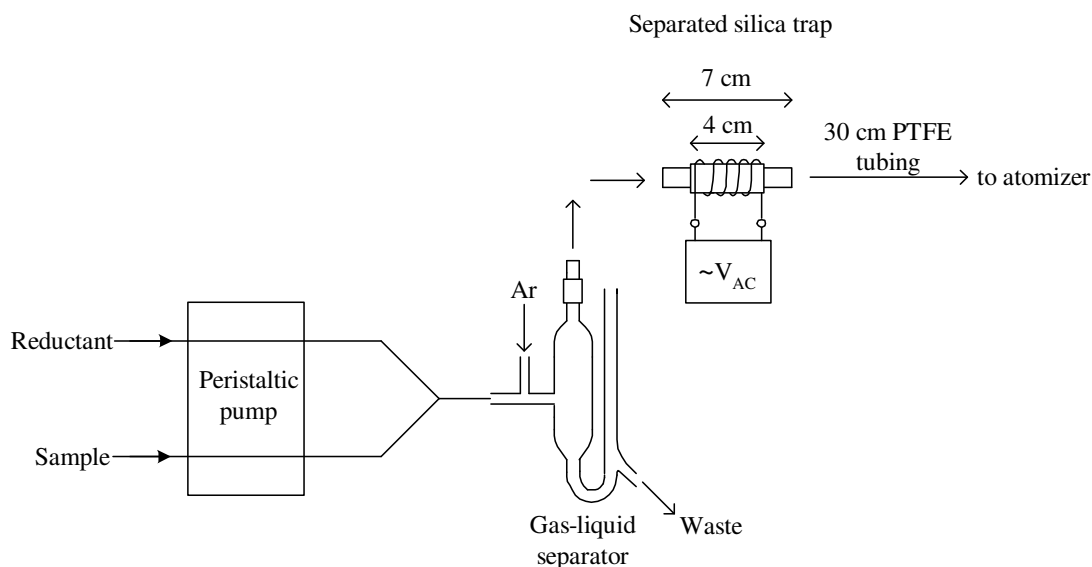


Figure 2.1 Continuous flow system with separated quartz trap on-line

2.1.5. Atomizer

Quartz tube atomizer was prepared in glass shop of Chemistry Department. Quartz tubings were supplied from Quartz Scientific Inc., Ohio. The atomizer was in T shape and the horizontal bar was aligned in the optical path (optical arm); this part was 135 mm in length, 13 and 15 mm in inner and outer diameters, respectively (Figure 2.2). The inlet arm had 4 mm inner and 6 mm outer diameters and was 90 mm long. The atomizer was heated by an air-acetylene flame.

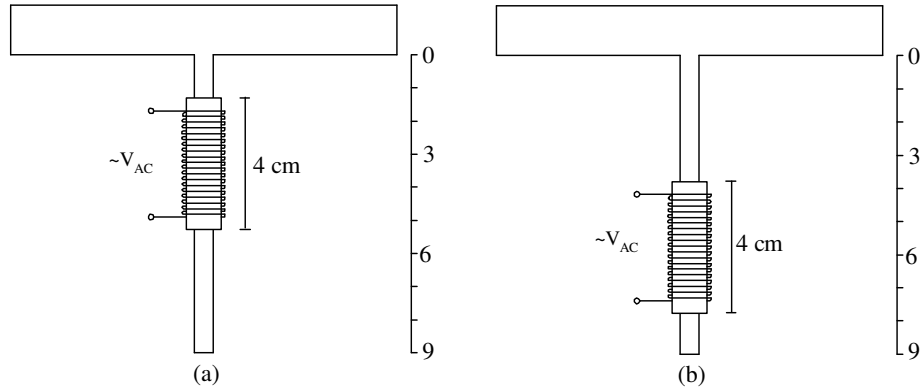


Figure 2.2 Top view of quartz tube atomizer with trap. Trap (a) close to (b) away from T-junction

Temperature measurements were done by a nickel-chromium thermocouple with a ceramic coated tip so that it could be easily in contact with even conducting surfaces. The temperatures reached vs. applied voltage differences for separated quartz trap are given in Table 2.1. Those temperatures were measured from the middle of the trap.

Table 2.1 The relation between voltage difference applied to the trap and the inside temperature for separated quartz trap

<i>Voltage, V</i>	<i>Temperature, °C</i>
10	175
20	338
30	455
40	521
50	655
60	721
70	791
80	845
90	912

2.1.6 Procedure

In order to preconcentrate the analyte on the inlet arm of the atomizer, the trap was positioned near to the T-junction (Fig. 2.2 a). Heating the trap to 500 °C, the analyte was trapped for 1 minute. Following the stage of trapping, the pump was stopped and revolatilization was realized by heating the trap further up to 900 °C, then resuming the flows of HCl and NaBH₄ streams by turning the pump on which generated a H₂ flow of approximately 75 ml min⁻¹ upon decomposition of NaBH₄. In the second part of the experiments, the trap was separated from the atomizer (Fig. 2.1) to check its ability to transport the revolatilized species to another source / atomizer. The trap was heated to 500 °C and analyte was trapped for 1 minute. The pump was not stopped, and the trap was further heated while the reagents HCl and NaBH₄ were flowing continuously. A sharp, transient signal was obtained when the trap reached to a temperature of 750 °C, i.e. 60 seconds after increasing the voltage

difference from 40 V to 90 V (Figure 2.3). The flow system has a waste output containing $K_3Fe(CN)_6$; this solution is toxic and thus should be disposed of properly.

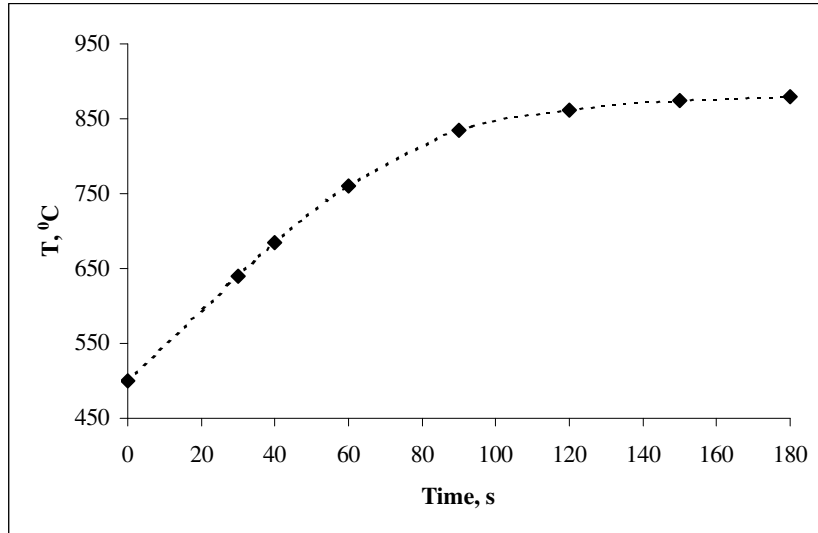


Figure 2.3 Temperature inside the separated quartz trap vs. time after increasing the applied voltage from 30 V (500 °C) to 90 V; temperature was at a steady state at $t = 0$

2.1.7 Accuracy Check

The accuracy of the method was tested using two certified reference materials (SRM); Natural Matrix Certified Reference Material, Metals on Soil/Sediment #4, IRM-008 (Ultra Scientific), containing 95.3 ± 5.3 mg/kg Pb and Trace Materials in Drinking Water, Cat # CRM-TMDW (High-Purity Standards), containing 40 $\mu\text{g/L}$ Pb.

0.100 g of soil/sediment SRM was digested with 3.0 ml of concentrated HNO_3 (Merck) and 1.0 ml of concentrated HF (Merck) in a Milestone Ethos Plus

microwave oven applying the microwave program given in Table 2.2. The solutions were evaporated to dryness. The residue was dissolved in 0.120 M HCl and diluted to 100.0 ml with 0.120 M HCl. 1.0-ml of the final solution was diluted to 100.0 ml using a solution of 0.5% (w/v) $K_3Fe(CN)_6$ in 0.120 M HCl.

2.0 ml of drinking water SRM was diluted to 50.0 ml using 0.5% (w/v) $K_3Fe(CN)_6$ in 0.120 M HCl.

Table 2.2 Microwave program for digestion

<i>Step</i>	<i>Time, min</i>	<i>Temperature, °C</i>
1	10	200
2	15	200

2.2 Sb

The experiments were carried out in Dr. Dědina's laboratory; Academy of the Sciences of the Czech Republic, Institute of Analytical Chemistry, Laboratory of Trace Element Analysis, Prague, Czech Republic, between September 9, 2002 and December 6, 2002.

2.2.1 Reagents

Working Sb(III) standards were prepared from 1000 mg ml⁻¹ stock Sb solution (BDH Laboratory Reagents) by dilution in 1.0 M HCl. The blank was 1.0 M HCl. The reductant was 0.5% (m/v) solution of NaBH₄ (Sigma) in 0.4% (m/v) KOH (Merck) prepared daily and filtered before use. Deionized water was used to prepare solutions.

2.2.2 Spectrometer

A Perkin Elmer model AAnalyst 800 atomic absorption spectrometer was used. An Sb electrodeless discharge lamp (Perkin Elmer system II), operated at 350 mA, was used as light source, the wavelength was set to 217.6 nm and the slit width was 0.2 nm. Background correction was not employed.

2.2.3 Hydride Generator

An in-house made, continuous flow hydride generation system similar as described in Ref.[135] was employed (Figure 2.4). Two T-pieces (PEEK- polyether ether ketone, 0.8 mm inner bore) were used to merge sample flow with the reductant flow and downstream to merge the reaction mixture flow with the carrier argon flow. Either blank or standard was introduced to the sample channel. The outlet from the second T-piece was connected by a 510 mm long, 1 mm i.d. PTFE tubing to a 3 ml inner volume gas-liquid separator with a forced outlet. The GLS was made from a 9/11 standard joint. A rubber septum was placed tightly to the bottom of the GLS through which two PTFE tubing passes: one from the reaction coil and one to the waste. The dead volume of the GLS could be adjusted by moving the septum inside. Another PEEK, 0.8 mm inner bore T-piece was inserted downstream of the gas-liquid separator to introduce auxiliary gases (see below). The gas outlet from the gas-liquid separator was connected with the trap (see below) by a 350 mm long PTFE tubing. If not explicitly stated otherwise, PTFE tubings (1.0 mm i.d. for gases and 0.5 mm i.d. for liquids) and Rheodyne 1/16" flangeless fittings were used for the hydride generator and also to connect the trap.

Sample and reductant solutions were delivered and the waste from the gas-liquid separator was removed by a multichannel minicartridge peristaltic pump (Ismatec).

Sample and reductant flow rates were 4.0 ml min^{-1} and 1.2 ml min^{-1} , respectively. Gas flow rates were controlled either by needle valves attached to calibrated rotameters (Cole-Parmer) or by mass flow controllers (Cole-Parmer).

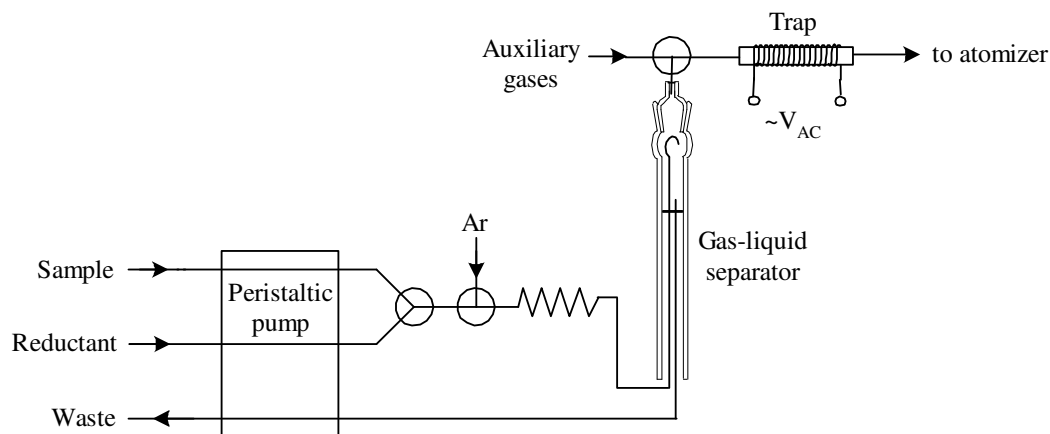


Figure 2.4 Scheme of the hydride generator

2.2.4 Trap

The trapping medium used was a 40 mm long quartz tube (i.d. 2 mm, o.d. 3 mm). No filling material was used. The upstream end of the trap tube was coupled to the inlet arm of the atomizer by a 5 mm Tygon[®] tubing (i.d. 3 mm). The trap was periodically cleaned in the same way as the atomizer (see Section 2.2.5).

A 0.8 mm Ni-Cr wire, 360 mm long, having a resistance of 1Ω was coiled around the quartz tube. The voltage differences applied to the wire was controlled by an autotransformer connected to the mains electricity, 220 V, and monitored with a multimeter. The inner wall temperature of the trap was measured with a thermocouple and calibrated with respect to the applied voltage (Table 2.3). The maximum feasible temperature was 1000°C . The employed heating control of the

trap did not make it possible to set other temperatures besides those shown in Table 2.3. It took some time before the trap temperature achieved the steady state level (Figure 2.5).

Table 2.3 The relation between voltage difference applied to the trap and the inside temperature for Sb

<i>Voltage, V</i>	<i>Temperature, °C</i>
3.0	440
4.0	620
4.4	650
5.0	700
6.0	800
7.0	900
8.0	1000

The temperatures given in Table 2.3 were measured under a flow rate of 75 ml min⁻¹ of Ar and 2.5 ml min⁻¹ of air. They did not change significantly when the gas flow rate was increased by an additional 100 ml min⁻¹ of H₂. The values given apply for the middle section of the trap, about 20 mm long, having a homogenous temperature. The outer trap sections were cooler.

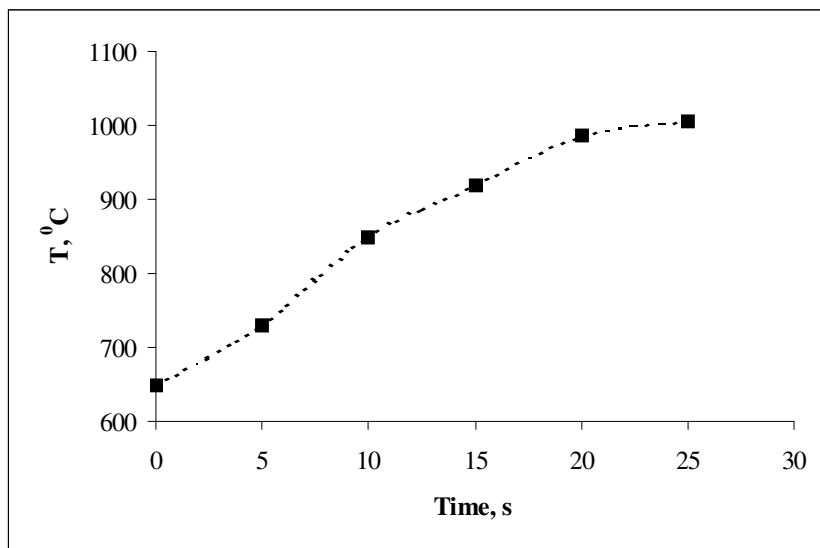


Figure 2.5 Temperature inside the trap vs. the time after increasing the applied voltage from 4.4 V (650 °C) to 8.0 V; temperature was at a steady state at t = 0

2.2.5 Atomizer

The multiple microflame quartz tube atomizer (multiatomizer) [136] was used as hydride atomizer without end windows. The multiatomizer (Figure 2.6) had an optical arm length of 125 mm, i.d. of 7 mm and o.d. of 14 mm. The length and i.d. of the inlet arm was 105 mm and 1.8 mm, respectively. The outer air flow was optimized to be 10 ml min⁻¹ which enters to the optical arm through the uniformly distributed orifices over its length. The diameter of orifices varied between 0.1 and 1 mm due to the manual procedure of making them, but the majority of the orifices were approximately 0.5 mm. The distance between the orifice pairs was 15 mm. The commercial heating device with temperature control produced by Perkin-Elmer for the system FIAS 400 was used for heating of the atomizer to 900°C. Prior to the first use or when sensitivity decreased significantly, the atomizer was cleaned by

leaching for 10 min in a mixture of conc. HNO_3 - conc. HF (7:3). Then it was rinsed by distilled water and left to dry.

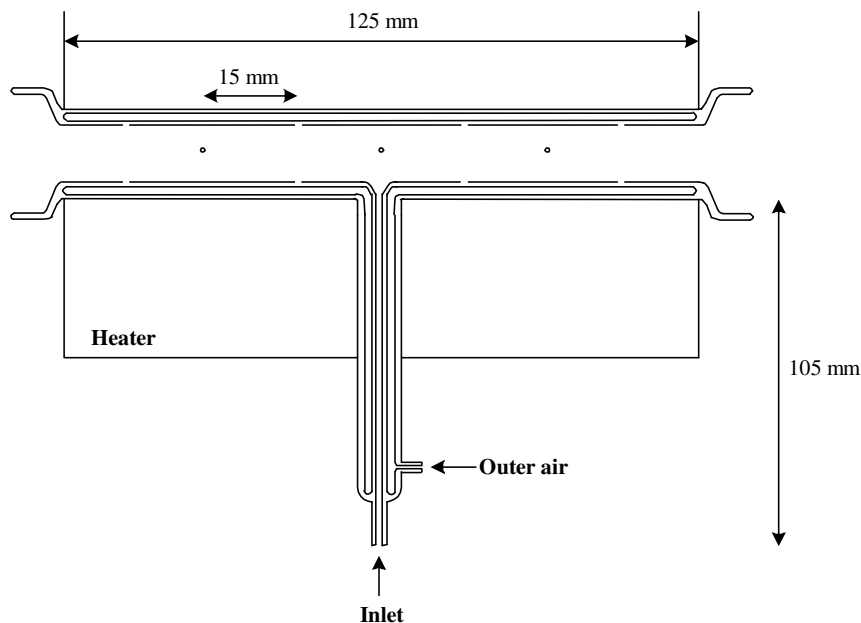


Figure 2.6 Multiple microflame quartz tube atomizer [136]

2.2.6 Procedure

Measurements were performed either in a collection mode (trapping) or in a direct transfer mode (continuous flow, no trapping). The flows of carrier Ar (75 ml min^{-1}) and auxiliary air (2.5 ml min^{-1}), respectively, were maintained throughout in both modes of measurement. The collection mode procedure consisted of the following two steps:

Step 1- collection:

The trap heating voltage was set to the collection level. If not stated otherwise, the voltage was 4.4 V, corresponding to the steady state trap of 650 °C (Fig. 2.4) It took about 30 s before the steady state temperature was achieved. The peristaltic pump was then switched then on to start hydride generation. At the start of Step 1, a standard solution was introduced to the sample channel. The standard solution introduction time was at least 30 seconds. If not explicitly stated otherwise, the standard solution introduction time and standard concentration, respectively, were 30 s and 2.5 ng ml⁻¹. This corresponds to a mass of 5 ng Sb. The standard was then replaced by the blank for 30 seconds to flush the system. The total gas flow rate introduced to the inlet arm of the atomizer during Step 2 was 92.5 ml min⁻¹ (75 ml min⁻¹ of carrier Ar, 2.5 ml min⁻¹ of auxiliary air, around 15 ml min⁻¹ of H₂ evolved from NaBH₄, assuming complete decomposition).

Step 2 - volatilization:

The peristaltic pump was switched off to stop hydride generation and, simultaneously, the heating voltage was set to the volatilization level of 8.0 V, corresponding to the steady state trap temperature of 1000 °C (Fig. 2.4). The total flow rate of gas introduced to the inlet arm of the atomizer was 77.5 ml min⁻¹ (75 ml min⁻¹ of carrier Ar and 2.5 ml min⁻¹ of auxiliary air). At a given time, corresponding to the selected volatilization temperature, hydrogen flow to the auxiliary channel was switched on in order to revolatilize the collected analyte species. If not stated otherwise, the hydrogen flow of 100 ml min⁻¹ was switched on at 920 °C, i.e. 15 seconds after increasing the applied voltage from collection to volatilization level (Fig. 2.4). After switching on the auxiliary hydrogen flow, the total gas flow introduced to the inlet arm of the atomizer was 177.5 ml min⁻¹ (75 ml min⁻¹ of carrier Ar, 2.5 ml min⁻¹ of auxiliary air and 100 ml min⁻¹ of auxiliary hydrogen). After recording the signal of volatilized analyte, the auxiliary hydrogen flow was switched off and, simultaneously, the heating voltage was reduced to the collection

level. It took about 30 s before the steady state collection temperature was achieved. The procedure then continued by the Step 1.

Some experiments were performed in the direct transfer mode: the trap was either removed (the 350 mm long PTFE tubing downstream the gas-liquid separator was connected to the inlet arm of the atomizer by the 5 mm long Tygon[®] tubing) or unheated. The procedure corresponded to the Step 2 described above with the only exception that the total gas flow rate (which was 92.5 ml min⁻¹ in Step 2 of the collection mode) could be higher by the hydrogen flow rate introduced to the auxiliary channel.

2.3 Cd

2.3.1 Reagents

Working solutions were prepared daily from the 1000 mg l⁻¹ stock Cd solution (Aldrich) by diluting appropriate aliquots with 0.25 M HCl. NaBH₄ (Merck) solutions were prepared daily and stabilized with 0.1% (w/v) NaOH (Carlo Erba). The reductant solution was stirred with a magnetic stirrer during analysis which improved precision of measurements.

2.3.2 Spectrometer

A Pye Unicam PU9200 atomic absorption spectrometer equipped with deuterium background correction was used. A Cd hollow cathode lamp (Unicam), was

employed as light source, operated at 6 mA, and set to 228.8 nm. The slit width was 0.5 nm.

2.3.3 Cold Vapour Generator

Figure 2.7 depicts the flow system used for both optimization of cold vapour generation and trapping of cadmium species. Both FI and continuous flow modes were employed. For optimization of generation step, a 6-port injection valve (Rheodyne, Model 5020) was inserted to sample stream. During these optimizations, no attempt was made to trap the analyte. After optimizing generation conditions in FI mode, trapping procedures were optimized. For this purpose, sample solution was fed continuously for a fixed time period and therefore injection valve was not employed.

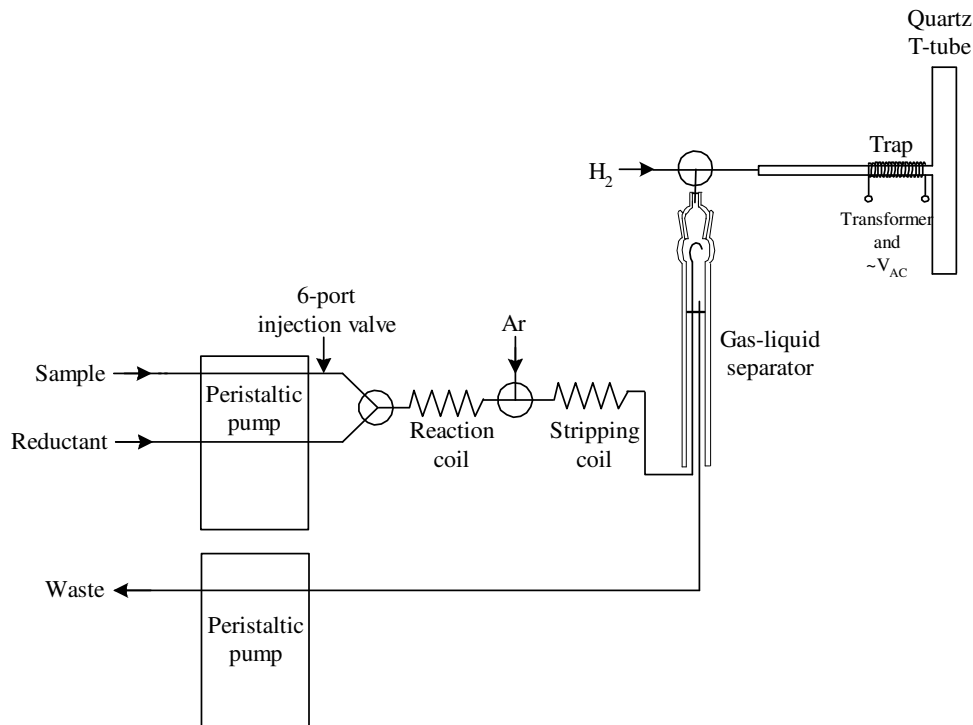


Figure 2.7 Scheme of the hydride generator

Two peristaltic pumps (Gilson Minipuls 3) were used: one for sample / carrier and reductant solutions and one to drain the GLS. A separate peristaltic pump was needed to maintain the balance between the feed and waste flow rates. Sample / carrier and reductant flow rates were 2.0 ml min^{-1} and 1.2 ml min^{-1} , respectively. In case of FI experiments, a $100 \mu\text{l}$ sample loop was used. The two streams were mixed in a chemifold and then along the 30.0 cm reaction coil. Cadmium species were then purged from the liquid mixture along a 20.0 cm stripping coil with an argon stream added from a T-piece, before their entrance to the gas-liquid separator. Argon flow was kept at 130 ml min^{-1} . The same GLS as used for Sb was employed for which the details were given in Section 2.2.3. The gas phase was introduced directly to the inlet arm of the quartz T-tube by 185 mm PTFE tubing. A T-piece was inserted between GLS and quartz T-tube in order to introduce H_2 whenever necessary. All the coils and transfer lines were made up of 0.8 mm i.d. PTFE tubings. Gas flow rates were controlled by calibrated flowmeters (Cole-Parmer).

2.3.4 Trap

The trapping medium used was the inlet arm of the quartz T-tube. The trap was placed to the closest possible position to the junction point of inlet and optical arms (Figure 2.7) taking the advantage that Cd was determined by cold vapour generation technique so that the quartz T-tube was unheated. In this way transport losses were minimized. Five or six pieces of broken quartz pieces were inserted in trapping region as filling material to increase trapping efficiency. Broken quartz pieces were produced by crashing a quartz tubing of 4 mm i.d. and 6 mm o.d.; among the pieces produced, those with longest dimension of about 3 mm were selected. In case of significant sensitivity drop, quartz T atomizer was cleaned in a mixture of concentrated $\text{HNO}_3:\text{HF}$ (7:3) for 10 minutes, devitrified filling material was

discarded and replaced with the unused ones. Devitrification of quartz can be identified by a hazy film caused by fine micro cracks.

The trapping medium was resistively heated with a 0.31 mm diameter Ni-Cr wire, 330 mm long, having a resistance of 1 Ω , coiled around the inlet arm of the quartz T-tube. Resultantly, the Ni-Cr coil covered a 20 mm portion of the inlet arm (Figure 2.9). The voltage differences applied to the wire was controlled by a variable potential power supply and a 750 W transformer. The input voltage of the variable potential power supply was 220 V. The inner wall temperature of the trap was measured with a thermocouple and calibrated with respect to the applied voltage (Table 2.4). Temperature was measured by means of a nickel-chromium thermocouple at the middle section of the trap.

Table 2.4 The relation between voltage difference applied to the trap and the inside temperature for Cd

<i>Voltage, V</i>	<i>Temperature, $^{\circ}C$</i>
0.7	155
1.4	351
2	623
2.7	793
3.4	941
4.1	1030

The temperature measurements were done keeping Ar flow rate constant at 130 ml min^{-1} . Introduction of H_2 for revolatilization cycle did not increase the temperatures. In fact, H_2 decreases the temperature inside the trap slightly owing to the higher thermal conductivity of this gas as compared to Ar. The heating rate of the trap is shown in Figure 2.8. Upon increasing the voltage difference from 1.4 V to 4.1 V the

maximum feasible temperature is reached within 30 seconds with an unfilled inlet arm.

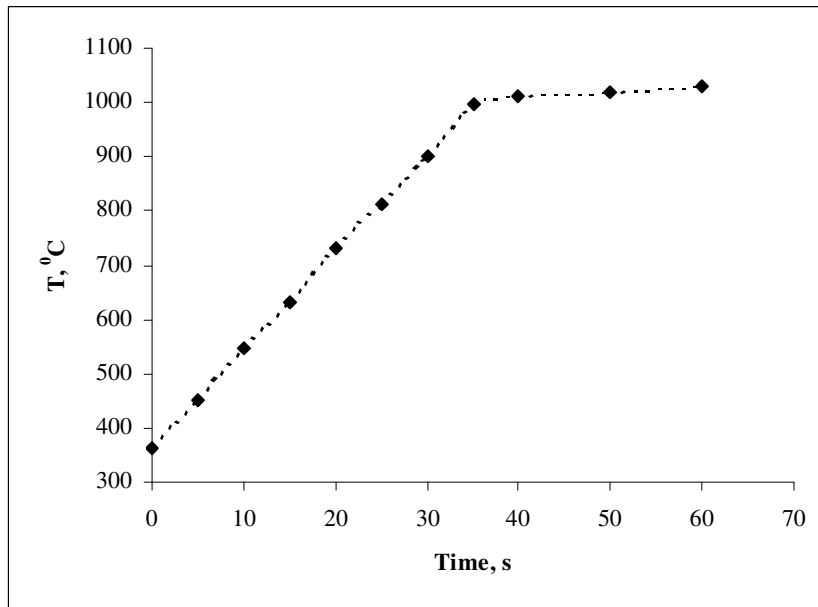


Figure 2.8 Temperature inside the the inlet arm vs. the time after increasing the applied voltage from 1.4 V (350 °C) to 4.4 V; temperature was at a steady state at t = 0

2.3.5 Quartz T-Tube

The mechanism of formation / atomization of Cd species is not well understood yet, therefore calling the quartz T-tube as atomizer would be a misnomer since it may only be serving as an absorption cell. A conventional quartz T-tube was used at room temperature whose inlet arm was also serving as the trapping medium (Figure 2.9).

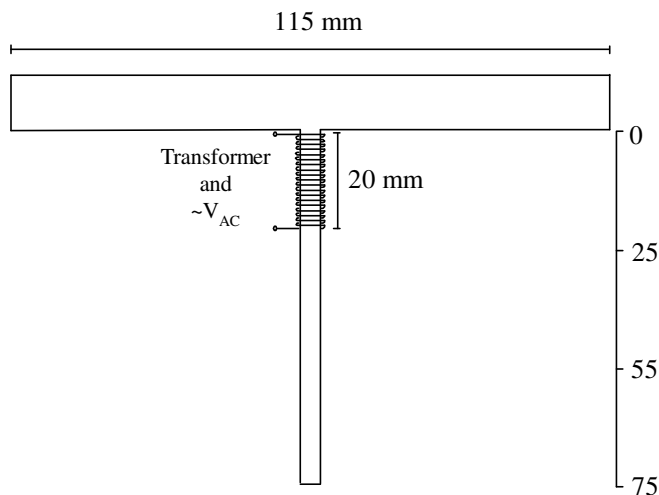


Figure 2.9 Top view of quartz T-tube with trap

The quartz T-tube (Figure 2.9) had an optical arm length of 115 mm, i.d. of 8 mm and o.d. of 10 mm. The inlet arm was 75 mm in length, 3.0 and 4.0 mm in inner and outer diameters, respectively.

2.3.6 Procedure

Collection of generated Cd species was realized upon heating the trap to 350 °C. After a certain preconcentration time in continuous flow mode, the peristaltic pump was stopped and the voltage difference was increased to 4.4 V. 60 seconds was needed in order to obtain the highest atomization signals; this was attributed to the fact that trapping medium was filled with quartz pieces and time was required to bring all the pieces to the same temperature. In addition to the H₂ from the decomposition of NaBH₄ (approximately 90 ml min⁻¹), only Ar, at a flow rate of 180 ml min⁻¹, was present in the medium as the carrier gas. For revolatilization of collected species, H₂ flow was switched on and H₂ was sent to the trap from a T-

piece inserted downstream of the gas-liquid separator. The flow rate of H₂ for was 200 ml min⁻¹ which made the total gas flow rate 380 ml min⁻¹ during revolatilization step. After obtaining the signal, H₂ flow was switched off, the voltage difference was brought to 1.1 V and 60 seconds was required to bring the temperature down to the collection level. Then another collection cycle was started.

2.3.7 Accuracy Check

SRMs 1573a Tomato Leaves and 1566b Oyster Tissue (Freeze-Dried) obtained from NIST, and Trace Elements in Seawater SRM obtained from BCR were used to validate the proposed method. 0.250 g of tomato leaves and oyster tissue samples were digested by adding 5.0 ml of concentrated HNO₃. An additional 0.5 ml of concentrated HF was added on tomato leaves samples. A Milestone Ethos Plus microwave oven was used for digestion. The same microwave program given in Table 2.5 was applied for both sample types. The resulting solutions were diluted to 50.0 ml with deionized water.

Trace Elements in Seawater SRM was acidified so that the final sample was in 0.40 M HCl. No other treatment was required. Tomato leaves and oyster tissue samples were further diluted 150 and 250 times, respectively, with 0.40 M HCl before analysis.

Table 2.5 Microwave program for digestion

<i>Step</i>	<i>Time, min</i>	<i>Temperature, °C</i>
1	5	180
2	5	180
3	5	200
4	5	200

CHAPTER 3

RESULTS AND DISCUSSIONS

3.1 Pb

3.1.1 Optimization of Conditions for Continuous Flow HGAAS

The effects of the variables that were considered to be dependent were investigated by a full factorial design for each variable pair. These were: potassium hexacyanoferrate(III) and HCl concentrations, NaBH₄ and NaOH concentrations, pumping rate and argon flow rate. In addition, the length of reaction coil was optimized. All the measurements were carried out at least in three replicates and peak heights of absorbance signals were recorded.

3.1.1.1 Potassium Hexacyanoferrate(III) and HCl Concentrations

The formation of lead hydride is highly dependant on the pH of the medium and confined to a restricted interval. Ten different HCl concentrations over the range 0.003 - 0.360 M and six different K₃Fe(CN)₆ concentrations over the range 0.025 - 3% (w/v) were investigated. 5 ng ml⁻¹ Pb was pumped continuously together with

1% (w/v) NaBH₄ in 0.1% (w/v) NaOH at a rate of 6 ml min⁻¹. Ar flow was 146 ml min⁻¹. Figure 3.1 shows the result of the optimization studies as a surface plot.

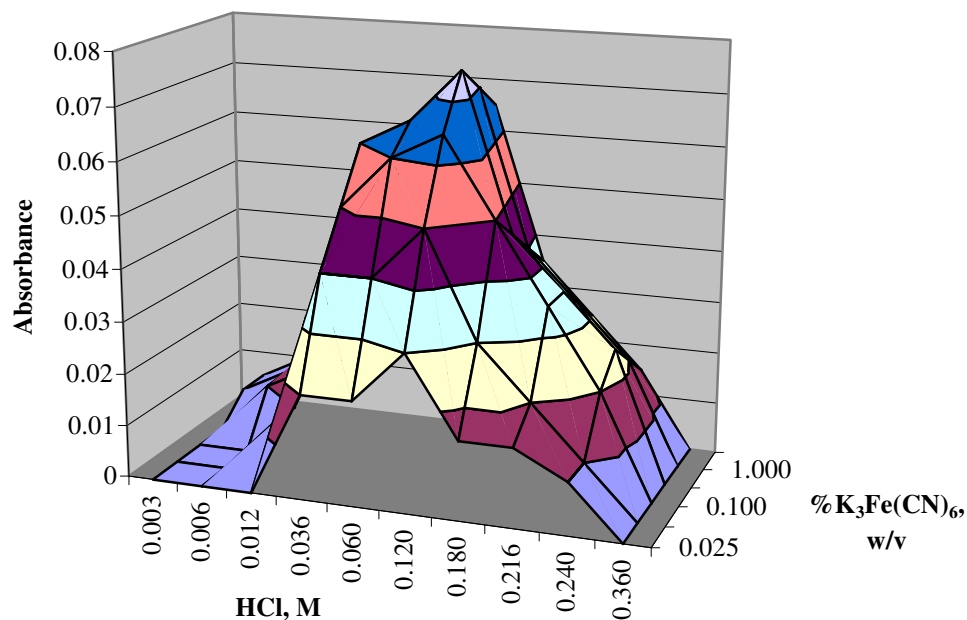
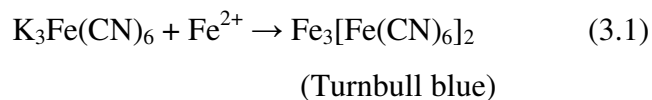


Figure 3.1 Surface plot for absorbance signal versus K₃Fe(CN)₆ and HCl concentrations

For any given oxidant concentration, the signal increased reaching a maximum at 0.120 M HCl, then decreased as the acid concentration was further increased (Figure 3.1). A similar trend was also observed by Tyson et al. [74]. Use of high amounts of K₃Fe(CN)₆ was to be avoided because of high blank values caused by this reagent. 0.5% (w/v) K₃Fe(CN)₆ prepared in 0.120 M HCl was used throughout the studies. The reagent should be prepared daily due to a blue precipitate formation in time according to the following reaction:



3.1.1.2 NaBH₄ and NaOH Concentrations

5 ng ml⁻¹ Pb in 0.5% (w/v) K₃Fe(CN)₆ and 0.120 M HCl was pumped continuously at a rate of 6 ml min⁻¹. Ar flow was kept at 146 ml min⁻¹. No signal was obtained when NaBH₄ concentration was lower than 0.4% (w/v). For NaOH concentrations higher than 0.5%, a considerable decrease in the signals was observed. The absorbance signals increased as the reductant concentration increased up to 1.0% (w/v) for a given NaOH concentration (Figure 3.2). Since this increment was not found to be very significant, 0.5% NaBH₄ (w/v) in prepared in 0.1% (w/v) NaOH was chosen for further studies for economical reasons.

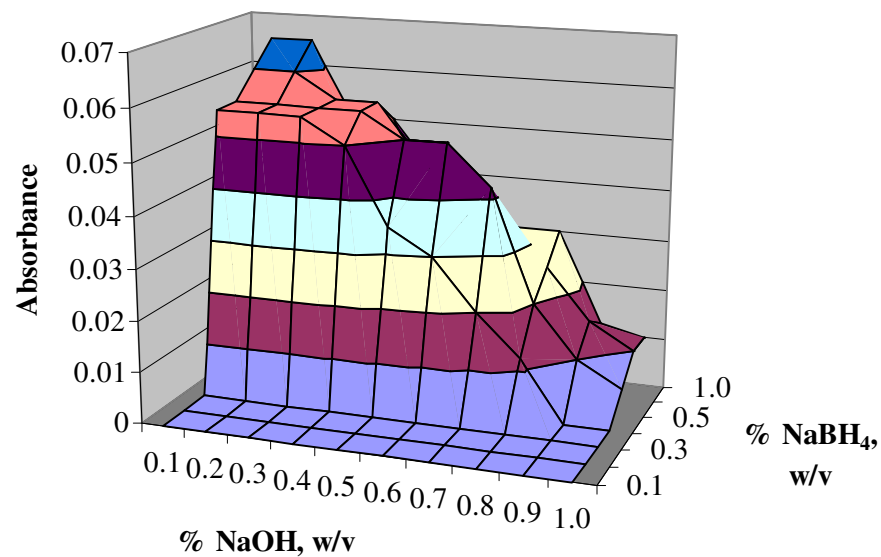


Figure 3.2 Surface plot for absorbance signal versus NaBH₄ and NaOH concentrations

3.1.1.3 Pumping Rate and Argon Flow Rate

5 ng ml⁻¹ Pb in 1.0% (w/v) K₃Fe(CN)₆ and 0.216 M HCl was pumped continuously at a varying rates together with 1% (w/v) NaBH₄ stabilized in 0.1% (w/v) NaOH. Pumping rate and Ar flow rate were found to be completely independent (Figure 3.3). An increase in argon gas flow beyond 300 ml min⁻¹ resulted in a slight decrease in absorbance values due to the dilution of analyte. The peak height values was observed to be insensitive to changes in Ar flow between 50-250 ml min⁻¹. High carrier gas flow rates prevented the condensation inside the tubings which worsened the reproducibility of the signal. An Ar flow rate of 146 ml min⁻¹ was chosen for further studies. As expected, the absorbance values increased as the pumping rate increased. 6 ml min⁻¹ was chosen as pumping rate.

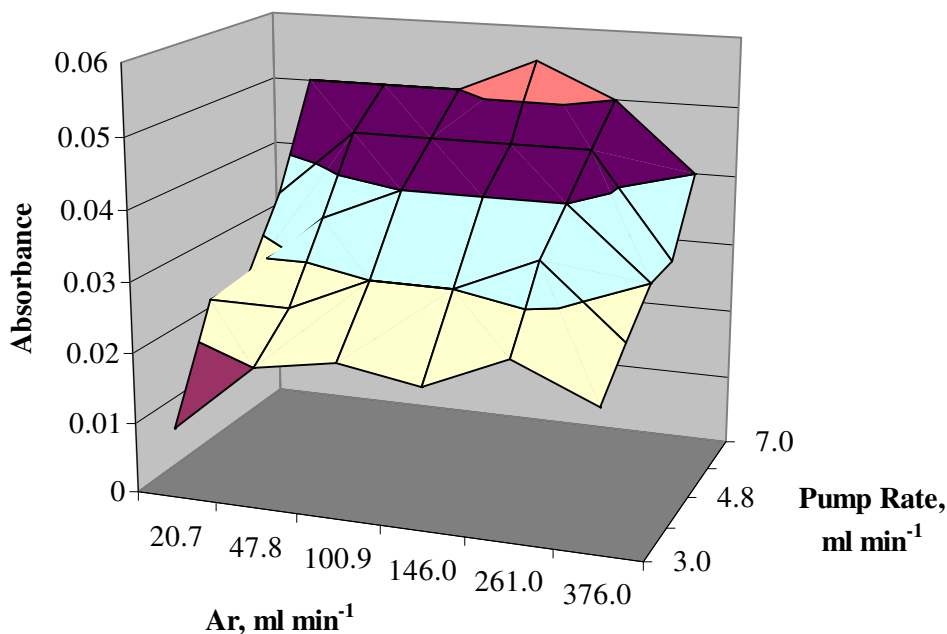


Figure 3.3 Surface plot for absorbance signal versus pumping rate and Ar flow

3.1.1.4 The Length of Reaction Coil

The PTFE reaction coil used in the experiments was 47.5 cm. The length was varied between 10.0 and 60.0 cm to understand its effect on the signal. No significant change was observed in the absorbance.

3.1.2 Trapping PbH_4 on Inlet Arm of Quartz Tube Atomizer

The changes in absorbance signal for continuous flow system when the inlet arm of quartz tube atomizer was heated can be seen in Figure 3.4, any reduction in signal indicates trapping. Argon was used as carrier gas. The heater was placed at two different positions as in Figure 2.2. Lead hydride generated was sent to flame heated quartz tube atomizer. When the trap was close to T-junction (Figure 2.2 a), absorbance increases by 50% at elevated trap voltages, showing that trapping of some analyte occurs in conventional hydride generation operation (no trap).

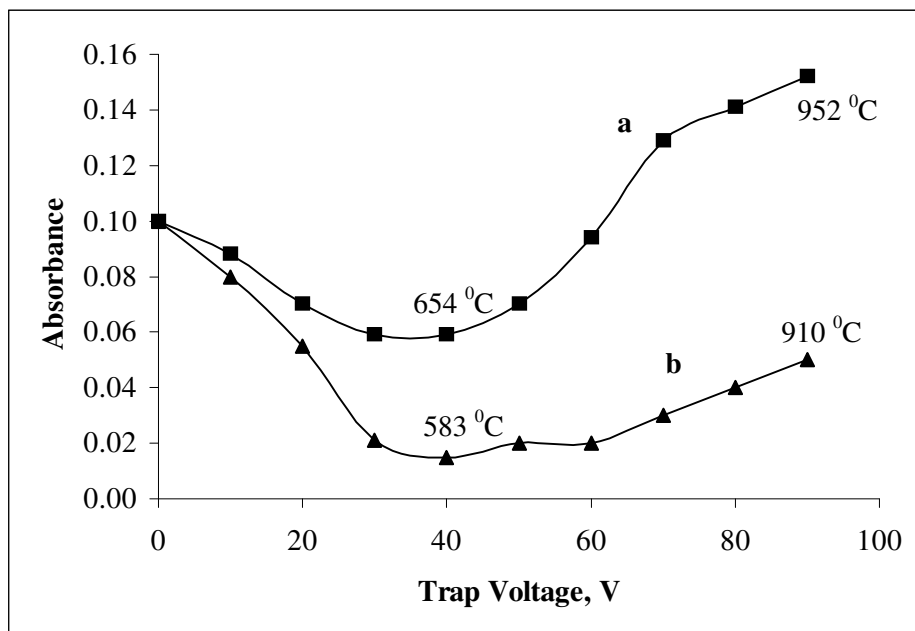
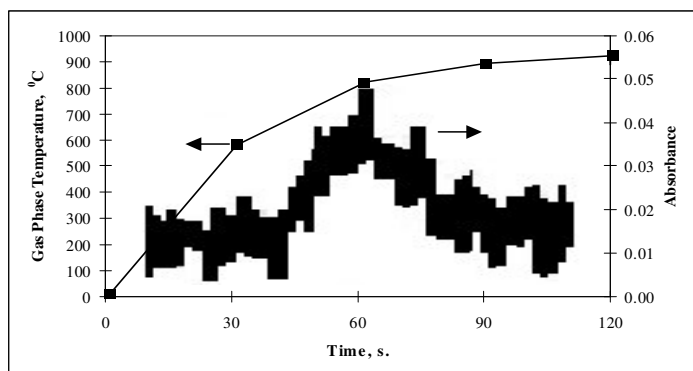


Figure 3.4 Changes in signal when the trap was operated during continuous flow of PbH_4 , 10 ng ml^{-1} Pb. Trap (a) close to (b) away from T-junction of quartz tube atomizer

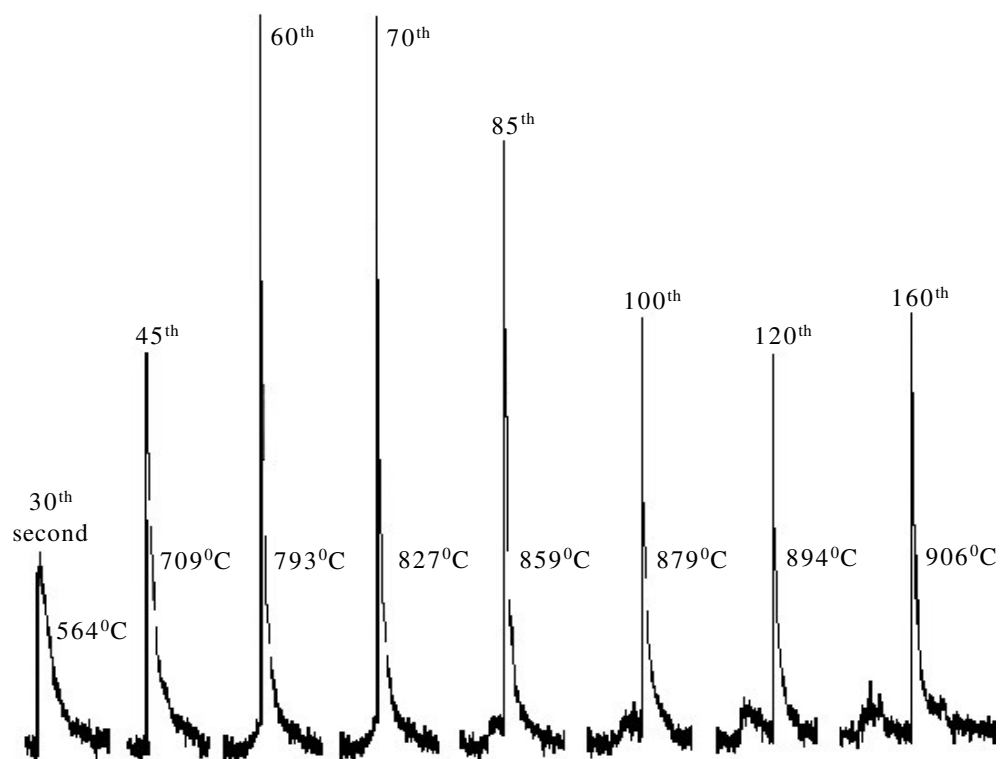
When the part that was away from the T-junction (Figure 2.2 b) was heated, much more trapping was realized as illustrated in Figure 3.4. The reason for this was that the unheated part of the inlet arm served as another trap between optical arm and heated trap, since there was an inevitable temperature gradient generated by the flame near the T-junction. Therefore, within this temperature gradient near the T-junction, there was a region of certain temperature which was ideal for trapping.

Experiments were carried out when the trap was close to the T-junction (Figure 2.2 a). After collecting up to 10 ng ml^{-1} Pb solutions for 1 minute at $500 \text{ }^\circ\text{C}$, pump was stopped and the temperature was increased to $900 \text{ }^\circ\text{C}$. No detectable signal was obtained unless the pump was reactivated, i.e. H_2 was formed. When the analyte

concentration was increased to 20 ng ml^{-1} , a broad signal (Figure 3.5 a) was obtained in absence of H_2 (pump off) with increasing temperature; this signal was believed to be due to the thermal atomization of collected analyte species on quartz. This signal lasted for approximately 2 minutes. If the pump was activated before the thermal signal terminated, a transient atomization signal was observed. The height and breadth of the absorbance signal was found to be dependent on the time the pump was turned on during the life time of the broad thermal signal (Figure 3.5 b). When the pump was started after 30 or 45 seconds of heating (when the temperature of gas phase was 564 and 709°C , respectively) the signal was rather broad. It reached to a maximum peak height when the temperature was approximately 800°C . Even after the thermal signal has ended, releasing H_2 into the trap caused an atomization signal indicating that heating did not cause the revolatilization and / or reatomization of all the collected species. The last signal in Figure 3.5 b illustrated this case. In this set of experiments, at the end of the sharp signal, no other signal was observed when the pump was stopped and then reactivated. It must be also mentioned that releasing H_2 into the heated quartz tube atomizer did not cause a significant temperature difference both on quartz surface and in gas phase. In general, the temperatures measured on the inner surfaces were not significantly higher than those measured in gas phase; the difference was in the range of $10\text{-}30^\circ\text{C}$; naturally, the surface was hotter.



(a)



(b)

Figure 3.5 Time profile of thermal atomization signal. 20 ng/mL Pb collected for 2 minutes on quartz T-tube, close to T-junction. No hydrogen was allowed into the atomizer during atomization (b) 20 ng/mL Pb collected for 2 minutes. Trap was heated and pump was activated on different instants of heating

The results implied that the presence of H₂ was required for revolatization and / or reatomization of some of the trapped analyte species. In addition, the trap must be heated to a certain temperature to realize revolatization and / or reatomization. Thermal atomization shown in Fig. 3.5 a took place if there was no hydrogen in the medium and will appear at the temperatures as high as 800 °C. It is then highly possible that formation of hydrogen radicals, formed by H₂ gas at certain temperature, played an important role in revolatization and atomization of Pb species, indicated by the sharp signals.

3.1.3 Observation of Pre-peaks

The pre-peaks in FI HGAAS were investigated by Welz et al. [137] in the determination of Sn. It was reported that these peaks appear when the pump was turned on before the first signal of a sequence of measurements. The height of these peaks depended on the time elapsed, during which the quartz tube atomizer was kept at a high temperature without a flow of H₂. The authors concluded that these peaks are due to impurities in quartz.

In our case, pre-peaks were observed with conventional HGAAS measurements without trap. In a series of experiments, these peaks appeared when the pump was activated as the first time; the freshly produced H₂ comes into contact with a certain location around the inlet arm of the quartz tube atomizer, thus causing the rapid atomization of species trapped during the previous measurements. As long as the hydrogen flow was continuous, no pre-peaks were observed. Stopping and re-tarting the flow of H₂ caused another pre-peak. The height of the pre-peak was proportional to the time elapsed while the pump was inactive. Therefore, it seemed that wherever the trapping occurred, a continuous flow of hydrogen could not prevent the

accumulation of some species. In other words, the species collected were not washed off by hydrogen. Presumably, when the pump was inactivated, air, and thus O_2 diffused into the system which was hot (since the flame was on) and the species collected did undergo a chemical change which could be now easily volatilized by a new front of H_2 gas when the pump was activated again. As the time elapsed during this change was longer, more species did undergo the transformation and a higher signal was then obtained.

One indication for this hypothesis was illustrated in Figure 3.4 a. When the heated trap was close to T-junction (Figure 2.2 a), the signal was approximately 50% higher than for the case with no trap when elevated temperatures were used. This may be caused by the fact that the location that acted as the trap is now as hot as the atomizer tube itself (approx. $900^{\circ}C$). It was very likely that a new trap location was not formed in this configuration; otherwise, at elevated temperatures, the absorbance would be same as in the case with no trap. However, the opposite was the case and the resulting absorbance signal was approximately 50% higher. In support of the discussion above, no pre-peaks were observed with this configuration as shown in Figure 2.2 a. When the ceramic heater was moved about 4.0 cm away from the T-junction as shown in Figure 2.2 b, the change in the continuous hydride signal as a function of trap voltage was given in Figure 3.4 b. Obviously, the location which previously caused the pre-peaks was not as hot as it was as with the configuration in Figure 2.2 a, thus this location was functional again. Indeed, the pre-peaks were observed with this configuration (Figure 2.2 b). With this configuration, even at elevated temperatures used with the quartz trap, continuous signal never reached to the value recorded at zero voltage, when trap was not heated at all.

3.1.4 Trapping PbH₄ on Separated Quartz Trap

The continuous flow signal decreased by 80% with this configuration (Figure 2.1). Inserting three pieces of quartz into the trapping region improved the trapping, and no detectable analyte signal was observed for analyte solutions with a concentration of 1 ng ml⁻¹ during collection cycle, provided the trap temperature was 500 °C. The carrier gas was 1% O₂ + 99% Ar. No atomization signal was observed with this configuration if the trap was heated without any H₂. It should be noted that the relatively low thermal peak shown in Figure 3.5 a for 20 ng ml⁻¹ Pb cannot be observed when significantly lower concentrations were used. Therefore, the sharp analytical peaks were observed on an almost flat background. Following the trapping at 500 °C, the analytical procedure for this set-up consisted of a continuous H₂ flow (pump on) while the trap was further heated to 750 °C. This technique was selected because the results were more reproducible compared to the case where the pump was reactivated after heating. The signal obtained by collecting 6 ng of analyte was compared to the signal for continuous flow HGAAS in Figure 3.6. The increase in signal was about 8 fold.

When the peak height of signals started to decrease after approximately 100 cycles, and when the signal reduction was as much as 5%, the small pieces of quartz inside the trap needed to be replaced with the new ones, but not the trap tubing itself.

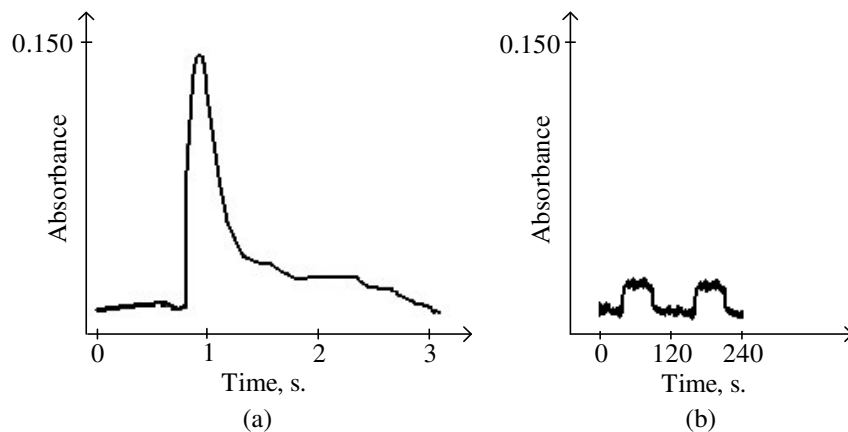


Figure 3.6 Time profile of atomization signal for (a) separated quartz trap, 6.0 ml of 1 ng ml^{-1} Pb collected for 60 s; (b) continuous flow HGAAS, 1 ng ml^{-1} Pb

3.1.5 Effect of Carrier Gas

For continuous flow HGAAS, use of pure Ar or a mixture of 1% O_2 + 99% Ar did not cause any significant difference in the absorbance signal. Using pure CO as carrier gas decreased the signal by 50%.

When the analyte species were trapped on the inlet arm of quartz tube atomizer close to the T-junction, a 1% O_2 + 99% Ar mixture increased the atomization signal by 20%. No atomization signal was obtained when pure CO was used as carrier gas. When the trap on inlet arm was moved 4.0 cm away from the T-junction (Figure 2.2 b), the signal became broad and the use of peak height was not feasible. In this case, there was no significant difference in the signals obtained when the carrier gas was pure Ar or 1% O_2 + 99%Ar.

When the analyte species were trapped on the separated quartz trap, no atomization signal was observed if pure Ar or pure CO were used as carrier gas. The signals

were observed only if 1% O₂ + 99% Ar mixture was used as the carrier; this showed that some oxygen must be present in the medium to realize revolatilization / reatomization from quartz surface. Atomization signals were obtained with Ar as the carrier only when the analyte species were trapped on the inlet arm of the atomizer (Figure 2.2 a). With this configuration, oxygen diffusing from the open ends of the quartz tube atomizer was sufficient to cause revolatilization / reatomization of most of the species collected. The suppressing effect of CO when used as the carrier gas may be due to the reaction of CO with O₂ in the medium, thus diminishing its concentration to very low values.

3.1.6 Effect of Hydrogen Radicals

In addition to their rather well demonstrated effects in the quartz tube atomizers [5, 25-28, 31, 32], hydrogen radicals might be affecting the signal in two ways regarding the trap system used in this study. They may cause revolatilization / reatomization of lead species collected on quartz and / or they may be effective in transporting the species to the atomizer in a cloud of radicals. In order to observe the effect of H₂ on revolatilization, analyte was collected on the separated quartz trap. Before the atomization cycle, gas-liquid separator was dismounted and then was connected to the system in such a way that the hydrogen stream was bypassed (Figure 3.7). In this set-up hydrogen could not enter into the trap, but can only meet the analyte species in the transport line after the trap if they were somehow revolatilized. No signal was obtained with this configuration. The signal reappeared if hydrogen was allowed to pass through the trap again. This experiment did not exclude the carrying effect of the radicals, but illustrated that radicals must be in contact with quartz trap surface to effect revolatilization / reatomization of trapped analyte species.

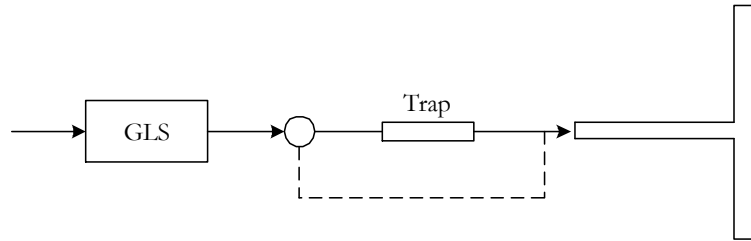


Figure 3.7 Experimental set-up to understand the effect of hydrogen radicals

3.1.7 The Form of Revolatilized Species

The species carried might be in atomic or molecular form. If they were in atomic form, an absorbance signal could be observed, even if the quartz tube atomizer was not heated by the flame. The flame was turned off and 100 ng ml^{-1} Pb was collected on inlet arm of the quartz tube atomizer. An atomization signal of about 0.3 absorbance units was obtained in the atomization cycle when the pump was started. When the experiment was repeated with the separated quartz trap, analyte concentration had to be increased to 300 ng ml^{-1} to detect an atomic signal. In time, some condensation was observed on inlet arm of the quartz tube atomizer which was due to water vapour, and no atomization signal was then obtained. When the inlet arm of quartz tube atomizer was electrically heated, atomization signal reappeared. It should be noted that the atomic signal was observed only at rather high analyte concentrations. Therefore, at least some of the trapped Pb species might be transported in atomic form. The decrease in sensitivity when the flame was not on could be due to the fact that most of the species entering the optical path are in molecular form, possibly some oxides of lead. Some of the species may be in atomic form to cause the signal. When the optical arm of the quartz tube atomizer was heated as in conventional analysis, the atomic population will obviously increase. This does not exclude, however, that a large free atomic population of analyte is possibly formed but later inactivated on cold walls.

3.1.8 Analytical Figures of Merit

Measurements were carried out using peak height of signals. An enhancement factor of 6 was obtained for the detection limit when 60 seconds trapping with the separated quartz trap was compared to continuous flow HGAAS. This factor can be improved using longer collection periods. The correlation coefficient of linear regression line was 0.997 with the equation $A = 0.126C + 0.02$ where C is in ng ml^{-1} (Figure 3.8).

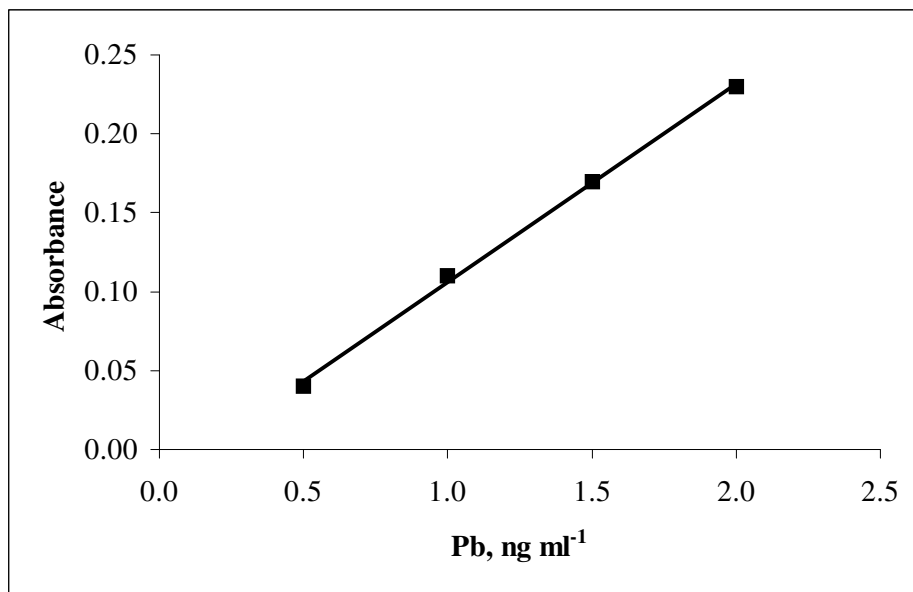


Figure 3.8 Calibration plot for 60 s trapping

The absorbance was found to be changing linearly up to 4 minutes of collection time when collecting 0.5 ng ml^{-1} Pb solution (Figure 3.9).

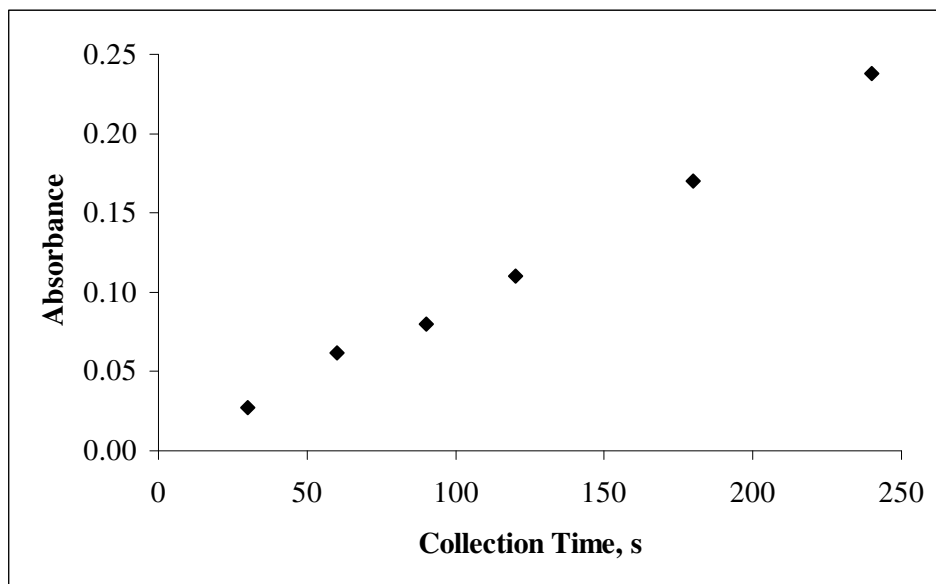


Figure 3.9 Analytical signal vs. collection time for $0.5 \text{ ng ml}^{-1} \text{ Pb}$

The system sensitivity was limited by rather high blank values caused by $\text{K}_3\text{Fe}(\text{CN})_6$; observed blanks could be as high as 0.200 ng ml^{-1} . Attempts were made to purify $\text{K}_3\text{Fe}(\text{CN})_6$ using mercapto resin, active carbon, Chelex-100 and amberlite XAD-2 resin. Extraction of Pb with diphenylthiocarbazon in chloroform as solvent was also tried. None of the trials had been successful.

The total efficiency of trapping and volatilization was found to be 49% comparing characteristic mass values. The concentration (c_0) and mass (m_0) sensitivities (i.e. the mass or concentration of analyte that provides a defined peak absorbance of 0.0044) and 3σ limit of detection (LOD) were compared in Table 3.1. The precision of the results was better than 5% relative standard deviation (RSD).

Table 3.1 Comparison of analytical figures of merit using peak height. Collection time for separated quartz trap was 60 s with a sample solution flow rate of 6.0 ml min⁻¹.

	$c_0, \text{ng l}^{-1}$	m_0, pg	$LOD, \text{ng l}^{-1}$
HGAAS (250 μl loop)	410	116	120
Separated quartz trap HGAAS	40	238	19

The amount of Pb in SRMs was found to be in good agreement with the certified values as given in Table 3.2. Direct calibration was used for analysis of both SRMs.

Table 3.2 Analysis results of standard reference materials

<i>SRM</i>	<i>Certified</i>	<i>Found</i>
Soil/Sediment #4, mg kg ⁻¹	95.3 \pm 5.3	97.2 \pm 2.5
CRM-TMDW, ng ml ⁻¹	40.0 \pm 0.2	41.0 \pm 1.0

3.2 Sb

3.2.1 Hydride Generation Conditions for Continuous Flow HGAAS

The generation conditions as previously optimized by Matoušek et al. [136] with the same hydride generator were used. The details were given in Sections 2.2.1 and 2.2.3. If not mentioned otherwise, integrated absorbance signals were employed; the precision given in the text, tables and figures, estimated from at least three replicate measurements was better than 4% RSD.

Hydride atomization in conventional externally heated quartz tube atomizers is facilitated by O₂ contamination of gases introduced to the atomizer [5]. The traces of O₂ thus react with hydrogen in the beginning of the heated portion of the atomizer to form hydrogen radicals which were proved to atomize hydrides at relatively low temperatures typical for conventional quartz tube atomizer as well as for the multiple microflame quartz tube atomizer [136]. However, O₂ traces in a gas containing hydrogen are removed by reactions with hydrogen above 500 °C. Consequently, oxygen content in the gas after passing through the heated trap, introduced to the conventional quartz tube atomizer could be too low to render the analyte atomization possible. Use of multiple microflame quartz tube atomizer was also useful in this respect [138].

3.2.2 Preliminary Observations

When trap was not heated, a signal typical for the continuous flow generation in the direct transfer mode was observed in the collection step, i.e. with a rising edge followed by the steady state plateau and by the falling edge observed after replacing the standard by the blank in the sample channel. To reach the steady state plateau, the standard had to be introduced for at least 60 s. However, the software of the employed spectrometer did not make it possible to integrate signals longer than 60 s. To cover the whole signal (including the rising edge as well as the falling edge) by the integration period of 60 s, the standard (of the concentration 2.5 ng ml⁻¹) was introduced for 30 s (at a flow rate of 4.0 ml min⁻¹), corresponding to a mass of 5 ng of Sb, even though this standard solution introduction time was too short to achieve the steady state signal plateau. The integrated area of the signal was 1.2 s, corresponding to the peak area characteristic mass (m₀) of 18 pg. The sensitivity observed in the absence of the trap did not differ significantly. m₀ is thus 2.2 times

higher than observed for Se in the same atomizer [33]. The ratio of sensitivity Se / Sb roughly corresponds to that observed recently [136].

At the trap temperature of 440 °C, the "breakthrough" signal, i.e. the signal observed during collection step, decreased to around 50%. At the temperature of 620 °C, no significant breakthrough signal was detected indicating that this was a minimum temperature useful for stibine collection. However, no significant breakthrough signal was detected also at temperatures higher than 620 °C up to the maximum applied trap temperature of 1000 °C.

To volatilize collected analyte, it was not sufficient just to heat the trap - at least some hydrogen flow through the trap was also required. This agrees to the observation on the volatilization of Pb. It should be noted that hydrogen is required, besides for analyte volatilization from the trap, also for atomization in conventional quartz tube atomizers [5] as well as in the multiatomizer [33, 136].

To prove that the signal observed in the volatilization step of the collection mode was due to analyte collected in the trap and not in any other part of the atomizer, the following experiment was conducted: after performing the collection step, the trap was disconnected and replaced by another "clean" trap. The volatilization step was subsequently performed and no signal was obtained. When the original trap was installed back and the volatilization step was activated, the signal of the analyte collected in the trap was observed.

3.2.3 Optimization of Collection and Volatilization

Qualitatively, the rate of volatilization increased with increasing hydrogen flow rate and volatilization temperature. The above mentioned necessity of hydrogen for

analyte volatilization made it possible to eliminate the slow heating of the trap: the volatilization was initiated by the switching on the flow of H₂ not before the trap achieved the selected temperature. When switching on the flow of H₂ in the beginning of Step 2 (see Section 2.2.6), simultaneously with setting the heating voltage to the volatilization level, unacceptably broad peaks were observed (Table 3.3). Introducing a H₂ flow to the atomizer reduces sensitivity because of dilution and, additionally, due to the influence of H₂ on the absorption line width [5]. The interaction of an emitting or absorbing atom with molecules of foreign gases perturb its energy levels and lead to a broadening of spectral lines. The broadening is a function of the density of the perturbing species and is therefore known as pressure broadening or Lorentz broadening according to the author of the associated theory [5].

Table 3.3 Integrated absorbances for introducing H₂ before or after reaching to volatilization temperature

<i>H₂, ml min⁻¹</i>	<i>Integrated Absorbance, s</i>	
	<i>H₂ in before volatilization temperature</i>	<i>H₂ in at volatilization temperature</i>
25	0.405	0.449
50	0.203	0.471
100	0.024	0.351

Consequently, in addition to collection and volatilization temperatures, also the hydrogen flow rate (in the volatilization step) had to be optimized. It appeared that the optimum collection and volatilization temperatures were 650°C and 920°C, respectively (Figure 3.10).

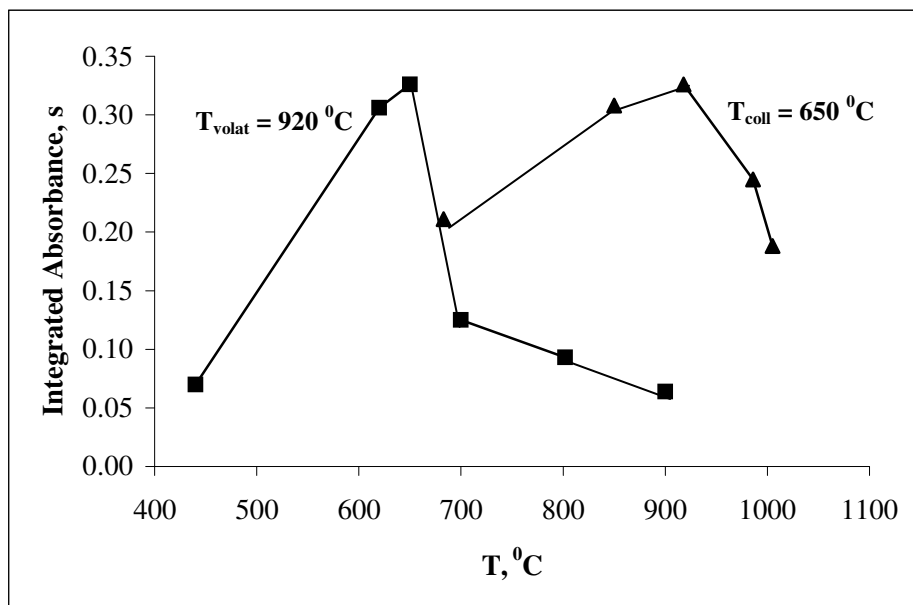


Figure 3.10 Influence of collection temperature (squares, volatilization temperature of 920 °C) and volatilization temperature (triangles, collection temperature of 650 °C) on the observed signal; 5 ng Sb

The optimum hydrogen flow rate was around 100 ml min⁻¹ as illustrated in Table 3.4. The table compares signals obtained in the direct transfer mode of measurement, i.e. for unheated trap with those obtained in the collection mode under essentially the same gas flow rates introduced to the inlet arm of the atomizer. This made it possible to assess the efficiency of the collection / volatilization as given in the last column of Table 3.4.

Table 3.4 The influence of the auxiliary H₂ flow rate on peak area for direct transfer and collection^a modes of measurements.

<i>H₂ flow, ml min⁻¹</i>	<i>Integrated Absorbance, s</i>		<i>Peak FWHM^b, s</i>	<i>Efficiency, %</i>
	<i>Direct transfer mode</i>	<i>Collection mode</i>		
0	1.21	0		
25	1.14	0.45	3.2	39
50	0.97	0.47	1.3	49
75	0.74	0.42	0.9	57
100	0.54	0.35	0.5	65
150	0.40	0.20	0.4	49
200	0.39	0.13	0.1	34

^a 5 ng Sb ^bIn the collection mode FWHM: Full width at half maximum

In the revolatilization step, signals of regular shape were observed for collection temperatures equal and lower than 650 °C - see Figure 3.11 as an example of a peak observed under the optimum collection temperature (650 °C) and volatilization temperature (920 °C). The typical full width of the peak at half maximum (FWHM) was 0.4 to 0.5 s.

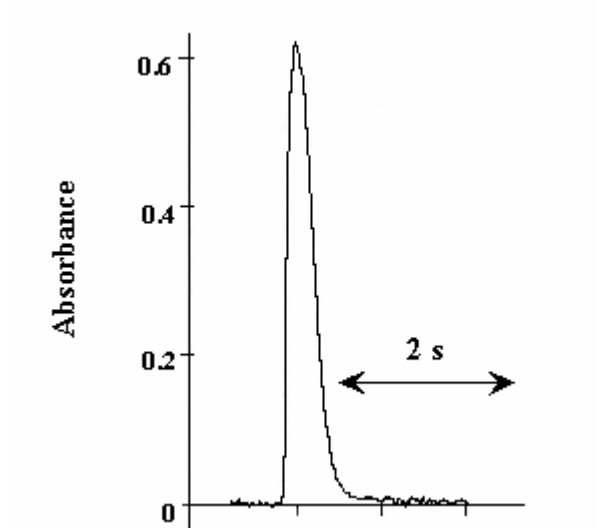


Figure 3.11 The typical signal shape observed. Collection temperature: 650 °C; revolatilization temperature: 920 °C; 4 ng Sb

At collection temperatures equal or higher than 700 °C, the peak area of the atomization signal was reduced (Figure 3.10) and also its shape changed - it appeared as two peaks, the "sooner" one having FWHM similar as for the optimum collection temperature and the "later" one which was much broader (Figure 3.12).

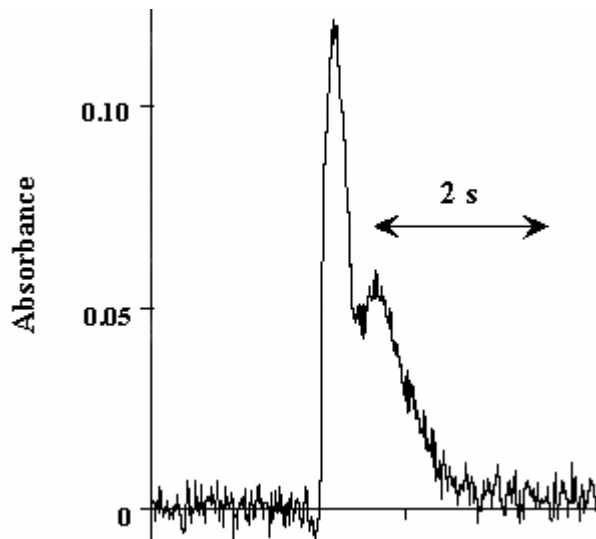


Figure 3.12 The signal observed for the collection temperature of 700 °C. Revolatilization temperature: 920 °C; 5 ng Sb

3.2.4 Influence of the Length of Inlet Arm of Atomizer

In order to see the effect of the length of the inlet arm, a multiple microflame quartz tube atomizer with a 45 mm long inlet arm was employed i.e. 60 mm shorter than the inlet arm of the original multiple microflame quartz tube. No significance difference was observed in the volatilization signal. This observation indicated that there was no significant loss of volatilized species from the trap at the first 60 mm of the inlet arm.

3.2.5 Influence of Oxygen

The influence of air flow rate introduced, in both steps of the procedure, to the auxiliary channel on signal observed in the volatilization step, is shown in Table 3.5.

A very small flow rate, up to 2.5 ml min⁻¹, made slight improvement in peak area, however, higher flow rates reduced peak area and made peaks markedly broader (Table 3.5). Also tailing was observed to appear at higher air flow rates.

Table 3.5 The influence of auxiliary air flow rate on signals observed in the collection mode of measurements; 5 ng Sb

<i>Air flow rate, ml min⁻¹</i>	<i>Integrated Absorbance, s</i>	<i>Peak FWHM, s</i>
0	0.32	0.5
2.5	0.35	0.5
5	0.20	0.8
10	0.10	1.9

The observed influence of the auxiliary air should not be accounted to processes taking place in the atomizer since any oxygen required for the atomization was covered by the oxygen flow introduced to the outer channel of the multiatomizer [33, 136]. Consequently, the influence of the introduced oxygen should be accounted for the processes taking place in the trap and / or in the tubing connecting the upstream end of the trap tube to the inlet arm of the atomizer. Reduction of area and the broadening of peaks in the presence of air flow rate of 5 ml min⁻¹ and higher could be attributed to partial conversion of elemental antimony retained in the trap to oxide. Sb₂O₃ is more volatile than the elemental Sb - the oxide sublimates at 1550°C [139]. The conversion of oxide to hydride could be slower than that of the elemental form. The oxidation should be occurring in the beginning of the volatilization step, before switching on the hydrogen flow. To prove that oxygen was active in the volatilization step, the flow of air at the rate of 5 ml min⁻¹ was introduced only during the volatilization step. The signal observed did not differ

significantly from that for the same air flow rate introduced in both steps of the procedure.

In their study, Narsito et al. [140] had reported that the addition of oxygen to the gas entering the atomizer in an amount greater than the stoichiometric ratio when compared with amount of H₂ present caused a sharp drop in the absorbance to nearly zero. They explained this observation by the formation of oxide of Sb.

3.2.6 Observation of Pre-peaks

Typically, narrow peaks (FWHM around 0.3 s) were observed when hydrogen flow to the atomizer was resumed (either by introducing hydrogen to the auxiliary channel or by switching on the peristaltic pump) after a time period during which the atomizer was kept at the atomization temperature in the absence of H₂. These "pre-peaks" were observed in the direct transfer mode in the absence of the trap. The height of pre-peaks depended on the length of time period during which the atomizer was heated in the absence of hydrogen: the longer the period the higher the pre-peak.

As mentioned before, a similar observation was reported for Sn determination (pre-peak intensity increased with the length of time period during which the atomizer was heated in the absence of H₂) and explained by analyte impurities, in the quartz material of the atomizer, diffusing at elevated temperatures from the bulk of the material to the inner atomizer surface [137]. However, this cannot be the explanation of pre-peaks appearing in our experiments with Sb since there were no pre-peaks observed in the atomizer after cleaning in the mixture of HNO₃ and HF. The pre-peaks could be due to the analyte species transported to the atomizer in the absence of H₂ similarly as the pre-peaks in Pb determination.

The observed pre-peaks can be explained by the slow mobility of certain fraction of elemental Sb with the following hypothesis:

In the presence of H₂, the migrating analyte is eventually converted to hydride and thus detected by the spectrometer. The corresponding, very weak, AAS signal is hidden in the baseline.

In the absence of H₂, the migration of elemental Sb may continue, however, it cannot be converted to much more volatile hydride. Even when the migrating analyte reaches the atomizer optical arm it cannot be atomized because of the absence of H₂. Moreover, elemental Sb present in any part of the line can react with traces of molecular oxygen, inevitably present in the absence of H₂. The oxidation rate is controlled by the temperature of the actual section of the line. Sb₂O₃ can thus migrate downstream faster than elemental Sb.

Upon resuming H₂ flow, either by starting hydride generation or by switching on H₂ to the auxiliary channel, at least some fraction of analyte present in hot parts of the atomizer could be converted to hydride and / or atomized.

3.2.7 Analytical Figures of Merit

The calibration plot, for the collection mode with standard solution introduction time of 120 s, is shown in Figure 3.13. The linear portions of calibrations extended up to Sb concentration of 1.25 ng ml⁻¹ (10 ng) - the corresponding peak height absorbance is 1.5. Straight lines show the linear best fits corresponding to a sensitivity of 1.203 ± 0.012 ml ng⁻¹ (correlation coefficient 0.998) and 0.470 ± 0.006 ml ng⁻¹ (correlation coefficient 0.997), respectively, for peak height and area. The sensitivity of the linear portion corresponds to the peak area characteristic mass of

75 pg. The curvature observed for higher analyte mass (peak height absorbance above 1.5) was obviously due to the stray light radiation.

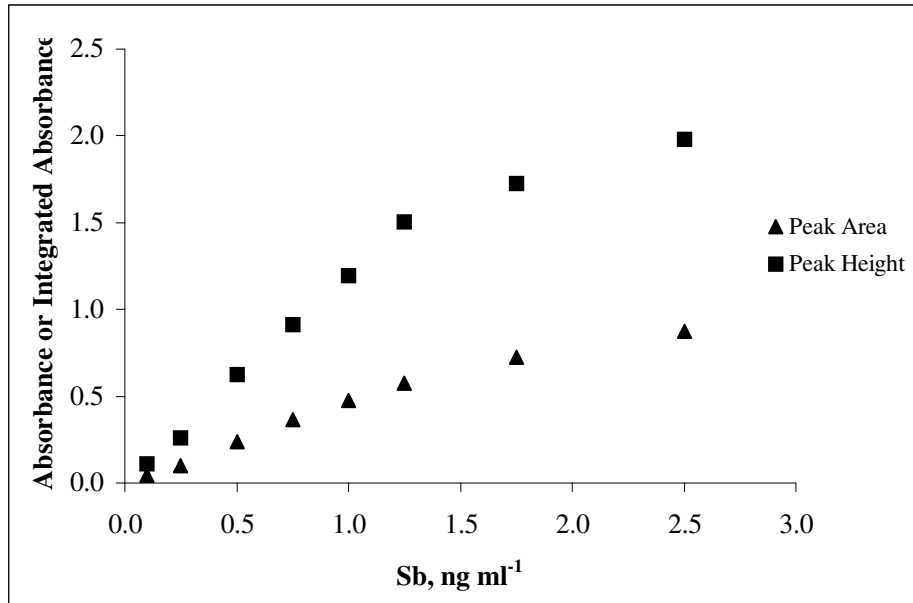


Figure 3.13 Peak area and peak height calibration for the collection mode. Collection time: 120 s; sample volume: 8 ml

RSDs were better than 5% and 4%, respectively, for peak height and area measurements in the collection mode. LOD (3σ) for peak height measurements were 130 pg ml^{-1} and 3.9 pg ml^{-1} , respectively, for the direct transfer and the collection modes (sample solution introduction time 120 s, sample consumption 8 ml). Sample throughput was 20 samples per hour in the collection mode for standard solution introduction time of 120 s. Lifetime of the trap was not less than 300 firings, having a stable performance throughout the whole period.

The achieved LOD is close to the best LOD achieved for stibine *in-situ* trapping in commercial graphite furnace with subsequent AAS detection: 2.9 pg ml⁻¹, with a sample consumption of 10 ml, reported by Sturgeon et al. [141], and it compares favorably with LODs (in pg ml⁻¹) given by other authors: 14 [142], 21 [143], 10 [144], 20 [145], 5 [146].

3.3 Cd

Cd was determined using cold vapour generation technique. Use of a flame heated quartz tube caused 50% reduction in the analytical signals. This was in agreement with the observation of Sanz Medel et al. [39]. In their work, the reduction was explained by the expansion of gases on heating, diluting the analyte and shortening its residence time in the optical path. Trapping of some of the species on the heated inlet arm before they enter to the optical path may also contribute to the decrease in the signal with an externally heated quartz tube. Nevertheless, this should be making a minor contribution, since with a bare inlet arm, trapping of Cd species was fairly inefficient.

3.3.1 Optimization of Conditions for FI Cold Vapour Generation of Cd

Literature data reveal much inconsistency and contradictory statements for the determination of Cd by cold vapour generation technique, probably because of the inherent instability and difficulties with generation, stripping off solution and transportation of volatile cadmium species [122]. In the light of previous studies in literature, it was decided to employ experimental design instead of “one factor at a time” approach to optimize the cold vapour generation conditions of volatile Cd

species. A two-level fractional factorial design was first employed for exploratory purposes. The aim was to screen a number of factors which could be affecting the analytical response or each other. The main factor or interacting factors which should be studied in detail later were sorted out with this design.

The factors which were considered to be significant were the lengths of reaction and stripping coils, carrier and sample acidities, and concentration of the reductant. The following two level fractional factorial design matrix was run to reduce the number of experiments to 2^{5-1} (Table 3.6). 4 additional experiments at the central point (0 level) were also added to the design. The experiments were done in random order. Real values of factors were chosen on the basis of the results of preliminary experiments. Factors were coded as -1 (low), 0 (center) and +1 (high). The coding of factors is shown in Table 3.7. The design matrix simplifies considerably with coded values as presented in Table 3.7. All the experiments were done for 3 replicate solutions. At least 3 measurements were made for each replicate.

Table 3.6 Uncoded design matrix

x_0 <i>Intercept</i>	x_1 <i>Reaction coil</i>	x_2 <i>Stripping coil</i>	x_3 <i>Carrier HCl</i>	x_4 <i>Sample HCl</i>	x_5 <i>NaBH₄</i>
1	10	10	0.1	0.05	3.0
1	30	10	0.1	0.05	1.0
1	10	20	0.1	0.05	1.0
1	30	20	0.1	0.05	3.0
1	10	10	0.3	0.05	1.0
1	30	10	0.3	0.05	3.0
1	10	20	0.3	0.05	3.0
1	30	20	0.3	0.05	1.0
1	10	10	0.1	0.25	1.0
1	30	10	0.1	0.25	3.0
1	10	20	0.1	0.25	3.0
1	30	20	0.1	0.25	1.0
1	10	10	0.3	0.25	3.0
1	30	10	0.3	0.25	1.0
1	10	20	0.3	0.25	1.0
1	30	20	0.3	0.25	3.0
1	20	15	0.2	0.15	2.0
1	20	15	0.2	0.15	2.0
1	20	15	0.2	0.15	2.0
1	20	15	0.2	0.15	2.0

Table 3.7 Coding of factors

<i>Factor</i>	<i>Unit</i>	<i>-1</i>	<i>0</i>	<i>+1</i>
Length of reaction coil	cm	10	20	30
Length of stripping coil	cm	10	15	20
Carrier HCl concentration	M	0.10	0.20	0.30
Sample HCl concentration	M	0.05	0.15	0.25
NaBH ₄ concentration	%, w/v	1.0	2.0	3.0

The two factor interaction terms in Table 3.7 (x_1x_2 , x_1x_3 , x_1x_4 , x_1x_5 , x_2x_3 , x_2x_4 , x_2x_5 , and x_3x_4) were simply obtained by multiplying the relevant factors.

3.3.2 Data Analysis

The experimental data can be described by forming a mathematical relationship between the factors and response as

$$y = b_0 + b_1x_1 + b_2x_2 + b_3x_3 + b_4x_4 + b_5x_5 + b_{12}x_1x_2 + b_{13}x_1x_3 + b_{14}x_1x_4 + b_{15}x_1x_5 + b_{23}x_2x_3 + b_{24}x_2x_4 + b_{25}x_2x_5 + b_{34}x_3x_4 \quad (3.2)$$

where y is the response, x 's are the value of the factors and b 's are the coefficients of the model [132].

Table 3.8 Coded design matrix with average response values

Exp	x_0	x_1	x_2	x_3	x_4	x_5	x_1x_2	x_1x_3	x_1x_4	x_1x_5	x_2x_3	x_2x_4	x_2x_5	x_3x_4	x_3x_5	x_4x_5	<i>Response (y)</i>
1	1	-1	-1	-1	-1	1	1	1	1	-1	1	1	-1	1	-1	-1	0.039
2	1	1	-1	-1	-1	-1	-1	-1	-1	-1	1	1	1	1	1	1	0.037
3	1	-1	1	-1	-1	-1	-1	1	1	1	-1	-1	-1	1	1	1	0.024
4	1	1	1	-1	-1	1	1	-1	-1	1	-1	-1	1	1	-1	-1	0.048
5	1	-1	-1	1	-1	-1	1	-1	1	1	-1	1	1	-1	-1	1	0.201
6	1	1	-1	1	-1	1	-1	1	-1	1	-1	1	-1	-1	1	-1	1.707
7	1	-1	1	1	-1	1	-1	-1	1	-1	1	-1	1	-1	1	-1	0.964
8	1	1	1	1	-1	-1	1	1	-1	-1	1	-1	-1	-1	-1	1	0.456
9	1	-1	-1	-1	1	-1	1	1	-1	1	1	-1	1	-1	1	-1	0.550
10	1	1	-1	-1	1	1	-1	-1	1	1	1	-1	-1	-1	-1	1	0.933
11	1	-1	1	-1	1	1	-1	1	-1	-1	-1	1	1	-1	-1	1	0.617
12	1	1	1	-1	1	-1	1	-1	1	-1	-1	1	-1	-1	1	-1	0.872
13	1	-1	-1	1	1	1	1	-1	-1	-1	-1	-1	-1	1	1	1	1.746
14	1	1	-1	1	1	-1	-1	1	1	-1	-1	-1	1	1	-1	-1	0.068
15	1	-1	1	1	1	-1	-1	-1	-1	1	1	1	-1	1	-1	-1	0.057
16	1	1	1	1	1	1	1	1	1	1	1	1	1	1	1	1	2.467
17	1	0	0	0	0	0	0	0	0	0	0	0	0	0	0	0	1.051
18	1	0	0	0	0	0	0	0	0	0	0	0	0	0	0	0	1.021
19	1	0	0	0	0	0	0	0	0	0	0	0	0	0	0	0	1.154
20	1	0	0	0	0	0	0	0	0	0	0	0	0	0	0	0	1.058

Factors: x_1 , length of reaction coil; x_2 , length of stripping coil; x_3 , carrier HCl concentration; x_4 , sample HCl concentration; x_5 , NaBH₄ concentration. y ; integrated abs

The relationship between the response, the coefficients and the experimental conditions can be expressed in matrix form by

$$y = D.b \quad (3.3)$$

as illustrated in Figure 3.14, where y is the vector of responses, D is the design matrix, and b is the vector of coefficients in the model.

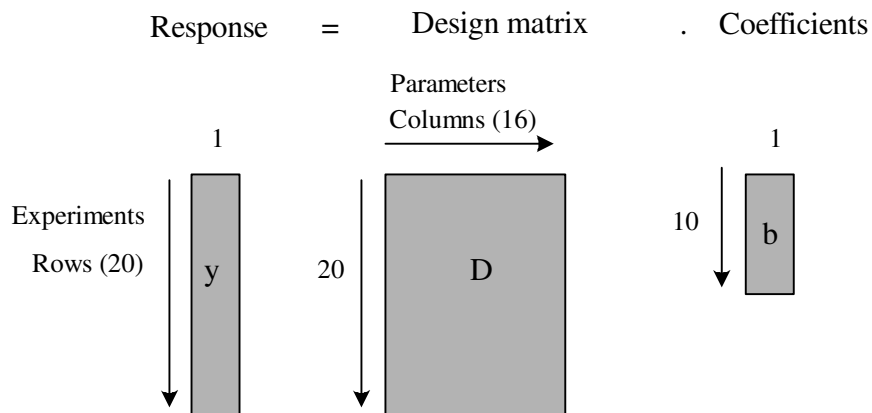


Figure 3.14 Relationship between response, design matrix and coefficients [132]

Since D was not a square matrix, the coefficient matrix was obtained by using pseudo inverse function

$$b = (D'.D)^{-1}. D' . y \quad (3.4)$$

in Excel. The size of the coefficients can be used to understand the significance of factors. The coefficients calculated for each replicate using coded design matrix (Table 3.8) are given in Table 3.9.

Table 3.9 The coefficients for the model

<i>Factors</i>	<i>Coefficients</i>	<i>Replicate1</i>	<i>Replicate2</i>	<i>Replicate3</i>	<i>Average</i>	<i>St dev</i>	<i>t</i>
x_0	b_0	0.754	0.732	0.775	0.754	0.022	34.744
x_1	b_1	0.149	0.143	0.156	0.149	0.006	24.214
x_2	b_2	0.013	0.015	0.014	0.014	0.001	11.413
x_3	b_3	0.276	0.286	0.291	0.284	0.008	36.590
x_4	b_4	0.240	0.227	0.252	0.240	0.012	19.468
x_5	b_5	0.384	0.384	0.406	0.391	0.013	31.228
x_1x_2	b_1b_2	0.122	0.122	0.126	0.123	0.002	51.525
x_1x_3	b_1b_3	0.061	0.068	0.071	0.067	0.005	12.570
x_1x_4	b_1b_4	0.024	0.020	0.022	0.022	0.002	12.401
x_1x_5	b_1b_5	0.075	0.074	0.074	0.074	0.001	110.477
x_2x_3	b_2b_3	0.015	0.015	0.011	0.014	0.003	5.446
x_2x_4	b_2b_4	0.073	0.076	0.078	0.075	0.003	26.782
x_2x_5	b_2b_5	-0.058	-0.050	-0.057	-0.055	0.005	-11.915
x_3x_4	b_3b_4	-0.113	-0.110	-0.118	-0.113	0.004	-27.720
x_3x_5	b_3b_5	0.360	0.373	0.382	0.372	0.011	34.142
x_4x_5	b_4b_5	0.140	0.129	0.140	0.136	0.006	21.189

One of the simplest approaches to determining the significance is simply to look at the t statistics calculated by dividing the average values in Table 3.9 by the standard deviation. For 4 degrees of freedom (20-16) and at 95% confidence level, the critical t value is 2.78. Therefore, all of the five factors investigated by fractional factorial design have shown to have significant effect on the response. For practical reasons, only the most significant three; namely the length of reaction coil (x_1), concentration of carrier HCl (x_3), and concentration of NaBH₄ (x_5), were chosen for further optimization with central composite design. A central composite design is constructed as several superimposed designs (Figure 1.3). The total number of experiments, N (=20) equals the sum of 2^k (=8) factorial points, often represented as

the corners of the cube; $2k + 1$ ($=7$) star points, often represented as axial points on or above the faces of the cube plus one in the center; and R ($=5$) replicate point, in the center where k , is the number of factors. [132]. The levels at $2k$ experiments are (-1) and $(+1)$; the levels at $2k$ experiments are $\pm \alpha$ and the level at replicate experiments is (0) . Construction of the central composite design for three factors is shown in Table 3.10.

Table 3.10 Construction of a central composite design for three factors

<i>Exp.</i>	x_1	x_2	x_3
1	-1	-1	-1
2	1	-1	-1
3	-1	1	-1
4	1	1	-1
5	-1	-1	1
6	1	-1	1
7	-1	1	1
8	1	1	1
9	0	0	0
10	$-\alpha$	0	0
11	α	0	0
12	0	$-\alpha$	0
13	0	α	0
14	0	0	$-\alpha$
15	0	0	α
16	0	0	0
17	0	0	0
18	0	0	0
19	0	0	0
20	0	0	0

The choice of the position of axial (or star) points determines whether the design would be rotatable or orthogonal. Rotatability implies that the confidence in the predictions depends only on the distance from the center of the design. For a two factor design, this means that all experimental points in a circle of a given radius

will be predicted equally well [132]. For a rotatable design, as in our case, α is calculated as:

$$\alpha = \pm (2^k)^{1/4} \quad (3.5)$$

Using Equation 3.5, α value was calculated as ± 1.682 . The real values corresponding to the coded levels are given in Table 3.11. The length of stripping coil was 20.0 cm, the concentration of HCl in sample solution was 0.40 M and the flow of Ar was 170 ml min⁻¹ during the following experiments.

Table 3.11 Real values corresponding to the coded levels

<i>Factor</i>	<i>Level</i>				
	<i>- 1.682 (α)</i>	<i>-1</i>	<i>0</i>	<i>1</i>	<i>+ 1.682 (α)</i>
Reaction coil length, cm	3.18	10	20	30	36.82
Carrier HCl concentration, M	0.13	0.20	0.30	0.40	0.47
%NaBH ₄ , w/v	2.16	2.50	3.00	3.50	3.84

Obviously, α values were calculated as:

$$\begin{aligned} +1.682 &= (x_1 - 20)/10, & x_1 &= 36.82 \\ -1.682 &= (x_1 - 20)/10, & x_1 &= 3.18 \end{aligned}$$

Using a model of the form

$$y = b_0 + b_1x_1 + b_2x_2 + b_3x_3 + b_{11}x_1^2 + b_{22}x_2^2 + b_{33}x_3^2 + b_{12}x_1x_2 + b_{13}x_1x_3 + b_{23}x_2x_3 \quad (3.6)$$

the coded design matrix for central composite design was set as in Table 3.12. The coefficients of the model were determined using pseudo-inverse function (Equation

3.3) and are given in Table 3.13. The predicted responses and residuals are presented in Table 3.14.

Table 3.12 Coded central composite design matrix with average response values

<i>Exp</i>	x_0	x_1	x_2	x_3	x_1x_1	x_2x_2	x_3x_3	x_1x_2	x_1x_3	x_2x_3	<i>y</i>
1	1	-1	-1	-1	1	1	1	1	1	1	1.973
2	1	1	-1	-1	1	1	1	-1	-1	1	2.223
3	1	-1	1	-1	1	1	1	-1	1	-1	1.672
4	1	1	1	-1	1	1	1	1	-1	-1	2.089
5	1	-1	-1	1	1	1	1	1	-1	-1	1.566
6	1	1	-1	1	1	1	1	-1	1	-1	2.070
7	1	-1	1	1	1	1	1	-1	-1	1	1.956
8	1	1	1	1	1	1	1	1	1	1	2.239
9	1	0	0	0	0	0	0	0	0	0	2.264
10	1	-1.682	0	0	2.829	0	0	0	0	0	1.841
11	1	1.682	0	0	2.829	0	0	0	0	0	2.347
12	1	0	-1.682	0	0	2.829	0	0	0	0	2.012
13	1	0	1.682	0	0	2.829	0	0	0	0	1.961
14	1	0	0	-1.682	0	0	2.829	0	0	0	2.231
15	1	0	0	1.682	0	0	2.829	0	0	0	2.127
16	1	0	0	0	0	0	0	0	0	0	2.276
17	1	0	0	0	0	0	0	0	0	0	2.243
18	1	0	0	0	0	0	0	0	0	0	2.331
19	1	0	0	0	0	0	0	0	0	0	2.220
20	1	0	0	0	0	0	0	0	0	0	2.236

Factors: x_1 , length of reaction coil; x_2 , carrier HCl concentration; x_3 , NaBH₄ concentration. *y*; integrated absorbance

Table 3.13 Coefficients for the model

b_0	b_1	b_2	b_3	b_{11}	b_{22}	b_{33}	b_{12}	b_{13}	b_{23}
2.2648	0.1688	0.002684	-0.02203	-0.08076	-0.1188	-0.05083	-0.00668	0.01503	0.1243

Table 3.14 The predicted responses and residuals

y	<i>Predicted y</i>	<i>Residual</i>
1.973	1.998	-0.025
2.223	2.319	-0.095
1.672	1.768	-0.096
2.089	2.062	0.027
1.566	1.675	-0.109
2.070	2.056	0.014
1.956	1.942	0.014
2.239	2.297	-0.057
2.264	2.265	0.000
1.841	1.752	0.089
2.347	2.320	0.027
2.012	1.924	0.088
1.961	1.933	0.028
2.231	2.158	0.073
2.127	2.084	0.043
2.276	2.265	0.011
2.243	2.265	-0.022
2.331	2.265	0.066
2.220	2.265	-0.045
2.236	2.265	-0.029
Residual sum of squares		0.067336
Mean square residual error (s)		0.006734

The variance of each of the ten parameters in the model was calculated as follows. The matrix $(D' \cdot D)^{-1}$ was calculated. This was a square matrix with dimensions equal to the parameters (10) in the model (Table 3.15). For each of the parameters, the appropriate number from the matrix is called the variance (v) for each parameter.

Table 3.15 Calculation of t-statistics

	b_0	b_1	b_2	b_3	b_{11}	b_{22}	b_{33}	b_{12}	b_{13}	b_{14}
b_0	0.166343	0	0	0	-0.05679	-0.05679	-0.05679	0	0	0
b_1	0	0.073216	0	0	0	0	0	0	0	0
b_2	0	0	0.073216	0	0	0	0	0	0	0
b_3	0	0	0	0.073216	0	0	0	0	0	0
b_{11}	-0.05679	0	0	0	0.069365	0.006895	0.006895	0	0	0
b_{22}	-0.05679	0	0	0	0.006895	0.069365	0.006895	0	0	0
b_{33}	-0.05679	0	0	0	0.006895	0.006895	0.069365	0	0	0
b_{12}	0	0	0	0	0	0	0	0.125	0	0
b_{13}	0	0	0	0	0	0	0	0	0.125	0
b_{14}	0	0	0	0	0	0	0	0	0	0.125
sv	0.00112	0.00049	0.00049	0.00049	0.00047	0.00047	0.00047	0.00084	0.00084	0.00084
(sv) ^{1/2}	0.03347	0.02220	0.02220	0.02220	0.02161	0.02161	0.02161	0.02901	0.02901	0.02901
b	2.26480	0.16882	0.00268	-0.02203	-0.08076	-0.11880	-0.05083	-0.00668	0.01503	0.12429
t	67.671	7.603	0.121	-0.992	-3.737	-5.497	-2.352	-0.230	0.518	4.284
	b_0	b_1	b_2	b_3	b_{11}	b_{22}	b_{33}	b_{12}	b_{13}	b_{23}

The diagonal elements were taken for each parameter and these were multiplied by the mean square residual error, s , (Table 3.14) as given as the first row under the matrix in Table 3.15. Mean square residual error was calculated by dividing the residual sum of squares to the degrees of freedom. For each coefficient b , t -statistics was calculated by

$$t = b/(sv)^{1/2} \quad (3.7)$$

The significance of the parameters can be assessed by this ratio; the higher this ratio, the more significant is the coefficient. This ratio is also used for t -test. The analysis of the results showed that out of all the three factors studied, the length of the reaction coil had the highest influence on the response. Some interactions and quadratic terms were also significant. Quadratic terms are important since they allow curvature which is one way of obtaining a maximum or minimum. The interaction terms shows that the influence of two factors on the response is dependent. For example, the results in Table 3.15 revealed that the effects of carrier HCl concentration and NaBH_4 concentration were depending on each other.

Taking partial derivatives of the equation,

$$y = 2.26480 + 0.16882x_1 + 0.00268 x_2 - 0.02203 x_3 - 0.08076x_1^2 - 0.11880 x_2^2 - 0.05083 x_3^2 - 0.00668 x_1x_2 + 0.01503 x_1x_3 + 0.12429 x_2x_3 \quad (3.8)$$

the optimum conditions were determined using coded values of the three factors. These were then converted to the real experimental values. Equations were set up as follows:

$$\partial y/\partial x_1 = 0.16882 - 0.16152 x_1 - 0.00668 x_2 + 0.01503 x_3 = 0 \quad (3.9)$$

$$\partial y/\partial x_2 = 0.00268 - 0.2376 x_2 - 0.00668 x_1 + 0.124 x_3 = 0 \quad (3.10)$$

$$\partial y / \partial x_3 = -0.02203 - 0.10166x_3 + 0.01503x_1 + 0.12429x_2 = 0 \quad (3.11)$$

Solving for these equations, the obtained coded and real values of the factors are given in Table 3.16.

Table 3.16 Coded and real optimum values for generation of Cd species

<i>Factor</i>	<i>Coded Value</i>	<i>Real Value</i>
Reaction coil length, cm	1.027	30
Carrier HCl, M	-0.140	0.30
%NaBH ₄ , (w/v)	-0.235	3.0

Response surfaces estimated from central composite design for the three parameters are shown in Figures 3.15-3.17. This is another way of locating the optimum.

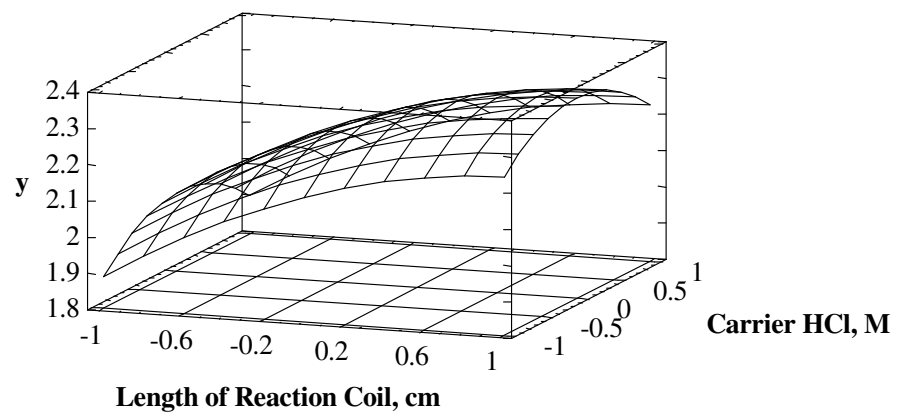


Figure 3.15 Estimated response surface for length of reaction coil vs carrier HCl concentration

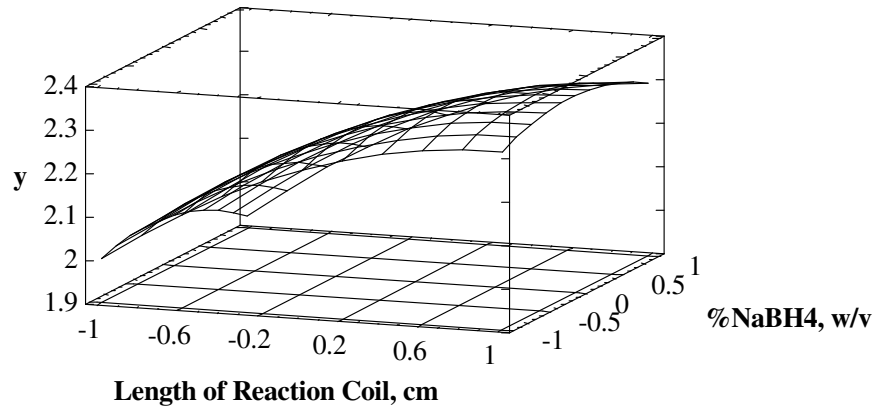


Figure 3.16 Estimated response surface for length of reaction coil vs NaBH_4 concentration

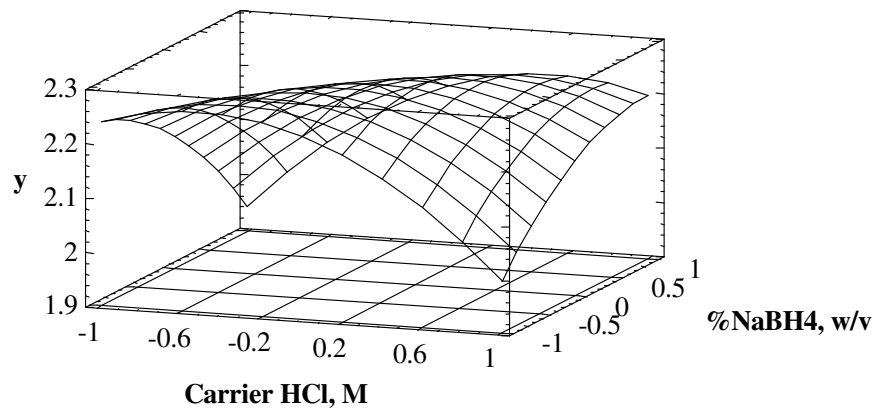


Figure 3.17 Estimated response surface for carrier HCl concentration vs NaBH_4 concentration

For the rest of the studies, the optimum values given in Table 3.16 were used for reaction coil length, carrier HCl and NaBH₄ concentrations. The length of the stripping coil was and flow of carrier Ar were kept constant at 20.0 cm and 170 ml min⁻¹, respectively. The effect of flow of Ar on response is shown in Figure 3.18.

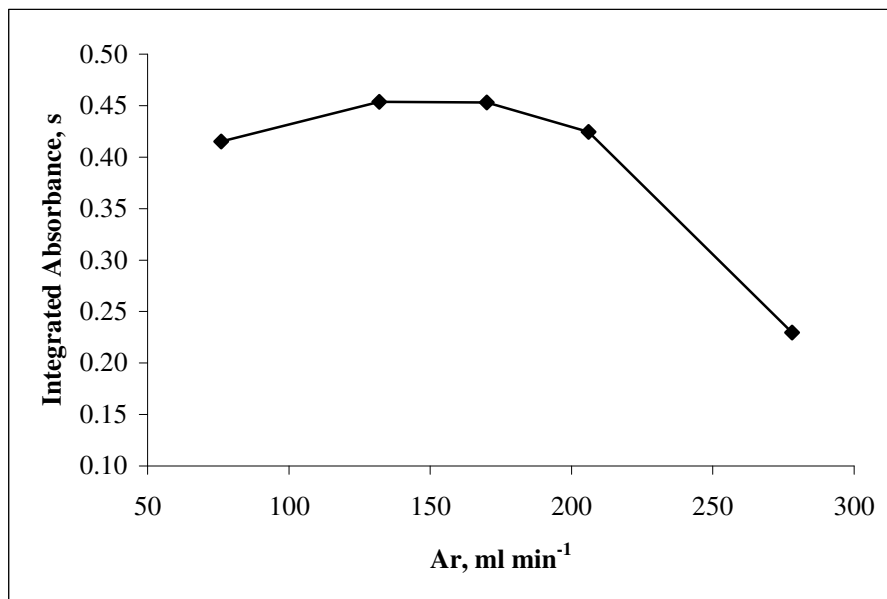


Figure 3.18 Effect of Ar flow on FI signal. 1 ng ml⁻¹ Cd, 100 µl loop

An Ar flow rate lower than 170 ml min⁻¹ was not preferred since it reduced the amount of condensation in the transfer tubings.

3.3.3 Double Peaks in FI Cold Vapour Generation of Cd

Generation conditions for volatile Cd species are rather critical and requires careful control of the parameters. Unlike the other hydrides, sample and carrier acid

concentrations may vary and are critical. The experiments showed that higher acid concentrations in the carrier as compared to sample (as an example, 0.2 M for sample and 0.3 M for carrier) resulted in double peaks in FI mode using 100 μL sample loop. Electronegativity (ϵ) of elements of interest, Sb ($\epsilon = 1.8$) and Pb ($\epsilon = 1.6$) as compared with the ϵ figure for the hydrogen atom ($\epsilon = 2.2$) represents an estimate of the covalent character of the E-H bond in the molecule of hydride produced. Generally, the elements in the upper right side of the Periodic Table yield hydrides with a more pronounced covalent character and relevant stability; they are generated and transported to the atomization cell with high efficiency (As, Se, Sb). On the contrary, the elements situated downwards (Sn, Bi, Pb) and particularly in the bottom left corner (In, Tl, Cd) are more problematic [11]. Lampugnani et al. [122] suggested that because of substantial differences in electronegativity of Cd ($\epsilon = 1.5$) and H, the covalent character of chemical bond in CdH_2 should be less pronounced than with other, more electronegative hydride forming elements; therefore this hydride could be expected to be less stable by itself as well as in acidic medium.

The resulting double peaks in our case could be explained by the incomplete generation of hydride; Cd^{2+} ions remaining in the reaction mixture or on the walls of the GLS could have been converted to the hydride with an additional hydrogen radical front.

3.3.4 Optimization of Collection and Revolatilization

The decrease in integrated absorbance values for Cd as a function of temperature of the trapping region was depicted in Figure 3.19. The peak area values were reduced by 90% when the inlet arm of quartz T tube was (Figure 2.10) heated to 350 $^{\circ}\text{C}$, indicating retention of Cd species on quartz surface. It should be mentioned that the

inlet arm was filled with 6-7 pieces of quartz in this configuration; with a bare inlet arm or with fewer pieces of quartz in the inlet arm, the reduction in the signal never exceeded 50%, indicating incomplete trapping. Even with this configuration, 100% trapping was not achieved but no further attempt was made to increase the amount of filling material in the trapping region since this would result in broader revolatilization peaks.

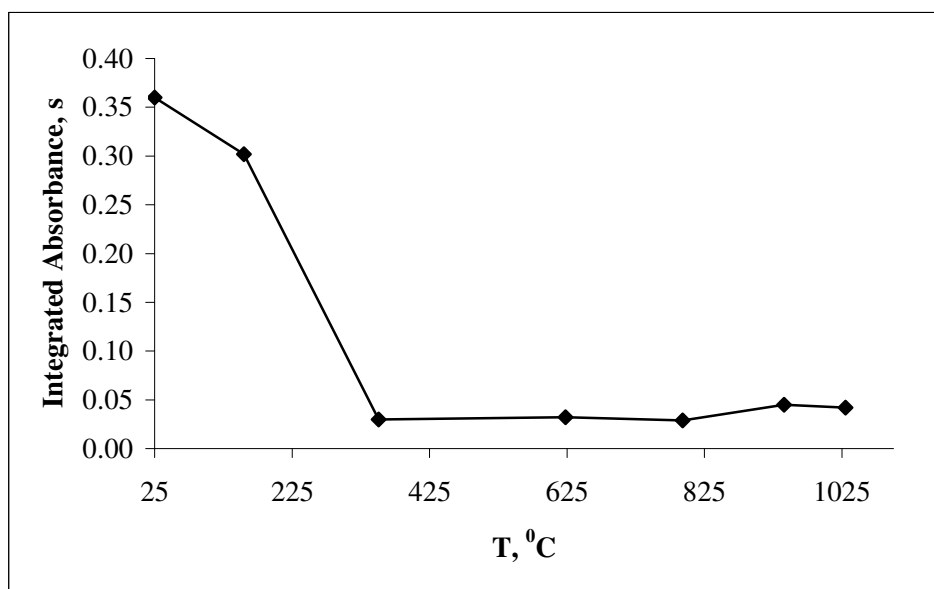


Figure 3.19 Changes in signal when the trap was operated during FI of 100 μl , 1.0 ng ml^{-1} Cd

The results for optimization of collection and revolatilization temperatures are given in Figure 3.20. The optimum trapping temperature found, 350 $^{\circ}\text{C}$, was relatively low as compared to Pb and Sb. The decrease in the signal for the collection temperatures higher than 350 $^{\circ}\text{C}$ was due to the release of some of the analyte species from the quartz surface (incomplete trapping). The optimum revolatilization temperature was reached 60 s after increasing the voltage difference from 1.4 to 4.1 V. Actually, with

a bare inlet arm, a temperature of 1000 °C was already reached 35 s after increasing the voltage difference (Figure 2.9). The need for an additional 25 s was attributed to the fact that the inlet arm was filled with quartz pieces and time was needed to bring all the pieces to the same temperature.

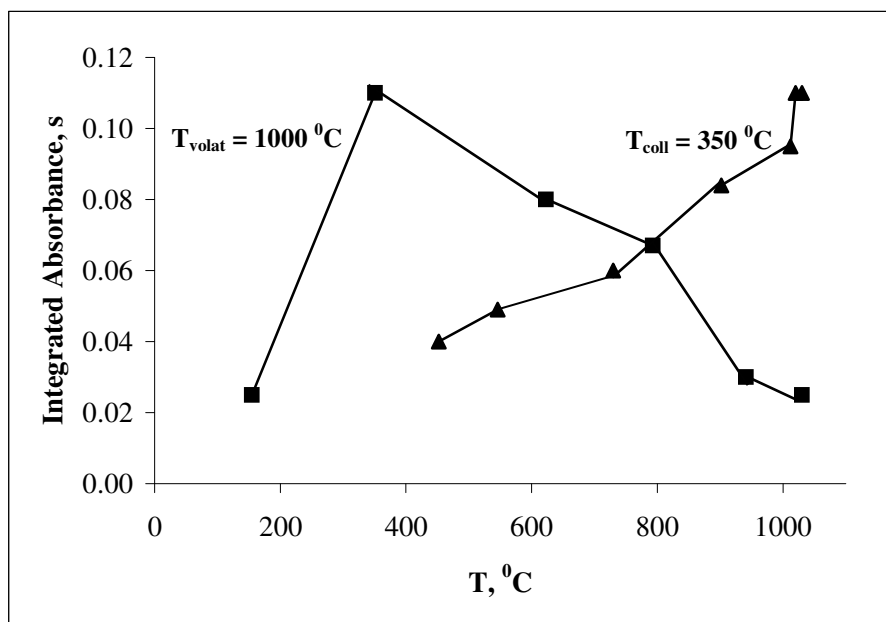


Figure 3.20 Influence of collection temperature (squares, volatilization temperature of 1000 °C) and revolatilization temperature (triangles, collection temperature of 350 °C) on the observed signal; 0.3 ng Cd

3.3.5 Effect of Carrier Gas

Use of a mixture of 1% O₂ + 99% Ar as carrier gas reduced the analytical response of Cd 25% even for the case of FI mode experiments in which the species were generated and detected at room temperature and no trapping was applied. This may be due to the formation of CdO, which may be remaining in the reaction mixture or

may not be atomizing even if it reaches the optical path. When mixture of Ar and O₂ was used in trap experiments the reduction in the atomization signal was 50% as compared to Ar alone. Here, the presence of O₂ should be affecting not only generation but also revolatilization step. Although these experiments were not direct evidences, the negative effect of O₂ may suggest that both the collected and revolatilized species were atomic Cd.

Use of a higher flow of Ar for revolatilization step was also tried to see if it would have any beneficial effect on the analytical signal. However, the flows higher than 170 ml min⁻¹ decreased the integrated absorbance values due to the dilution effect. Therefore, Ar gas at a flow of 170 ml min⁻¹ for both collection and revolatilization steps.

3.3.6 Effect of H₂ Flow

In order to revolatilize the collected species, only heating the trap to the revolatilization temperature was not sufficient. The presence of H₂ gas at was essential which was in accordance with the observations for Pb and Sb. As for Sb, H₂ gas was introduced after reaching the revolatilization temperature; introduction of H₂ at the beginning of revolatilization step caused broad signals. 200 ml min⁻¹ was chosen as optimum for H₂ flow (Figure 3.21).

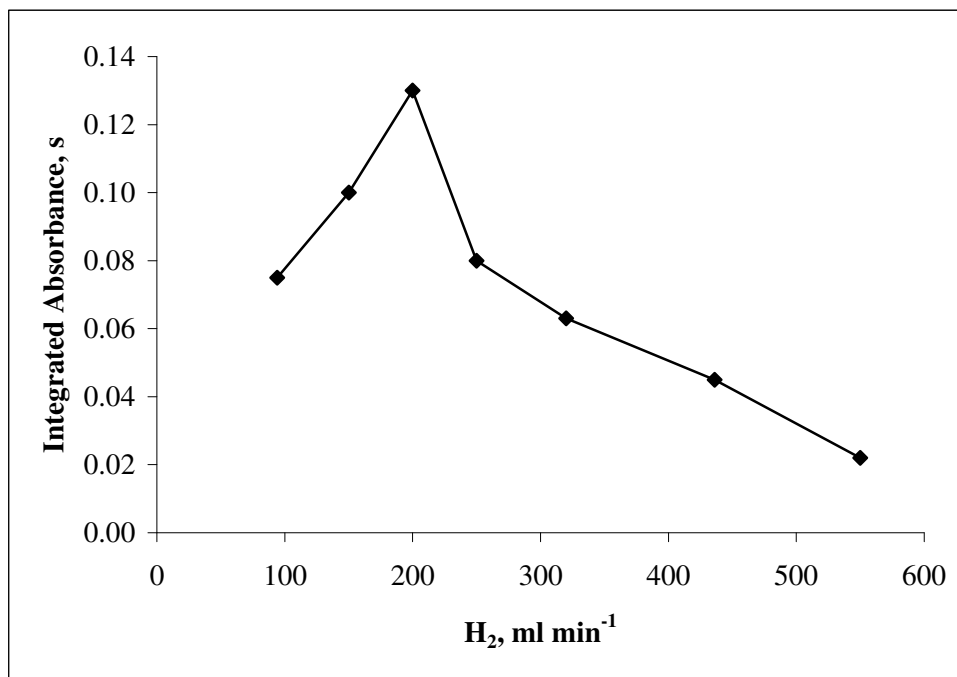


Figure 3.21 The influence of the H₂ flow rate on peak area for revolatilization

3.3.7 Effect of Filling Materials

Apart from the quartz pieces, quartz frit (porous quartz disc) pieces were also tried as filling material to understand if they would act as a better trapping medium for Cd. Unfortunately, it was not possible to revolatilize the analyte from quartz frit, possibly due to the diffusion of analyte species into the pores.

Use of 6-7 pieces of quartz pieces was necessary to efficiently trap the hydride. The typical analytical signal shape observed with this configuration is shown in Figure 3.22. The FWHM is approximately 0.9 s, use of more filling material caused broader peaks.

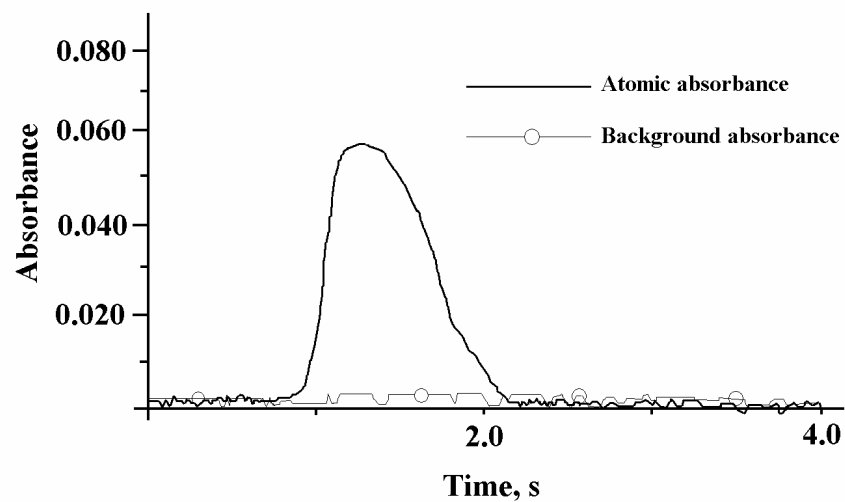


Figure 3.22 The typical signal shape observed. Collection temperature: 350 °C; revolatilization temperature: 1000 °C; 20 pg ml⁻¹ Cd, 3 min. collection. Peak height: 0.057; peak area: 0.051. Seven pieces of quartz piece as filling material in the trapping medium

In Figure 3.23, the signal profile for 3 pieces of quartz is seen for the same collection and revolatilization conditions. Here, release of the species is faster but the sensitivity drops significantly due to incomplete trapping.

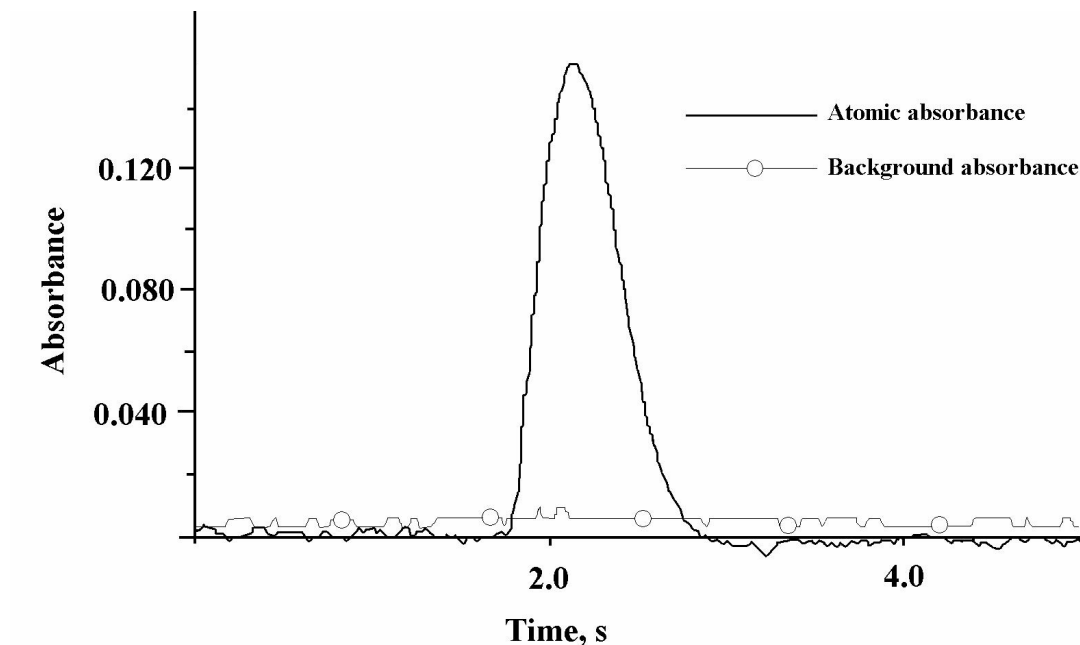


Figure 3.23 The signal shape observed for 3 pieces of quartz piece as filling material in the trapping medium. Collection temperature: 350 °C; revolatilization temperature: 1000 °C; 75 pg ml⁻¹ Cd, 3 min. collection. Peak height: 0.155; peak area: 0.079

3.3.8 Analytical Figures of Merit

3σ LODs, characteristic masses (m_0) and characteristic concentrations (c_0), calculated by using integrated absorbances, were summarized in Table 3.17. The enhancement factor for the LOD for a collection time of 180 s (corresponding to sample volume of 6.0 ml) was found to be 90 as compared to FI HGAAS. The precision of measurements was 5% RSD ($n = 10$). For a collection time of 3 minutes, the calibration plot was linear between 20-100 pg ml⁻¹ with a best line equation and correlation coefficient of $y = 0.0025x - 0.0001$ and 0.999, respectively,

where C was the concentration of Cd in pg ml^{-1} (Figure 3.24). No purification of the used reagents were required owing to the low blank values.

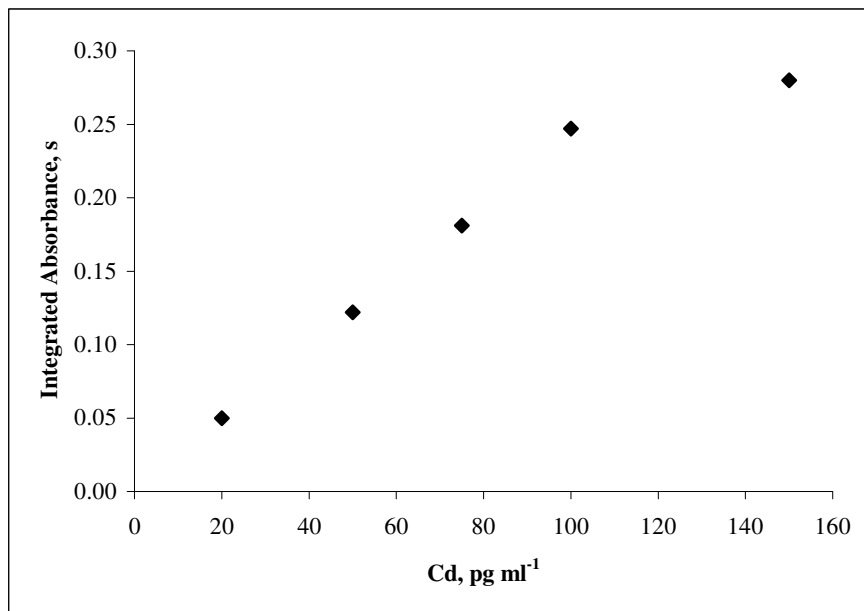


Figure 3.24 Calibration plot for 180 s collection; total sample volume was 6.0 ml

Collection times more than 180 s were not used for practical reasons. Sample throughput rate for a collection of 180 s was 12 per hour. Better rates can be obtained using lower collection times (Figure 3.25). The lifetime of filling material was not less 100 measurements.

Table 3.17 Comparison of analytical figures of merit using integrated absorbances. Collection time for quartz trap was 180 s with a sample solution flow rate of 2.0 ml min⁻¹.

	$c_0, \text{pg ml}^{-1}$	m_0, pg	$LOD, \text{pg ml}^{-1}$
FI HGAAS (100 μl loop)	12.2	1.2	164
Quartz Trap	1.7	10.2	1.8

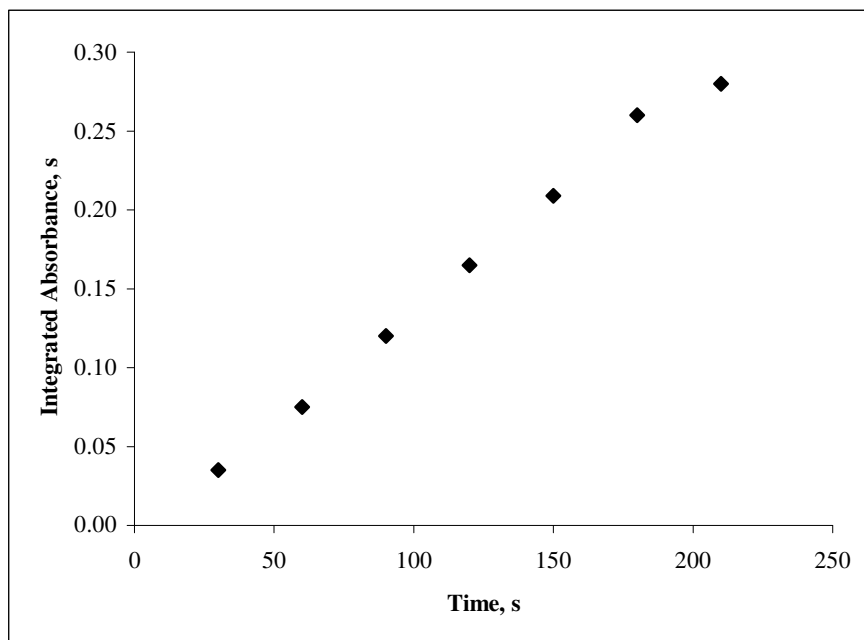


Figure 3.25 Analytical signal vs collection time for 0.1 ng ml⁻¹ Cd flowing at a rate of 2 ml min⁻¹

The proposed method was applied to the analysis of standard reference materials for accuracy assessment. The results were presented in Table 3.18. Good agreement with the certified values is evident. For the analysis of sea water SRM,

direct calibration was applied. Calibration by standard additions was adopted for the analysis of tomato leaves and oyster tissue SRMs.

Table 3.18 Determination of Cd in SRMs

<i>SRM</i>	<i>Certified</i>	<i>Found</i>
Trace Elements in Seawater, nmol kg ⁻¹	0.175 ± 0.018	0.180 ± 0.009
1573a Tomato Leaves, mg kg ⁻¹	1.52 ± 0.04	1.50 ± 0.06
1566b Oyster Tissue, mg kg ⁻¹	2.48 ± 0.08	2.45 ± 0.15

The LOD obtained is the same as the best attained as compared to the values in the literature obtained with *in-situ* trapping in graphite furnace; in pg ml⁻¹, 10 [113, 119], 5 [118], 7 [120] and 2 [122].

CHAPTER 4

CONCLUSIONS

One of the inherent advantages of generation of volatile forms of analyte for analytical atomic spectrometry is that the analyte can be easily preconcentrated either in a special collection device, usually by cryogenic trapping, or directly in the atomizer. The cryogenic collection is time consuming and much labor is involved therefore, in-atomizer trapping is the most convenient way of analyte collection. Until recently, the only widely used approach to in-atomizer trapping was *in-situ* trapping in commercial graphite furnaces. The main advantage of this technique is a very high sensitivity made possible by the collection.

This study illustrated the use of heated quartz surface for trapping of Pb and Sb hydrides and Cd species. The novel on-line quartz trap could possibly be used for other hydride forming elements. It should be noted that since the separated quartz trap worked, the device can be coupled with any system for atomic measurements, such as inductively coupled plasma atomic emission spectrometer or inductively coupled plasma mass spectrometer.

The trap may also be interpreted as a result of efforts to study and eliminate the pre-peaks; these are normally a source of nuisance, but now after proper taming a powerful analytical tool has been obtained.

The trap is interesting in that it works as an on-line preconcentration device. In addition, the related studies may shed a light on the mechanisms of trapping, revolatilization and atomization of analyte species. In the case of the analytes studied in this work, the presence of hydrogen radicals should be playing an important role on revolatilization, since hydrogen gas and a temperature of at least 750⁰C were needed simultaneously. Oxygen seems to be required for process of revolatilization of Pb and Sb. The transported species are believed to be at least partially atomic for the case of Pb. The need for O₂ in revolatilization may suggest that some of the transported species may be oxides. The negative effect of oxygen on both FI and trap signals of Cd suggests that Cd species were both collected and revolatilized in atomic form. Further studies are required to clearly understand the nature of the species collected on quartz surface.

Following the stage of trapping, the performance of the device and the problems related are quite similar to the case of electrothermal vaporizers (ETV). The role of carrier species in ETV devices are well known. Similar carriers may also be effective in our novel quartz trap.

A side product of this study is useful for conventional HGAAS determination of Pb, heating the inlet arm of the quartz tube atomizer results in a sensitivity enhancement of approximately 50%.

The incomplete collection / revolatilization (50-65% efficiency) indicates that the present system is not at an optimum. Significantly better performance should be expected when the efficiency was improved. For the optimum performance of the technique, it is desirable to trap hydride and transport the revolatilized analyte to the atomizer completely. Otherwise, not only the maximum sensitivity is not reached but a deviation in an experimental parameter may lead to significant change in

collection / revolatilization efficiencies, and thus also in sensitivity. This can negatively influence both the accuracy and repeatability of the analysis.

It should be emphasized that as long as a simple quartz tube atomizer is used in connection with this quartz trap, the overall analytical technique is very economical, yet quite powerful, operating in the range of ng l⁻¹. For Sb and Cd, the detection limits provided are the same as the best detection limits attained with *in-situ* trapping in graphite furnace. 3 σ LODs and characteristic masses (m_0) attained for the elements of interest are summarized in Table 4.1.

Table 4.1 Summary of 3 σ LODs and characteristic masses (m_0) attained

<i>Element</i>	<i>Technique</i>	<i>m_0, pg</i>	<i>LOD, pg ml⁻¹</i>
<i>Pb</i>	HGAAS (250 μ l loop)	116	120
	Quartz trap (60 s collection)	238	19
<i>Sb</i>	HGAAS (2.0 ml sample)	18	130
	Quartz trap (120 s collection)	75	3.9
<i>Cd</i>	Cold Vapour Generation (100 μ l loop)	1.2	164
	Quartz trap (180 s collection)	10.2	1.8

The following two articles were published from this work.

1. D. K. Korkmaz, N. Ertaş, O. Y. Ataman, A Novel Silica Trap for Lead Determination by Hydride Generation Atomic Absorption Spectrometry, *Spectrochim. Acta Part B*, 2002, **57**, 571-580.

2. D. Korkmaz, J. Dědina, O. Y. Ataman, Stibine Preconcentration in a Quartz Trap with Subsequent Atomization in the Quartz Multiatomizer for Atomic Absorption Spectrometry, *J. Anal. At. Spectrom.*, 2004, **19**, 255-259.

REFERENCES

1. B. Welz, M. Sperling, Atomic Absorption Spectrometry, Third, Completely Revised Edition, Wiley, Weinheim, 1999.
2. A. Walsh, The Application of Atomic Absorption Spectra to Chemical Analysis, *Spectrochim. Acta*, 1955, **7**, 108-117.
3. J. A. C. Broekaert, Analytical Atomic Spectrometry with Flames and Plasmas, Wiley, Weinheim, 2002.
4. T. A. M. Ure, L. R. P. Butler, B. V. L'Vov, I. Rubeska, R. Sturgeon, Nomenclature, Symbols, Units and Their Usage in Spectrochemical Analysis – XIII. Terms Related to Chemical Vapour Generation (IUPAC Recommendations 1992), *Spectrochim. Acta Part B*, 1997, **52**, 2021-2024.
5. J. Dědina, D. L. Tsalev, Hydride Generation Atomic Absorption Spectrometry, Wiley, Chichester, 1995.
6. W. Holak, Gas-Sampling Technique for Arsenic Determination by Atomic Absorption Spectrometry, *Anal. Chem.*, 1969, **41**, 1712-1713.
7. D. Yan, Z. Yan, G. -S. Cheng, A. -M. Li, Determination of Indium and Thallium by Hydride Generation and Atomic Absorption Spectrometry, *Talanta*, 1984, **31**, 133-134.

8. K. Fujiwara, M. A. Mignardi, G. Petrucci, B. W. Smith, J. D. Winefordner, Determination of Phosphorous by ICP-AES Using Solid-Phase Hydride Generation, *Spectrosc. Lett.*, 1989, **22**, 1125-1140.
9. A. G. Howard, D. W. Russell, Borohydride-Coupled HPLC-FPD Instrumentation and Its Use in the Determination of Dimethylsulfonium Compounds, *Anal. Chem.*, 1997, **69**, 2882-2887.
10. D. L. Tsalev, Hyphenated Vapour Generation Atomic Absorption Spectrometric Techniques, *J. Anal. At. Spectrom.*, 1999, **14**, 147-162.
11. D. L. Tsalev, Vapor Generation or Electrothermal Atomic Absorption Spectrometry? – Both!, *Spectrochim. Acta Part B*, 2000, **55**, 917-933.
12. E. Denkhaus, A. Golloch, X.-M. Guo, B. Huang, Electrolytic Hydride Generation (EC-HG) – A Sample Introduction System with Some Special Features, *J. Anal. At. Spectrom.*, 2001, **16**, 870-878.
13. J. S. Blais, G. M. Momplaisir, W. D. Marshall, Determination of Arsenobetaine, Arsenocholine, and Tetramethylarsonium Cations by Liquid Chromatography – Thermochemical Hydride Generation – Atomic Absorption Spectrometry, *Anal. Chem.*, 1990, **62**, 1161-1166.
14. F. Laborda, E. Bolca, J. R. Castillo, Tubular Electrolytic Hydride Generator for Continuous and Flow Injection Sample Introduction in Atomic Absorption Spectrometry, *J. Anal. At. Spectrom.*, 2000, **15**, 103-107.
15. J. S. Blais, G. M. Momplaisir, W. D. Marshall, Determination of Arsenobetaine, Arsenocholine, and Tetramethylarsonium Cations by Liquid Chromatography – Thermochemical Hydride Generation – Atomic Absorption Spectrometry, *Anal. Chem.*, 1990, **62**, 1161-1166.
16. Y.-L., Feng, R. E. Sturgeon, J. W. Lam, Chemical Vapor Generation Characteristics of Transition and Noble Metals Reacting with Tetrahydroborate, *J. Anal. At. Spectrom.*, 2003, **18**, 1435-1442.

17. W. B. Robbins, J. A. Caruso, Development of Hydride Generation Methods for Atomic Spectroscopic Analysis, *Anal. Chem.*, 1979, 51, 889A-899A.
18. A. D'Ulivo, C. Baiocchi, E. Pitzalis, M. Onor, R. Zamboni, Chemical Vapor Generation for Atomic Spectrometry. A Contribution to the Comprehension of Reaction Mechanisms in the Generation of Volatile Hydrides Using Borane Complexes, *Spectrochim. Acta Part B*, 2004, **59**, 471-486.
19. F. Laborda, E. Bolea, M. T. Baranguan, J. R. Castillo, Hydride Generation in Analytical Chemistry and Nascent Hydrogen: When is it Going to be Over?, *Spectrochim. Acta Part B*, 2002, **57**, 797-802.
20. S. A. Pergantis, W. Winnik, E. H. Heithmar, W. R. Cullen, Investigation of Arsine-Generating Reactions Using Deuterium-Labelled Reagents and Mass Spectrometry, *Talanta*, 1997, **44**, 1941-1947.
21. R. M. Jr. Brown, R. C. Fry, J. L. Moyers, S. J. Northway, M. B. Denton, G. S. Wilson, Interference by Volatile Nitrogen Oxides and Transition Metal Catalysis in the Preconcentration of Arsenic and Selenium as Hydrides, *Anal. Chem.*, 1981, **53**, 1560-1566.
22. A. D'Ulivo, V. Loti, M. Onor, E. Pitzalis, R. Zamboni, Chemical Vapor Generation Atomic Spectrometry Using Amineboranes and Cyanotrihydroborate(III) Reagents, *Anal. Chem.*, 2003, **75**, 2591-2600.
23. D. D. Siemer, L. Hagemann, An Improved HG AA Apparatus for Se Determination, *Anal. Lett.*, 1975, **8**, 323-337.
24. J. Dědina, Hydride Generation and Atomization for AAS, *Prog. Analyt. Spectrosc.*, 1988, **11**, 251-360.
25. J. Dědina, I. Rubeska, Hydride Atomization in a Cool Hydrogen-Oxygen Flame Burning in a Quartz Tube Atomizer, *Spectrochim. Acta Part B*, 1980, **35**, 119-128.

26. J. Dědina, B. Welz, QTAs for HGAAS: Mechanism for the Atomization of Arsine, *J. Anal. At. Spectrom.*, 1992, **7**, 307-314.
27. J. Dědina, B. Welz, Quartz Tube Atomizers for Hydride Generation Atomic Absorption Spectrometry: Fate of Free Arsenic Atoms, *Spectrochim. Acta Part B*, 1993, **48**, 301-314.
28. S. Tesfalidet, G. Wikander, K. Irgum, Determination of Hydrogen Radicals in Analytical Flames Using Electron Spin Resonance Spectroscopy Applied to Direct Investigations of Flame-Based Atomization Units for Hydride Generation Atomic Absorption Spectrometry, *Anal. Chem.*, 1999, **71**, 1225-1231.
29. K. C. Thompson, D. R. Thomerson, AA Studies on the Determination of Sb, As, Bi, Ge, Pb, Se, Te and Sn by Utilising the Generation of Covalent Hydrides, *Analyst*, 1974, **99**, 595-601.
30. R. C. Chu, G. P. Barron, P. A. W. Baumgarner, Arsenic Determination at Sub Microgram Levels by Arsine Evolution and Flameless Atomic Absorption Spectrophotometric Technique, *Anal. Chem.*, 1972, **44**, 1476-1479.
31. B. Welz, M. Melcher, Investigations on Atomisation Mechanisms of Volatile Hydride-Forming Elements in a Heated Quartz Cell Part 1. Gas-Phase and Surface Effects; Decomposition and Atomisation of Arsine, *Analyst*, 1983, **108**, 213-224.
32. B. Welz, M. Schubert-Jacobs, M. Sperling, D. L. Styris, D. A. Redfield, Investigation of Reactions and Atomization of Arsine in a Heated Quartz Tube Using Atomic Absorption and Mass Spectrometry, *Spectrochim. Acta Part B*, 1990, **45**, 1235-1256.
33. J. Dědina , T. Matoušek, Multiple Microflame –A New Approach to Hydride Atomization for Atomic Absorption Spectrometry, *J. Anal. At. Spectrom.*, 2000, **15**, 301-304.

34. H. Matusiewicz, R. E. Sturgeon, Atomic Spectrometric Detection of Hydride Forming Elements Following In-Situ Trapping within a Graphite Furnace, *Spectrochim. Acta Part B*, 1996, **51**, 377-397.
35. J. Dědina, Quartz Tube Atomizers for Hydride Generation Atomic Absorption Spectrometry: Mechanism of Selenium Hydride Atomization and Fate of Free Atoms, *Spectrochim. Acta Part B*, 1992, **47**, 689-700.
36. A. D'Ulivo, J. Dědina, Interferences in Hydride Atomization Studied by Atomic Absorption and Atomic Fluorescence Spectrometry, *Spectrochim. Acta Part B*, 1996, **51**, 481-498.
37. P. Grinberg, I. Takase, R. Calixto de Campos, Characterization and Vapour Phase Interference Studies of a Flame Heated Holed Quartz T-Tube as Atomization Cell for Hydride Generation Atomic Absorption Spectrometry, *J. Anal. At. Spectrom.*, 1999, **14**, 827-830.
38. X. Hou, B. T. Jones, Tungsten Devices in Analytical Atomic Spectrometry - Review, *Spectrochim. Acta Part B*, 2002, **57**, 659-688.
39. A. Sanz-Medel, M. C. Valdes-Hevia y Temprano, N. Bordel Garcia, M. R. Fernandez de la Campa, Generation of Cadmium Atoms at Room Temperature Using Vesicles and Its Application to Cadmium Determination by Cold Vapour Atomic Absorption Spectrometry, *Anal. Chem.*, 1995, **67**, 2216-2223.
40. P. Pohl, Recent Advances in Chemical Vapour Generation via reaction with Sodium Tetrahydroborate, *Trends in Anal. Chem.*, 2004, **23**, 21-27.
41. A. S. Luna, R. E. Sturgeon, R. C. de Campos, Chemical Vapor Generation: Atomic Absorption by Ag, Au, Cu, and Zn Following Reduction of Aquo Ions with Sodium Tetrahydroborate(III), *Anal. Chem.*, 2000, **72**, 3523-3531.
42. C. Moor, J. W. Lam, R. E. Sturgeon, A Novel Introduction System for Hydride Generation – Inductively Coupled Plasma Mass Spectrometry:

Determination of Selenium in Biological Materials, *J. Anal. At. Spectrom.*, 2000, **15**, 143-149.

43. Y.-L. Feng, J. W. Lam, R. E. Sturgeon, Expanding the Scope of Chemical Vapor Generation for Noble and Transition Metals, *Analyst*, 2001, **126**, 1833-1837.
44. T. Matoušek, J. Dědina, M. Vobecky, Continuous Flow Chemical Vapour Generation of Silver for Atomic Absorption Spectrometry Using Tetrahydroborate(III) Reduction – System Performance and Assessment of the Efficiency Using Instrumental Neutron Activation Analysis, *J. Anal. At. Spectrom.*, 2002, **17**, 52-56.
45. A. S. Luna, H. B. Pereira, I. Takase, R. A. Gonçalves, R. E. Sturgeon, R. C. de Campos, *Spectrochim. Acta Part B*, 2002, **57**, 2047-2056.
46. X. Duan, R. L. McLaughlin, I. D. Brindle, A. Conn, Investigations into the Generation of Ag, Au, Cd, Co, Cu, Ni, Sn and Zn, by Vapour Generation and Their Determination by Inductively Coupled Plasma Atomic Emission Spectrometry Together with a Mass Spectrometric Study of Volatile Species. Determination of Ag, Au, Co, Cu, Ni and Zn in Iron, *J. Anal. At. Spectrom.*, 2002, **17**, 227-231.
47. T. Matoušek, R. E. Sturgeon, Surfactant Assisted Chemical Vapour Generation of Silver for AAS and ICP-OES: A Mechanistic Study, *J. Anal. At. Spectrom.*, 2003, **18**, 487-494.
48. X. Du, S. Xu, Flow-Injection Chemical Vapor-Generating Procedure for the Determination of Au by Atomic Absorption Spectrometry, *Fresenius J. Anal. Chem.*, 2001, **370**, 1065-1070.
49. P. Pohl, W. Zyrnicki, Study of Chemical Vapour Generation of Au, Pd and Pt by Inductively Coupled Plasma Atomic Emission Spectrometry, *J. Anal. At. Spectrom.*, 2001, **16**, 1442-1445.

50. H. Ma, X. Fan, H. Zhou, S. Xu, Preliminary Studies on Flow-Injection in Situ Trapping of Volatile Species of Gold in Graphite Furnace and Atomic Absorption Spectrometric Determination, *Spectrochim. Acta Part B*, 2003, **58**, 33-41.
51. P. Pohl, W. Zyrnicki, On the Transport of Some Metals into Inductively Coupled Plasma During Hydride Generation Process, *Anal. Chim. Acta*, 2001, **429**, 135-143.
52. R. E. Sturgeon, J. Liu, V. J. Boyko, V. T. Luong, Determination of Copper in Environmental Matrices Following Vapor Generation, *Anal. Chem.*, 1996, **68**, 1883-1887.
53. P. Pohl, W. Zyrnicki, Study of the Reaction of Ir, Os, Rh and Ru Ions with NaBH_4 in the Acid Medium by the Inductively Coupled Plasma Atomic Emission Spectrometry, *J. Anal. At. Spectrom.*, 2002, **17**, 746-749.
54. X. -M. Guo, B. Huang, Z. Sun, R. Ke, Q. Wang, Z. B. Gong, Preliminary Study on a Vapor Generation Technique for Nickel Without Using Carbon Monoxide by Inductively Coupled Plasma Atomic Emission Spectrometry, *Spectrochim. Acta Part B*, 2000, **55**, 943-950.
55. J. Marrero, P. Smichowski, Evaluation of vapor Generation for the Determination of Nickel by Inductively Coupled Plasma – Atomic Emission Spectrometry, *Anal. Bioanal. Chem.*, 2002, **374**, 196-209.
56. H. Sun, R. Suo, Y. Lu, Determination of Zinc in Food Using Atomic Fluorescence Spectrometry by Hydride Generation from Organized Media, *Anal. Chim. Acta*, 2002, **457**, 305-310.
57. P. Smichowski, S. Farias, S. P. Arisnabarreta, Chemical Vapour Generation of Transition Metal Volatile Species for Analytical Purposes: Determination of Zn by Inductively Coupled Plasma Optical Emission Spectrometry, *Analyst*, 2003, **128**, 779-785.

58. N. Panichev, R. E. Sturgeon, Atomic Absorption by Free Atoms in Solution Following Chemical Reduction from the Ionic State, *Anal. Chem.*, 1998, **70**, 1670-1676.
59. X. -M. Guo, X. -W. Guo, Determination of Ultra-Trace Amounts of Selenium by Continuous Flow Hydride Generation AFS and AAS with Collection on Gold Wire, *J. Anal. At. Spectrom.*, 2001, **16**, 1414-1418.
60. O. Cankur, N. Ertaş, O. Y. Ataman, Determination of Bismuth Using On-Line Preconcentration by Trapping on Resistively Heated W Coil and Hydride Generation Atomic Absorption Spectrometry, *J. Anal. At. Spectrom.*, 2002, **17**, 603-609.
61. F. Barbosa Jr., S. S. de Souza, F. J. Krug, In Situ Trapping of Selenium Hydride in Rhodium-Coated Tungsten Coil Electrothermal Atomic Absorption Spectrometry, *J. Anal. At. Spectrom.*, 2002, **17**, 382-388.
62. R. J. Watling, The Use of a Slotted Quartz Tube for the Determination of Arsenic, Antimony, Selenium and Antimony, *Anal. Chim. Acta*, 1977, **94**, 181-186.
63. C. Lau, A. Held, R. Stephens, Sensitivity Enhancements to Flame AAS by Use of a Flame Atom Trap, *Can. J. Spectrosc.*, 1976, **21**, 100-104.
64. N. Ertaş, R. S. Helles, S. Kumser, O. Y. Ataman, Federation of Analytical Chemistry and Spectroscopy Societies, FACSS XX, Annual Conference, October 17-22 1993, Detroit, Michigan, USA.
65. S. Kumser, N. Ertaş, D. Karadeniz, R. S. Helles, H. Çalık, O. Y. Ataman, Federation of Analytical Chemistry and Spectroscopy Societies, FACSS XXIII, Annual Conference, September 29 – October 4 1996, Detroit, Michigan, USA.

66. D. Korkmaz, S. Kumser, N. Ertaş, M. Mahmut, O. Y. Ataman, Investigations on Nature of Revolatilization from Atom Trap Surfaces in Flame AAS, *J. Anal. At. Spectrom.*, 2002, **17**, 1610-1614.
67. G. Huang, S. Qian, H. Yang, Study of Slotted Quartz Tube Atom Trapping Atomic Absorption Spectrometry, *Ziran Kexueban Hua Xue Fen Xi*, 1995, **41**, 707-712.
68. N. Ertaş, D. Karadeniz Korkmaz, S. Kumser, O. Y. Ataman, Novel Traps and Atomization Techniques for Flame AAS, *J. Anal. At. Spectrom.*, 2002, **17**, 1415-1420.
69. D. Korkmaz, M. Mahmut, R. Helles, N. Ertaş, O. Y. Ataman, Interference Studies in Slotted Silica Tube Trap Technique, *J. Anal. At. Spectrom.*, 2003, **18**, 99-104.
70. D. R. Juberg, C. F. Kleiman, S. C. Kwon, Position Paper of the American Council on Science and Health: Lead and Human Health, *Ecotox. Environ. Safe.*, 1997, **38**, 162-180.
71. C. Camara, Y. Madrid, Lead Hydride Generation Atomic Absorption Spectrometry: An Alternative to Electrothermal Atomic Absorption Spectrometry, *Analyst*, 1994, **119**, 1647-1658.
72. K. Jin, M. Taga, Determination of Lead by Continuous Flow Hydride Generation and Atomic Absorption Spectrometry Comparison of Malic Acid – Dichromate, Nitric Acid – Hydrogen Peroxide and Nitric Acid – Peroxodisulfate Reaction Matrices in Combination with Sodium Tetrahydroborate, *Anal. Chim. Acta*, 1982, **143**, 229-236.
73. J. R. Castillo, J. M. Mir, C. Martinez, J. Val, M. P. Colon, Influence of Oxidising Agents in Lead Determination by Hydride Generation Direct Flame Atomic Absorption Spectroscopy, *Mikrochim. Acta*, 1985, **1**, 253-263.

74. J. F. Tyson, R. I. Ellis, G. Carrick, F. Fernandez, Flow Injection Hydride Generation Electrothermal Atomic Absorption Spectrometry with In-Atomizer Trapping for the Determination of Lead in Calcium Supplements, *Talanta*, 2000, **52**, 403-410.
75. I. Brindle, R. McLaughlin, N. Tangtreamjitmun, Determination of Lead in Calcium Carbonate by Flow-Injection Hydride Generation with DC Plasma Atomic Emission Detection, *Spectrochim. Acta Part B*, 1998, **53**, 1121-1129.
76. S. -Z. Zhang, H. -B. Han, Z. -M. Ni, Determination of Lead by Hydride Generation Atomic Absorption Spectrometry in the Presence of Nitroso-R Salt, *Anal. Chim. Acta*, 1989, **221**, 85-90.
77. H. Chen, F. Tang, C. Gu, I. D. Brindle, The Influence of Chelating Reagents on Plumbane Generation: Determination of Lead in the Presence of PAN-S, *Talanta*, 1993, **40**, 1147-1155.
78. A. D'Ulivo, P. Papoff, Non-Dispersive Atomic-Fluorescence Spectrometric Determination of Lead by the Hydride-Generation Technique, *Talanta*, 1985, **32**, 383-386.
79. Y. Madrid, D. Chakraborti, C. Camara, Evaluation of Flow-Injection in Lead Hydride Generation Atomic Absorption Spectrometry, *Mikrochim. Acta*, 1995, **120**, 63-72.
80. D. Erber, L. Quick, F. Winter, K. Cammann, Investigations for the determination of Lead by In-Situ Hydride Trapping Within a Graphite Electrothermal Atomizer for Routine Analysis, *Talanta*, 1995, **42**, 927-936.
81. M. Chikuma, H. Aoki, Preconcentration of Lead (II) in Environmental Waters Using a Chelating Resin and Subsequent Determination as a Resin-Water Suspension by Hydride Generation Atomic Absorption Spectrometry, *J. Anal. At. Spectrom.*, 1993, **8**, 415-417.

82. M. Chikuma, H. Aoki, Preconcentration Atomic Absorption Spectrophotometric Determination of Trace Lead (II) by Hydride Generation Combined with an Adsorbent Water Suspension Sampling Technique, *Microchem. Journal*, 1994, **49**, 368-377.
83. H. O. Haug, Study on Stable Coatings for determination of Lead by Flow-Injection Hydride Generation and In-Situ Concentration in Graphite Furnace Atomic Absorption Spectrometry, *Spectrochim. Acta Part B*, 1996, **51**, 1425-1433.
84. M. C. Valdes-Hevia y Temprano, M. R. Fernandez de la Campa, A. Sanz-Medel, Comparison of Plumbane and Tetraethyllead for the Determination of Lead by Inductively Coupled Plasma Atomic Emission Spectrometry, *Anal. Chim. Acta*, 1995, **309**, 369-378.
85. P. Bermejo-Barrera, J. Moreda-Pineiro, A. Moreda-Pineiro, A. Bermejo-Barrera, Direct Trace Determination of Lead in Estuarine Water Using in Situ Preconcentration of Lead Hydride on Ir, Zr, and W-Coated Graphite Tubes, *Anal. Chim. Acta*, 1998, **368**, 281-289.
86. J. Aznarez, F. Palacios, J. C. Vidal, J. Galban, Extraction – Atomic Absorption Spectrophotometric Determination of Lead by Hydride Generation in Non-Aqueous Media, *Analyst*, 1984, 109, 713-715.
87. P. C. Hauser, Z. –P. Zhang, Flow-Injection Determination of Lead by Hydride Generation and Conductometric Detection, *Fresenius J. Anal. Chem.*, 1996, **355**, 141-143.
88. J. Li, F. Lu, T. Umemura, K. –I. Tsunoda, Determination of lead by Hydride Generation Inductively Coupled Plasma Mass Spectrometry, *Anal. Chim. Acta*, 2000, **419**, 65-72.
89. N. Maleki, A. Safavi, Z. Ramezani, Determination of Lead by Hydride Generation Atomic Absorption Spectrometry (HGAAS) Using a Solid

Medium for Generating Hydride, *J. Anal. At. Spectrom.*, 1999, **14**, 1227-1230.

90. H. -W. Sun, J. Ha, J. -M. Sun, L. -L. Yang, D. -Q. Zhang, Derivative Hydride Generation Atomic Absorption Spectrometry and Determination of Lead Traces in Waters, *Fresenius J. Anal. Chem.*, 2001, **371**, 1154-1157.
91. S. Chen, Z. Zhang, H. Yu, W. Liu, M. Sun, Determination of Trace lead by Hydride Generation Inductively Coupled Plasma Mass Spectrometry, *Anal. Chim. Acta*, 2002, **463**, 177-188.
92. X. Liu, S. Xu, Z. Fang, Determination of Trace Amounts of Lead in Biological Materials by Flow Injection-Hydride Generation-AAS with Sensitivity Enhancements Using Nitroso-R-Salt, *Atom. Spectrosc.*, 1994, **15**, 229-233.
93. M. T. Barangan, F. Laborda, J. R. Castillo, Reagent Injection FIA System for Lead Determination by Hydride Generation – Quartz – Tube Atomic Absorption Spectrometry, *Anal. Bioanal. Chem.*, 2002, **374**, 115-119.
94. M. C. Valdes-Hevia y Temprano, B. Aizpun Fernandez, M. R. Fernandez de la Campa, A. Sanz-Medel, Study of the Influence of Ordered Media on the Determination of Lead by Hydride Generation Inductively Coupled Plasma Atomic Emission Spectrometry, *Anal. Chim. Acta*, 1993, **283**, 175-182.
95. Y. Madrid, J. Meseguer, M. Bonilla, C. Camara, Lead Hydride Generation in a Lactic Acid – Potassium Dichromate Medium and Its Application to the Determination of Lead in Fish, Vegetable and Drink Samples, *Anal. Chim. Acta*, 1990, **237**, 181-187.
96. J. Li, Y. Liu, T. Lin, Determination of Lead by Hydride Generation Atomic Absorption Spectrometry, Part 1. A New Medium for Generating Hydride, *Anal. Chim. Acta*, 1990, **231**, 151-155.

97. J. F. Tyson, R. I. Ellis, G. Carnrick, F. Fernandez, Flow Injection Hydride Generation Electrothermal Atomic Absorption Spectrometry with In-Atomizer Trapping for the Determination of Lead in Calcium Supplements, *Talanta*, 2000, **52**, 403-410.
98. D. S. Forsyth, W. D. Marshall, Performance of an Automated Gas Chromatograph – Silica Furnace – Atomic Absorption Spectrometer for the Determination of Alkyllead Compounds, *Anal. Chem.*, 1985, **57**, 1299-1305.
99. M. Johansson, D. C. Baxter, K. E. A. Ohlsson, W. Frech, Mechanism of Formation and Spatial Distribution of Lead Atoms in Quartz Tube Atomizers, *Spectrochim. Acta Part B*, **52**, 1997, 643-656.
100. M. Filletta, N. Belzile, Y.-W. Chen, Antimony in the Environment: A Review Focused on Natural Waters I. Occurrence, *Earth-Sci. Rev.*, 2002, **57**, 125-176.
101. M. Krachler, H. Emons, J. Zheng, Speciation of Antimony for the 21st Century: Promises and Pitfalls, *Trends in Anal. Chem.*, 2001, **20**, 79-90.
102. N. N. Greenwood, A. Earnshaw, Chemistry of the Elements 2nd Edition, Butterworth-Heinemann, Oxford, 1997.
103. Monographs of International Agency for Research on Cancer (Cadmium and Cadmium Compounds),
<http://monographs.iarc.fr/htdocs/monographs/vol58/mono58-2.htm>
104. A. D'Ulivo, Y. Chen, Determination of Cadmium in Aqueous Samples by Vapour Generation with Sodium Tetraethylborate(III) Reagent, *J. Anal. At. Spectrom.*, 1989, **4**, 319-322.
105. J. Cacho, I. Beltran, C. Nerin, Generation of a Volatile Cadmium Species in an Organic Medium, *J. Anal. At. Spectrom.*, 1989, **4**, 661-663.

- 106.** L. Ebdon, P. Goodall, S. J. Hill, P. B. Stockwell, K. C. Thompson, Ultra-trace Determination of Cadmium by Vapour Generation Atomic Fluorescence Spectrometry, *J. Anal. At. Spectrom.*, 1993, **8**, 723-729.
- 107.** X. Guo, X. Guo, Studies on the Reaction Between Cadmium and Potassium Tetrahydroborate in Aqueous Solution and Its Application in Atomic Fluorescence Spectrometry, *Anal. Chim. Acta*, 1995, **310**, 377-385.
- 108.** Y. -K. Lu, H. -W. Sun, C. -G. Yuan, X. -P. Yan, Simultaneous Determination of Trace Cadmium and Arsenic in Biological Samples by Hydride Generation – Double Channel Atomic Fluorescence Spectrometry, *Anal. Chem.*, 2002, **74**, 1525-1529.
- 109.** M. C. Valdes-Hevia y Temprano, M.R. Fernandez de la Campa, A. Sanz-Medel, Generation of Volatile Cadmium Species with Sodium Tetrahydroborate from Organized Media: Application to Cadmium Determination by Inductively Coupled Plasma Atomic Emission Spectrometry, *J. Anal. Atom. Spectrom.*, 1993, **8**, 847-852.
- 110.** M. C. Valdes-Hevia y Temprano, M.R. Fernandez de la Campa, A. Sanz-Medel, Sensitive Inductively Coupled Plasma Atomic Emission Spectrometric Determination of Cadmium by Continuous Alkylation with Sodium Tetraethylborate, *J. Anal. Atom. Spectrom.*, 1994, **9**, 231-236.
- 111.** T. -J. Hwang, S. -J. Jiang, Determination of Cadmium by Flow Injection Isotope Dilution Inductively Coupled Plasma Mass Spectrometry with Vapour Generation Sample Introduction, *J. Anal. Atom. Spectrom.*, 1997, **12**, 579-584.
- 112.** D. Pozebon, V. L. Dressler, A. J. Curtius, Determination of Copper, Cadmium, Lead, Bismuth and Selenium in Sea-Water by Electrothermal Vaporization Inductively Coupled Plasma Mass Spectrometry After On-line Separation, *J. Anal. Atom. Spectrom.*, 1998, **13**, 363-369.
- 113.** H. Goenaga Infante, M. L. Fernandez Sanchez, A. Sanz-Medel, Vesicle-Assisted Determination of Ultratrace Amounts of Cadmium in Urine by

Electrothermal Atomic Absorption Spectrometry and Inductively Coupled Plasma Mass Spectrometry, *J. Anal. Atom. Spectrom.*, 1998, **13**, 899-903.

- 114.** J. P. Valles Mota, M. R. Fernandez de la Campa, J. I. G. Alonso, A. Sanz-Medel, Determination of Cadmium in Biological and Environmental Materials by Isotope Dilution Inductively Coupled Plasma Mass Spectrometry: Effect of Flow Sample Introduction Methods, *J. Anal. Atom. Spectrom.*, 1999, **14**, 113-120.
- 115.** S. Cerutti, M. F. Silva, J. A. Gasquez, R. A. Olsina, L. D. Martinez, On-line Preconcentration/Determination of Cadmium in Drinking Water on Activated Carbon Using 8-Hydroxyquinoline in a Flow Injection System Coupled to an Inductively Coupled Plasma Optical Emission Spectrometer, *Spectrochim. Acta Part B*, 2003, **58**, 43-50.
- 116.** S. Tao, T. Kumamaru, Inductively Coupled Plasma Atomic Emission Spectrometric Determination of Cadmium in Biological and Environmental Materials Using Electrothermal Vaporization After in Situ Alkylation, *Anal. Chim. Acta*, 1995, **310**, 369-375.
- 117.** H. Goenaga Infante, M. L. Fernandez Sanchez, A. Sanz-Medel, Ultratrace Determination of Cadmium by Atomic Absorption Spectrometry Using Hydride Generation with In-situ Preconcentration in a Palladium-Coated Graphite Atomizer, *J. Anal. Atom. Spectrom.*, 1996, **11**, 571-575.
- 118.** H. Goenaga Infante, M. L. Fernandez Sanchez, A. Sanz-Medel, Vesicular Hydride Generation In-Situ Preconcentration Electrothermal Atomic Absorption Spectrometry Determination of Sub-Parts-Per-Billion Levels of Cadmium, *J. Anal. Atom. Spectrom.*, 1997, **12**, 1333-1336.
- 119.** H. Matusiewicz, M. Kopras, R. E. Sturgeon, Determination of Cadmium in Environmental Samples by Hydride Generation with In Situ Concentration and Atomic Absorption Detection, *Analyst*, 1997, **122**, 331-336.
- 120.** P. Bermejo-Barrera, J. Moreda-Pinerio, A. Moreda-Pinerio, A. Bermejo-Barrera, Iridium-Coated Graphite Tubes for the Direct Determination of As,

Cd, Hg, and Pb in Seawater by Vapor Generation ETAAS, *Atom. Spectrosc.*, 1998, **19**, 100-106.

- 121.** J. Moreda-Pineiro, C. Moscoso-Perez, P. Lopez-Mahia, S. Muniategui-Lorenzo, E. Fernandez-Fernandez, D. Prada-Rodriguez, Multivariate Optimisation of Hydride Generation Procedures for Single Element Determinations of As, Cd, Sb and Se in Natural Waters by Electrothermal Atomic Absorption Spectrometry, *Talanta*, 2001, **53**, 871-883.
- 122.** L. Lampugnani, C. Salvetti, D. L. Tsalev, Hydride Generation Atomic Absorption Spectrometry with Different Flow Systems and in-atomizer Trapping for Determination of Cadmium in Water and Urine - Overview of Existing Data on Cadmium Vapour Generation and Evaluation of Critical Parameters, *Talanta*, 2003, **61**, 683-698.
- 123.** X. -W. Guo, X.-M. Guo, Determination of Cadmium at Ultratrace Levels by Cold Vapour Atomic Absorption Spectrometry, *J. Anal. At. Spectrom.*, 1995, **10**, 986-991.
- 124.** Y. -L. Feng, R. E. Sturgeon, J. W. Lam, Generation of Atomic and Molecular Cadmium Species from Aqueous Media, *Anal. Chem.*, 2003, **75**, 635-640.
- 125.** M. Fernandez de la Campa, E. Segovia Garcia, M. C. Valdes-Hevia y Temprano, B. Aizpun Fernandez, J. M. Marchante Gayon, A. Sanz-Medel, Effects of Organised Media on the Generation of Volatile Species for Atomic Spectroscopy, *Spectrochim. Acta Part B*, 1995, **50**, 377-391.
- 126.** M. L. Garrido, R. Munoz-Olivas, C. Camara, Determination of Cadmium in Aqueous Media by Flow Injection Cold Vapour Atomic Absorption Spectrometry. Application to Natural Water Samples, *J. Anal. At. Spectrom.*, 1998, **13**, 295-300.
- 127.** M. Liu, S. Xu, The Determination of Trace Cadmium by Flow Injection Cold Vapor Generation AAS, *Atom. Spectrosc.*, 1997, **18**, 195-201.

- 128.** M. L. Garrido, R. Munoz-Olivas, C. Camara, Interference Removal for Cadmium Determination in Waste Water and Sewage Sludge by Flow Injection Cold Vapour Generation Atomic Absorption Spectrometry, *J. Anal. At. Spectrom.*, 1998, **13**, 1145-1149.
- 129.** M. Liva, R. Munoz-Olivas, C. Camara, Determination of Cd in Sonicate Slurries and Leachates of Biological and Environmental Materials by FI-CV-AAS, *Talanta*, 2000, **51**, 381-387.
- 130.** C. Vargas-Razo, J. F. Tyson, Determination of Cadmium by Flow Injection-Chemical Vapor Generation Atomic Absorption Spectrometry, *Fresenius J. Anal. Chem.*, 2000, **366**, 182-190.
- 131.** M. Otto, *Chemometrics Statistics and Computer Applications in Analytical Chemistry*, Wiley, Weinheim, 1999.
- 132.** R. G. Brereton, *Chemometrics Data Analysis for the Laboratory and Chemical Plant*, Wiley, Chichester, 2003.
- 133.** J. N. Miller, J. C. Miller, *Statistics and Chemometrics for Analytical Chemistry Fourth Edition*, Prentice Hall, Essex, 2000.
- 134.** E. Morgan, *Chemometrics: Experimental Design*, Wiley, Chichester, 1995.
- 135.** T. Matoušek, M. Johansson, J. Dědina , W. Frech, Spatially Resolved Absorption Measurements of Antimony Atom Formation and Dissipation in Quartz Tube Atomizers Following Hydride Generation, *Spectrochim. Acta Part B*, 1999, **54**, 631-643.
- 136.** T. Matoušek, J. Dědina , A. Selecká, Multiple Microflame Quartz Tube Atomizer – Further Development Towards the Ideal Hydride Atomizer for Atomic Absorption Spectrometry, *Spectrochim. Acta Part B*, 2002, **57**, 451-462.

137. B. Welz, M. Schubert-Jacobs, T. Guo, Investigations for the Determination of Tin by Flow Injection Hydride Generation Atomic Absorption Spectrometry, *Talanta*, 1992, **39**, 1097-1105.
138. J. Dědina, private communication.
139. CRC Handbook of Chemistry and Physics, 52nd Edition, 1971-1972, Chemical Rubber Publishing Company, 1971.
140. Narsito, J. Agterdenbos, S. J. Santosa, Study of Processes in the Hydride Generation Atomic Absorption Spectrometry of Antimony, Arsenic and Selenium, *Anal. Chim. Acta*, 1990, **237**, 189-199.
141. R. E. Sturgeon, S. N. Willie, G. I. Sproule, P. T. Robinson, S. S. Berman, Sequestration of Volatile Element Hydrides by Platinum Group Elements for Graphite Furnace Atomic Absorption, *Spectrochim. Acta Part B*, 1989, **44**, 667-682.
142. P. Niedzielski, M. Siepak, Determination of Sb(III) and Sb(V) in Water Samples by Hydride Generation Atomic Absorption Spectrometry with *In-Situ* Trapping in a Graphite Tube, *Anal. Letters*, 2003, **36**, 971-986.
143. H. Matusiewicz, M. Mikolajczak, Determination of As, Sb, Se, Sn and Hg in Beer and Wort by Direct Hydride Generation Sample Introduction – Electrothermal AAS, *J. Anal. At. Spectrom.*, 2001, **16**, 652-657.
144. H. O. Haug, Y. –P. Liao, Investigation of the Automated Determination of As, Sb and Bi by Flow-Injection Hydride Generation Using In-Situ Trapping on Stable Coatings in Graphite Furnace Atomic Absorption Spectrometry, *Fresenius J. Anal. Chem.*, 1996, **356**, 435-444.
145. W. –W. Ding, R. E. Sturgeon, Evaluation of Electrochemical Hydride Generation for the Determination of Total Antimony in Natural Waters by Electrothermal Atomic Absorption Spectrometry with *In-Situ* Concentration, *J. Anal. At. Spectrom.*, 1996, **11**, 225-230.

146.J. Y. Cabon, C. L. Madec, Determination of Major Antimony Species in Seawater by Continuous Flow Injection Hydride Generation Atomic Absorption Spectrometry, *Anal. Chim. Acta*, 2004, **504**, 209-215.

VITA

Deniz Korkmaz was born in Ankara on November 30, 1974. She was graduated from Özel Yükseliş Lisesi in 1992. She received her B.S. degree in June 1996 from Chemistry Department of the Middle East Technical University. She received her M.S. degree from the same department in June 1998. She started her PhD studies in September 1998. She has been working as teaching assistant in the Chemistry Department of the Middle East Technical University since 1996.